Review

Strategies and methods for fabricating high quality metal halide perovskite thin films for solar cells

Helian Sun[a], Pengfei Dai[a], Xiaotong Li[a], Jinyan Ning[a], Shenghao Wang[a,b,*], Yabing Qi[b,*]

[a] *Materials Genome Institute, Shanghai University, Shanghai 200444, China*
[b] *Energy Materials and Surface Sciences Unit (EMSSU), Okinawa Institute of Science and Technology Graduate University (OIST), 1919-1 Tancha, Onna-son, Okinawa 904-0495, Japan*

*Corresponding authors.

E-mail addresses: shenghaowang@shu.edu.cn, shenghao.wang@oist.jp (S. Wang); Yabing.Qi@OIST.jp (Y. B. Qi)

ABSTRACT

With the development of human society, the problems of environmental deterioration and energy shortage have become increasingly prominent. In order to solve these problems, metal halide perovskite solar cells (PSCs) stand out because of their excellent properties (*i.e.*, high optical absorption coefficient, long carrier lifetime and carrier diffusion length, adjustable band gap) and have been widely studied by researchers. PSCs with low cost, high power conversion efficiency and high stability are the future development trend. The quality of perovskite film is essential for fabricating PSCs with high performance. To provide a full picture of realizing high performance PSCs, this review focus on the strategies for preparing high quality perovskite films (including antisolvent, Lewis acid-base, additive engineering, scaleable fabrication, strain engineering and band gap adjustment), and therefore to fabricate high performance

1

PSCs and to take the commerilization forward.

Keywords: Halide perovskite; Solar cell; Photovoltaic; Antisolvent

Helian Sun received her B.E. degree in Materials science and Engineering from Changzhou University in 2019. She is currently studying for a Master's Degree in the Materials Genome Institute, Shanghai University. At present, her research focuses on the preparation of perovskite solar cells by antisolvent method.
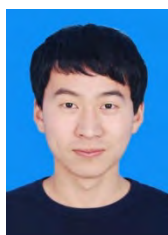
Pengfei Dai received his B.S. degree in Materials Chemistry from Shandong University of Science and Technology in 2018. He is currently studying for a Master's Degree in the Materials Genome Institute, Shanghai University. His research interest focuses on all-inorganic perovskite solar cells.

Xiaotong Li received her B.S. degree in Polymer Materials and Engineering from Qingdao University of Science and Technology. She is currently studying for a Master's Degree in the Materials Genome Institute, Shanghai University. Her research interest focuses on lead-free perovskite solar cells.

Jinyan Ning obtained a Doctor's degree in Engineering in Materials Science of Donghua University in 2014. During 2011–2014, she carried out doctoral research in Kawamura Institute of Chemical Research in Japan. She entered Shanghai University in 2014 and is currently working in the Materials Genome Institute, Shanghai University. She mainly engaged in high-throughput preparation and characterization of materials.

Shenghao Wang is a professor in Materials Genome Institute, Shanghai University, China. He received Ph.D. from University of Tsukuba in 2013. Prior to his current appointment, he worked as a postdoctoral scholar in Prof. Yabing Qi's Unit at the OIST from 2013 to 2016, and then he worked in Institute of Applied Physics, University of Tsukuba from 2017 to 2018. His research interests include surface and interface sciences, photoemission spectroscopy techniques, and solar cells (https://www.x-mol.com/groups/shu-ASOMD-lab).

Yabing Qi is a Professor and Unit Director of Energy Materials and Surface Sciences Unit (EMSSU) at Okinawa Institute of Science and Technology Graduate University (OIST) in Japan, and a Fellow of the Royal Society of Chemistry (FRSC). Before joining OIST, Prof. Qi was a postdoctoral fellow at Princeton University. Prof. Qi received his B.S., M.Phil., and Ph.D. from Nanjing University, Hong Kong University of Science and Technology, and University of California Berkeley, respectively. His research interests include surface/interface sciences, perovskite solar cells, lithium ion batteries, organic electronics, energy materials and devices (https://groups.oist.jp/emssu).

1. Introduction

With massive consumption of fossil fuels across the globe, the energy shortage and environment pollution have become serious challenges. To solve these issues, the utilization of renewable energy (such as solar energy) is under intensive studies. Metal halide perovskite solar cells (PSCs), as an emerging solar technology in the spotlight. In the past ten years, PSCs have attracted considerable attention because of their unique optoelectronic properties (e.g., large absorption coefficient, long diffusion length, high mobility [1,2]). The chemical formula of traditional perovskite materials is ABX_3, in which the A-site is univalent cation, such as Cs^+, MA^+ ($MA=CH_3NH_3$), FA^+ ($FA=HC(NH_2)_2$), B-site is divalent metal cation (Pb^{2+} and/or Sn^{2+}) and X-site is halogen anion (I^-, Br^-, and/or Cl^-). The crystal structure of the ABX_3 type perovskite can be regarded as a framework structure of the $[BX_6]^{4-}$ octahedral network connected by vertices in three-dimensional space, in which B-site is the central position and A-site cation is located in the $[BX_6]^{4-}$ framework interstices [3]. In 2009, $MAPbI_3$ perovskite was first introduced into dye-sensitized solar cells with a power conversion efficiency (PCE) of 3.81% [4]. After a decade, PCE of PSCs has reached 25.5% [5], which is attributed to tremendous effort by the perovskite research community.

Perovskite are versatile. Generally, pure lead-based perovskite and lead-less (or lead free) perovskite are the two classes. In each classification, in addition to the variation at the B site, the A site and X site can also be tuned, which leads to the adjustable band gap of perovskite materials. Fig. 1 shows the PCE enhancement of various PSCs in the last decade. Pure lead-based device possesses the highest PCE

4

(25.5%). Large variations of perovskite compositions can be witnessed. Even for the same type perovskite (*i.e.*, the same composition elements and the same structure), there are variations. For example, for Pb-Sn based perovskites, perovskites with 75% Pb or 50% Pb (note that both are in molar percentage), *i.e.*, $MAPb_{0.75}Sn_{0.25}I_3$, $MAPb_{0.38}Sn_{0.62}I_3$ are found in the figure. Take another example, for MA-FA based perovskites, both $MA_{0.4}FA_{0.6}$- and $MA_{0.3}FA_{0.7}$- based perovskites are found in the figure. It should be noted that the PCE record of different kinds of perovskite are different, where the PCEs are limited by the opto-electronic properties of them. Overall, the PCEs for different type perovskites gradually increase. Although the record PCE is already very close to that of commercialized silicon-based photovoltaic, there is still strong demand to further increase the PCE, and there is still room to further improve the device performance because of the theoretical PCE of PSCs is ~32% [6].

CsSnI$_{3-x}$Br$_x$ MASn$_x$Pb$_{1-x}$I$_3$ CsGe$_x$Sn$_{1-x}$I$_3$

MASnI$_{3-x}$Br$_x$ MA$_x$FA$_y$Cs$_{1-x-y}$Sn$_z$Pb$_{1-z}$I$_3$ MAGeI$_{3-x}$Br$_x$

FASnI$_{3-x}$Br$_x$ CsPb$_{0.9}$Sn$_{0.1}$IBr$_2$ FA$_x$MA$_{1-x}$Pb$_y$Sn$_z$Ge$_{1-y-z}$I$_3$

FA$_x$MA$_y$Cs$_{1-x-y}$SnI$_3$ 2D perovskite

FASn$_x$Pb$_{1-x}$I$_3$ PEA$_{0.15}$FA$_{0.85}$SnI$_3$

Lead-based perovskite

25.5%

22.09% — Lead-based perovskite

FA$_{0.83}$MA$_{0.17}$Ge$_{0.03}$Pb$_{0.97}$(I$_{0.9}$Br$_{0.1}$)$_3$

21.1% — FA$_{0.7}$MA$_{0.3}$Pb$_{0.5}$Sn$_{0.5}$I$_3$

19.03% — FA$_{0.5}$MA$_{0.5}$Pb$_{0.5}$Sn$_{0.5}$I$_3$

20.4% — FA$_{0.475}$MA$_{0.5}$Cs$_{0.025}$Pb$_{0.5}$Sn$_{0.5}$I$_3$

17.6% — FA$_{0.6}$MA$_{0.4}$Sn$_{0.6}$Pb$_{0.4}$I$_3$

17.6% — FAPb$_{0.7}$Sn$_{0.3}$I$_3$

18.95% — FA$_{0.7}$MA$_{0.2}$Cs$_{0.1}$Pb$_{0.5}$Sn$_{0.5}$I$_3$

17.25% — FA$_{0.6}$MA$_{0.4}$Sn$_{0.6}$Pb$_{0.4}$I$_3$

17.6% — FA$_{0.5}$MA$_{0.5}$Pb$_{0.5}$Sn$_{0.5}$I$_3$

16.26% — FAPb$_{0.7}$Sn$_{0.3}$I$_3$

15.4% — FA$_{0.75}$Cs$_{0.25}$Pb$_{0.6}$Sn$_{0.4}$I$_3$

15.08% — FA$_{0.6}$MA$_{0.4}$Sn$_{0.6}$Pb$_{0.4}$I$_3$

14.35% — FAPb$_{0.75}$Sn$_{0.25}$I$_3$

14.01% — MAPb$_{0.75}$Sn$_{0.25}$I$_3$

14.04% — MAPb$_{0.38}$Sn$_{0.62}$I$_3$

14.1% — FA$_{0.75}$Cs$_{0.25}$Sn$_{0.5}$Pb$_{0.5}$I$_3$

13.9% — MAPb$_{0.75}$Sn$_{0.25}$I$_3$

10.1% — MAPb$_{0.85}$Sn$_{0.15}$I$_{3-x}$Cl$_x$

10.2% — FAPb$_{0.5}$Sn$_{0.5}$I$_3$

11.3% — CsPb$_{0.9}$Sn$_{0.1}$IBr$_2$

10.07% — MA$_{0.9}$Cs$_{0.1}$Pb$_{0.5}$Sn$_{0.5}$I$_3$

9.06% — FA$_{0.75}$MA$_{0.25}$SnI$_3$

9.41% — FASnI$_3$

10.1% — FASnI$_3$

12.4% — PEA$_{0.15}$FA$_{0.85}$SnI$_3$

8.9% — FASnI$_3$

8.4% — 3D FASnI$_3$+2D PEA$_2$SnI$_4$

8.12% — (FA)$_{0.75}$(MA)$_{0.25}$SnI$_3$

7.9% — EA$_{0.08}$2D(PEA$_2$FASn$_2$I$_7$)/3D(FASnI$_3$)

7.78% — MASnI$_3$

6.4% — MASnI$_3$

5.73% — MASnIBr$_2$

5.48% — MASnI$_2$Br

6.22% — FASnI$_3$

7.09% — FASnI$_3$

7.13% — MASnI$_3$

7.11% — CsGe$_{0.5}$Sn$_{0.5}$I$_3$

4.81% — CsSnI$_3$

3.56% — CsSnI$_3$

3.2% — CsSnIBr$_2$

6.08% — Cs$_{0.08}$FA$_{0.92}$SnI$_3$

4.79% — FA$_{0.75}$MA$_{0.25}$Sn$_{0.95}$Ge$_{0.05}$I$_3$

2.76% — CsSnI$_3$

2.02% — CsSnI$_3$

2.10% — FASnI$_3$

1.38% — Cs$_{0.1}$MA$_{0.9}$SnI$_3$

1.72% — FASnI$_2$Br

0.88% — CsSnI$_3$

0.11% — CsGeI$_3$

0.20% — MAGeI$_3$

0.33% — Cs$_{0.1}$MA$_{0.9}$SnI$_3$

0.57% — MAGeI$_{2.7}$Br$_{0.3}$

2012 2013 2014 2015 2016 2017 2018 2019 2020

Fig. 1. The PCE enhancement of various PSCs in the last decade.

To accelerate the commercialization of PSCs, low cost and high stability are the two essential factors. To reduce the cost, there are three considerations. First, raw materials should be inexpensive. Fortunately, the constituent elements of perovskites (such as C, H, Cs, Pb, Sn, Cl, I and Br) are earth abundant. Hence, the cost of raw materials will not hinder the commercialization of PSCs.

Secondly, the fabrication process should be based on low-cost equipment and processes. Again, perovskites fabrication fortunately possess the low-cost feature, because of easy formation of perovskite films (*i.e.*, low formation energy or easy reaction between metal halide and organic halide), cheap equipment (such as spin coater [7,8], doctor blade [9], chemical vapor deposition [10,11], spray [12]) and non-harsh environment requirement (*i.e.*, no need of high vacuum system). Solution method is

one of the most commonly used methods to prepare perovskite thin films because of its simple process and low cost. The rapid development of PSCs is closely related to the development of solution method. However, solution method also has some drawbacks, such as pinhole, inhomogeneity, low coverage. The poor film quality (pinhole will reduce the parallel resistance, and the uneven film will increase the series resistance) will lead to lower PCE and poor stability of PSCs. In order to improve the quality of thin films and promote the improvement of PCE, a large number of methods have been used to treat perovskite films, such as vapor-assisted annealing, adding additives in precursor, surface passivation layer capping, and so on. Among them, the combination of solution method and the antisolvent [13], Lewis acid-base [14], or additives [15] plays an important role in preparation of high-quality perovskite films and improving the efficiency of different kinds of PSCs.

Perovskite are often instable, especially when they are exposed to environmental conditions (such as moisture or/and oxygen). The instability of perovskite includes poor chemical stability and poor thermal stability [16], which would lead to defects and degradation of perovskite, and eventually damage the performance of PSCs [17]. The structural and morphological properties, as well as the intrinsic defects also affect the stability of perovskite itself [18,19]. For example, poor morphology not only leads to low light absorption and ineffective charge transfer, it also induces easy degradation because of the hydrophilic nature of perovskite and the easy reaction with water. The volatilization of organic cations can accelerate the degradation of perovskite films during thermal annealing [20]. Ion migration in perovskite also results in poor stability,

so the structure confinement or reducing defect in crystals are very important [21,22]. Stability of PSCs is strongly correlated with the fabrication method, and stability properties can vary from group to group. It should be emphasized that from the viewpoint of practical applications, stability is as important as PCE.

In this review, we examine various strategies for fabricating high-quality perovskite films (and therefore enhancing device performance), including the antisolvent method (such as the role of it, the influencing factors and the methods to expand the dripping time window), the Lewis acid−base adduct approach, utilization of additives in precursor or surface of perovskite layer and the methods of scaleable fabrication. Strain engineering and the band gap adjustment are also discussed. At the end, we present the current challenges and future directions for commercialization of PSCs.

2. Antisolvent

A solution contains solute and solvent. An antisolvent is a liquid that does not dissolve the solute but is miscible with the solvent. When perovskite is prepared by the solution method, perovskite precursor (such as MAI, PbI_2, etc.) are dissolved in solvents. The commonly used solvents are dimethylformamide (DMF) [23], dimethyl sulfoxide (DMSO) [24], gamma-butyrolactone (GBL) [25] and N-Methyl pyrrolidone (NMP) [26], etc. In the spin coating process, most of the solvent is removed due to the centrifugal force generated by high-speed rotation. However, there is still residual solvent in the film formed by spin coating because the film is wet. The remaining solvent needs to be removed by thermal annealing. However, due to the relatively high

boiling point of these solvents, they evaporate slowly in the annealing process, leading to poor film morphology, which can seriously affect the performance of PSCs. In the spin coating process, the introduction of an antisolvent can rapidly reduce the solubility of perovskite precursor and promote the rapid crystallization and film formation of perovskite, which helps improve the performance of PSCs.

2.1. Basic role of antisolvent

2.1.1. Improving surface coverage

Sometimes, the perovskite film is not a complete film and there are pinholes in the conventional one-step spin coating method, which has a detrimental effect on the performance of PSCs. The antisolvent method can increase the film coverage. The coverage of the film has a great influence on the performance of the device: (1) The film with low coverage will lead to no light absorption in the uncovered area, and the photocurrent will be reduced; (2) in the low coverage area, the hole transport layer (HTL) contacts with the electron transport layer (ETL), forming a high-frequency shunt channel, reducing the filling factor (FF) and open circuit voltage (V_{oc}), and reducing the PCE of the device [7]. Only when the perovskite film with high coverage is used as the absorption layer, the best photovoltaic performance can be obtained. In 2014, Xiao *et al.* [27] prepared smooth, uniform and dense perovskite thin films by antisolvent treatment. They used DMF as solvent to prepare $MAPbI_3$ film. In the process of spin coating, they added another solvent: Chlorobenzene (CB). CB can reduce the solubility of perovskite instantaneously by rapidly extracting solvent, thus promoting the crystallization of perovskite. Here, the solvents like CB are called antisolvent. Fig. 2(a)

shows the morphologies of the films prepared without/with antisolvent. The film

prepared by the conventional spin coating method shows non-continuous coverage, and

the grains are small (panel i of Fig. 2a), while the perovskite film prepared by CB

antisolvent has no pinholes (panel ii of Fig. 2a), and the surface is covered completely

with large grains. There are many kinds of antisolvent, such as CB and anisole. Due to

the different physicochemical properties of the antisolvents (details can be seen in

Section 2.3), as well as the variety of perovskites, the morphology of perovskite thin

films may differ.
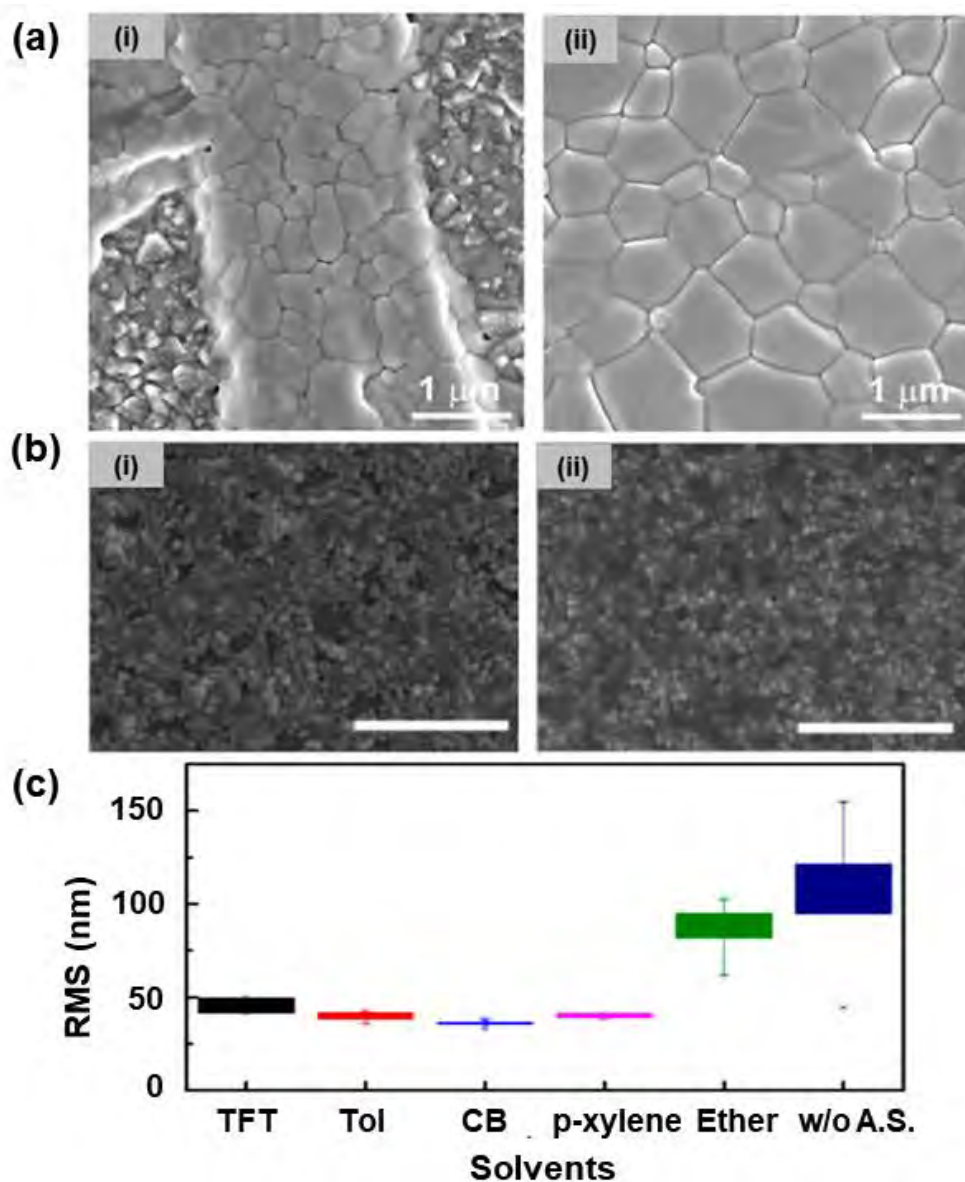
Fig. 2. (a) Scanning electron microscope (SEM) images of MAPbI$_3$ perovskite films prepared by the conventional spin-coating method (i) and the CB antisolvent treatment (ii) [27]. Copyright 2014, Wiley-VCH. (b) SEM images (scale bar: 2 μm) of MAPbI$_3$ films prepared by conventional spin coating (N/A) (i) and Tol washing (ii). [28]. Copyright 2014, Royal Society of Chemistry. (c) Root mean-squared (RMS) statistics of (FAPbI$_3$)$_{0.85}$(MAPbBr$_3$)$_{0.15}$ perovskite films prepared by different antisolvents [29]. TFT is trifluorotoluene. Copyright 2017, American Chemical Society.

2.1.2. Increasing grain size and crystallinity

In Fig. 2(a), we can see that the grain size of perovskite films prepared by conventional solution method is usually small (panel i of Fig. 2a), while CB antisolvent increases the grain size (panel ii of Fig. 2a). However, the antisolvent does not always increase the grain size. Some antisolvents (such as CB) have salient effect on increasing grain size, as described previously, while other antisolvent (such as Tol) have no obvious effect (panels i and ii of Fig. 2b). Therefore, the grain size is dependent on antisolvents. The physicochemical properties (the details can be seen in Section 2.3) of the antisolvent itself, the prepare condition of the antisolvent and the perovskite itself affect the grain size of perovskite [30,31]. It is well known that the larger grain size leads to the higher roughness of the film and the greater light scattering, thus reducing the light absorption of the perovskite layer. At the same time, large crystal grains also mean higher crystallinity and less grain boundaries (GBs) [32]. It has been reported that the presence of appropriate amount of GBs in perovskite thin films contributes to carrier separation and collection [33]. For example, Chen *et al.* found that the PbI_2 phase at GBs of perovskite thin film has a passivation effect, which can improve the photovoltaic performance of PSCs [34]. Similarly, Son *et al.* added excess MAI into the precursors to form a thin MAI layer on the $MAPbI_3$ GBs, which passivated the GBs, improved the ion conduction and increased the carrier lifetime [35]. Finally, it resulted in 20.1% of PCE. Note that the excess PbI_2 [34] and MAI [35] here are for different preparation methods, and the quality of the film depends on the preparation method.

On the other hand, the small grain size decreases the roughness and therefore the

light absorption will be enhanced. At the same time, small grain size indicates more GBs, which leads to more non-radiative recombination of carriers because that most defects are concentrated in the GBs of perovskite films [36,37]. In addition, more GBs can also lead to the water and oxygen penetration into the film through GBs channels, resulting in the degradation of perovskite [38]. Therefore, it is necessary to adjust the grain size by antisolvent to balance the roughness, crystallinity, light absorption and GBs, so as to enhance the photovoltaic performance of PSCs.

2.1.3. Reducing film roughness

When there is no antisolvent, the surface of the film fluctuates greatly which means large roughness. This can be witnessed in Fig. 2(c). The use of antisolvent can reduce the roughness of the film. Due to the different properties of antisolvents, they have different effects on the surface roughness of perovskite films. The fluctuation of the film surface is slightly improved with ether. The RMS of the films prepared by p-xylene, CB, tol and TFT are much smaller than that of ether, indicating that the surface tends to be more uniform. Effect of low boiling point antisolvent (such as ether) on improving the surface roughness of perovskite film is obviously weaker than other high boiling point antisolvent [29].

2.1.4. Improving photovoltaic performance

The combination of the effects of the antisolvent mentioned above on the quality (coverage, grain size, crystallinity, and surface roughness) of the perovskite film eventually results in the enhancement of the PSCs performance. In details, full coverage enhances light absorption meanwhile avoiding contact between the transport layers.

Large grains reduce the GBs, which reduce the trap states, leading to decrease in non-radiative recombination. While more GBs lead to shorten the life of carriers, thereby reducing the performance of the device. In addition, the higher crystallinity can increase the light absorption and increase the carrier mobility of the perovskite layer. Obviously, it can increase the generated photocurrent.

The hysteresis of PSCs prepared by conventional solution method (spin-coating) is obvious (Fig. 3a), which is closely related to the number of defects in the perovskite thin film, as well as the transport layers. The ion migration in the perovskite layer and the charge imbalance of the interface will lead to the hysteresis [39,40]. The introduction of antisolvent in the spin coating process can improve the film quality, and then reduce the hysteresis (Fig. 3a). At the same time, the selection of ETL will also affect the hysteresis of PSCs [41].

2.1.5. Enhancing stability

Usually, PSCs prepared by the conventional spin coating method (*i.e.*, no antisolvent) show poorer stability when exposed to air. The antisolvent can change this phenomenon by improving the quality of perovskite films. It leads to the improvement of device performance, which will eventually be accompanied by the improvement of stability. Fig. 3(b) shows the stability test of FAMACs PSCs prepared with or without antisolvent. When the device without antisolvent was exposed to air condition for 4320 h, only 50% PCE was remained. On the other hand, the device with antisolvent can still reach more than 80% of the original PCE, suggesting the effective enhancement for stability. When the same perovskite is prepared using the antisolvent with various

physicochemical properties, their influence on the stability is unequal. Fig. 3(c) shows

the stability test of $(FA_{0.85}MA_{0.15}) Pb(I_{0.85}Br_{0.15})_3$ PSCs prepared by CB, EA and MB

respectively. Among the three antisolvents, CB had the worst effect on improving the

stability, followed by EA and MB. The PSCs treated by MB could still reach 90% PCE

of the original efficiency after being exposed to air for 1400 hours (Fig. 3c) [42].
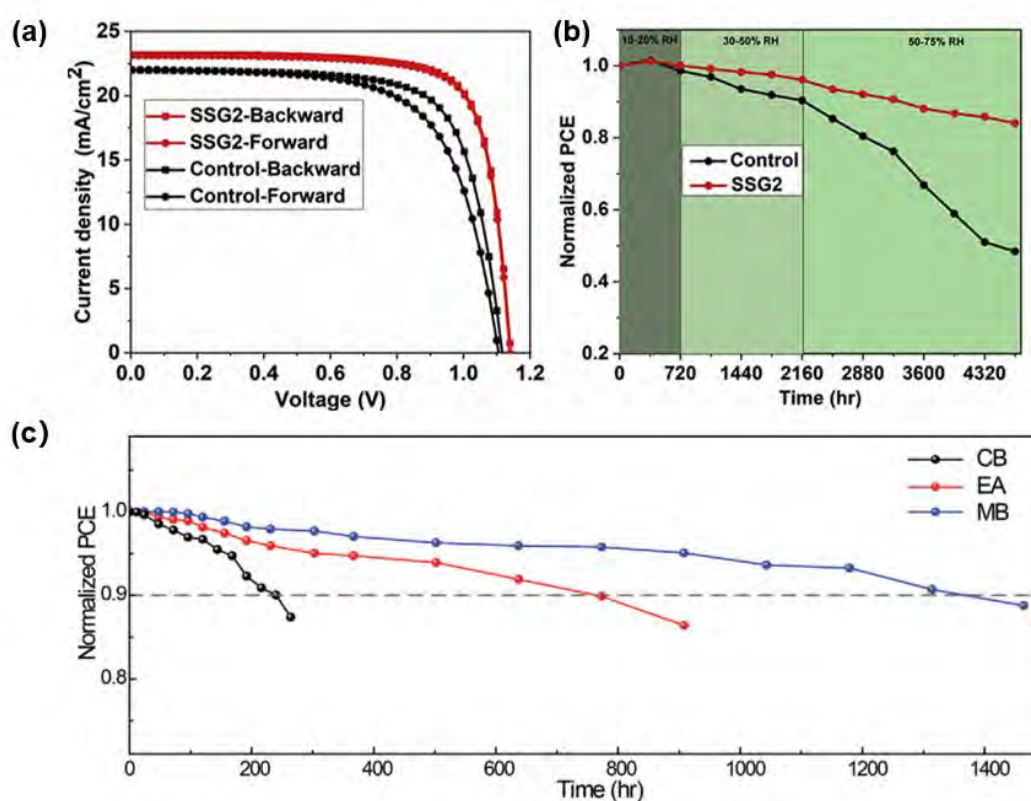
Fig. 3. (a) Current density-voltage curves and (b) stability test of triple-cation

(FAMACs) PSCs without (control)/with antisolvent. Here, SSG2 represents self-

seeding growth, which is actually the antisolvent method [43]. Copyright 2019, Elsevier.

(c) Stability tests of $(FA_{0.85}MA_{0.15})Pb(I_{0.85}Br_{0.15})_3$ PSCs prepared by CB, ethyl acetate

(EA) and methyl benzoate (MB) [42]. Copyright 2020, Wiley-VCH.

2.2. Ways to add an antisolvent

2.2.1. Dripping

In the process of spin-coating (one step or two step), there are several ways to add antisolvent. One of the most widely used is dripping [8]. Dripping can be divided into static dripping and dynamic dripping. During static dripping, antisolvent such as CB, Tol or ether is dripped on the center of the film surface during spin coating (Fig. 4a). After spin coating the perovskite precursor, the film is annealed in nitrogen atmosphere or air condition for evaporating solvent and promoting perovskite crystallization at the same time.
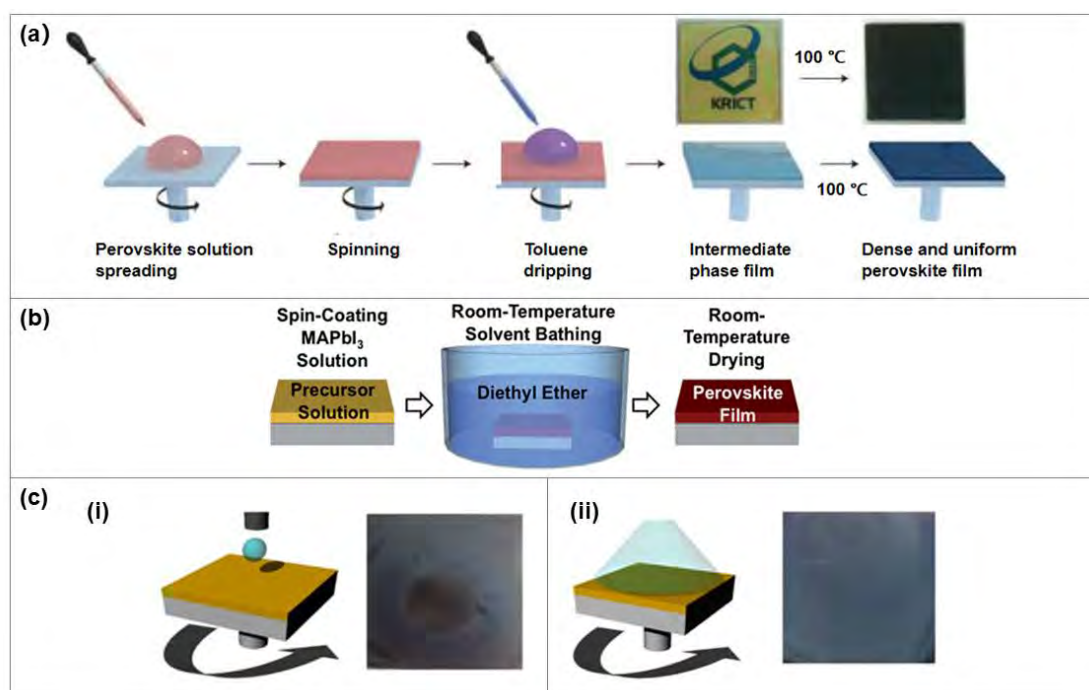
Fig. 4. (a) Schematic diagrams of perovskite film prepared by dripping antisolvent [8]. Copyright 2014, Springer Nature. (b) Schematic diagrams of preparation of large area uniform perovskite film in antisolvent bathing [44]. Copyright 2015, Royal Society of Chemistry. (c) Schematic diagrams of dripping (i) and spraying (ii) antisolvent device,

with optical image of $(FAPbI_3)_{0.85}(MAPbBr_3)_{0.15}$ perovskite film prepared by them [12]. Copyright 2019, Wiley-VCH.

The static dripping method usually results in uneven film morphology between edge and center, which is determined by the spin coating technique itself. So the static dripping is not suitable for the preparation of large area perovskite. To enlarge the scale, a dynamic antisolvent process for spin coating is explored [45]. In this report, the four corners and center of the film were inhomogeneous when the sample was prepared by traditional spin coating. While in the process of dynamic dripping, the pipette gun containing antisolvent moves from the center of the film to the top angle position, and the antisolvent is continuously dripped. The resultant perovskite film has good uniformity from the center to the edge.

2.2.2. Antisolvent bathing

In addition to dripping, antisolvent bathing is another way to incorporate the antisolvent. The antisolvent bathing, as the name implies, is to soak the wet film of perovskite precursor in the antisolvent. In the soaking process, the solvent extraction and the perovskite crystallization process happen simultaneously. Then, the film is taken out from the antisolvent bathing and subsequently annealed/naturally dried (Fig. 4b) [44]. The films prepared by this method have high phase purity, large area coverage and super smoothness. So the antisolvent bathing is suitable for preparing large area high-quality perovskite film. When the temperature of the antisolvent bathing is room temperature, the performance of large-area PSC is inferior to that prepared by dripping method because of the lack of controllability for large area crystallization orientation

[46]. By adjusting the temperature of the antisolvent, the nucleation rate of perovskite

can be reduced or accelerated, and the crystal orientation can be controlled [46,47]

(Section 2.8 for a detailed description). The antisolvent bath can also be combined with

gas blowing [48] and stirring [49] to control the morphology of perovskite better.

2.2.3. Spraying of antisolvent

The diffusion rate of some antisolvent itself (such as ACN) on the substrate is

faster than that caused by spin coating. In the process of spin coating, dripping this kind

of antisolvent will lead to the non-uniform diffusion of antisolvent, leaving a circular

mark on the substrate, as shown in panel i of Fig. 4(c) [12]. This can be avoided by

spraying this antisolvent on the substrate. The perovskite film prepared by spraying is

uniform without circular mark (panel ii of Fig. 4c).

2.3. Various antisolvent and their physicochemical properties

Table 1. Physicochemical properties of common antisolvent.

Antisolvent	Chemical formula	Chemical structure	Toxic or green	Polarity	Boiling point (°C)	DMSO miscibility	DMF miscibility
Toluene(Tol)	C_7H_8			~2.3	110	√	√
Trifluorotoluene (TFT)	$C_7H_5F_3$				102		
Chlorobenzene (CB)	C_6H_5Cl			~2.6	132	√	√
Bromobenzene (BrB)	C_6H_5Br				156.2	√	√
Dichlorobenzene (DCB)	$C_6H_4Cl_2$			~2.7	180.4		
Diethyl ether (ether)	$CH_3CH_2OCH_2CH_3$			~2.9	34	×	√
Dichloromethane (DCM)	CH_2Cl_2			~3.4	40	√	√
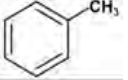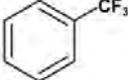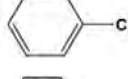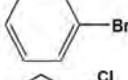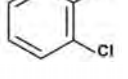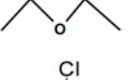
Name	Formula	Structure	Icon		Boiling point (°C)		
Trichloromethane	$CHCl_3$			~4.4	61	√	√
Acetonitrile (ACN)	C_2H_3N			~5.8	81	√	√
Petroleum ether (PE)	C_5H_{12}, C_6H_{14}, C_7H_{16}			~0.01	30–80	×	×
N-hexane	C_6H_{14}			~0.06	69	×	×
Isooctane	$(CH_3)_2CHCH_2C(CH_3)_3$			~0.1	99.3	×	×
Phenetole	$C_8H_{10}O$				170		
Anisole	C_7H_8O				153.8		
Diisopropyl ether	$(CH_3)_2CHOCH(CH_3)_2$			~2.4	68	×	√
Iodobenzene (IB)	C_6H_5I				188	√	√
1-Butanol	$C_4H_{10}O$			~3.9	117	√	√
Sec-butyl alcohol (SBA)	$C_4H_{10}O$				99.5		
Isobutanol	$CH_3CH(CH_3)CH_2OH$			~3	107.9	√	√
Ethanol (EtOH)	C_2H_5OH			~4.25	78	√	√
Ethyl acetate (EA)	$C_4H_8O_2$			~4.3	77	√	√
Methyl-acetate	CH_3COOCH_3				57.8		
Propyl acetate	$C_5H_{10}O_2$				107		
Methyl butyrate	$C_5H_{10}O_2$				102.8		
Methyl benzoate (MB)	$C_8H_8O_2$				198		
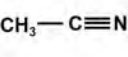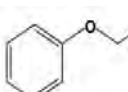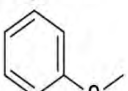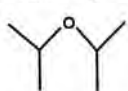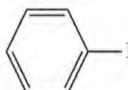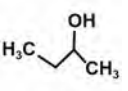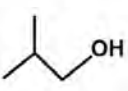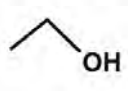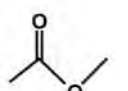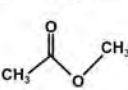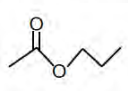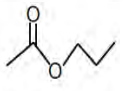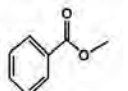
| Isopropanol (IPA) | $(CH_3)_2CHOH$ | | | ~4.3 | 82 | √ | √ |
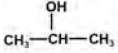
Various antisolvents were investigated in literature, which are listed in Table 1. The physical and chemical properties of the antisolvents, especially the polarity and boiling points, play an important role in the quality of the films and the photovoltaic performance of the devices. The polarity, boiling point, toxicity, chemical structure and miscibility with DMF or DMSO of each antisolvent are also shownTable 1. Antisolvent is usually added to the perovskite film after its formation or during its growth. So it should not dissolve, decompose and react with perovskite. According to the theory of similarity and miscibility, those with similar structure may be mutually soluble and those with similar polarity may be mutually soluble. If the polarity of antisolvent is as strong as DMF, DMSO and NMP. it will dissolve perovskite. For FAMA lead-based perovskite, Bu *et al.* determined the polarity of suitable antisolvent as 2–4.5 [50]. When the polarity of antisolvent is more than 4.5, it can not only extract solvent, but also dissolve perovskite, which is harmful to the growth of perovskite film. The polarity of antisolvent also determines the miscibility of antisolvent to solvent, which determines the extraction effect of antisolvent on solvent. The higher the polarity, the more miscible the antisolvent is with the solvent, which indicates that the solvent removal rate is higher. On the contrary, antisolvent with too low polarity will lead to poor solvent extraction effect [29].

Suitable antisolvent depends not only on the polarity, but also on the boiling point. The boiling point of antisolvent controls the crystal growth time of perovskite [31]. The

drying rate of high boiling point antisolvent is slow in spin coating process, which prolongs the growth time of crystal. The existence of antisolvent in the film provides enough fluidity, which makes the adjacent nuclei larger and increases the grain size. If the boiling point is low, the antisolvent will evaporate too fast, which will lead to poor extraction effect of solvent [51]. Chen *et al.* [31] prepared MAPbI$_3$ films using Tol, CB, iodobenzene (IB) and bromobenzene (BrB) as antisolvents. It was found that the short-circuit current (J_{sc}) increased with the increase of the relative polarity of the antisolvent, while the V_{oc} decreased with the increase of the relative polarity of the antisolvent. Li *et al.* used Tol, CB, ether, IPA and EtOH, to prepare PSCs [51]. It was found that the antisolvent (ether) with low boiling point and good polarity can produce high quality and high PCE (18.47%). Overall, the PSCs prepared by antisolvent with poor miscibility (low polarity) and boiling point have low PCE and poor reproducibility, while the films with high boiling point and miscible (polarity in appropriate range) antisolvent can obtain high density coverage and PCE.

2.4. Dripping time effect

Take an example for fabricating MAPbI$_3$ perovskite thin film by antisolvent [27], the film-forming process can be divided into three stages. The stage 1 is a few seconds (3 s) of spinning with precursor solution, mainly to remove the excess precursor solution. At this stage, the perovskite solution does not reach the supersaturated state. If the antisolvent is added at this stage, the growth of perovskite will be affected, resulting in incomplete coverage. The stage 2 is 4–6 s. In this stage, antisolvent is introduced to extract the residual solvent quickly, accelerate the crystallization of

perovskite and promote the formation of uniform and dense film. The stage 3 (after 7 s): The wet film becomes dry and begins to nucleate heterogeneous. However, the reported dripping time usually differ in different groups. Table 2 listed some reports regarding fabrication perovskites using CB, EA, Tol and ether. We can see that even for the same antisolvent and the same perovskite composition, the dripping time is different, and the device performance differs too. Early or too late dripping will cause poor film morphology, which would affect PCE of PSCs (Fig. 5a and c). So, the quality of perovskite thin film is very sensitive to the time of antisolvent dripping. The specific time of adding antisolvent needs to be continuously optimized to obtain the best PCE.
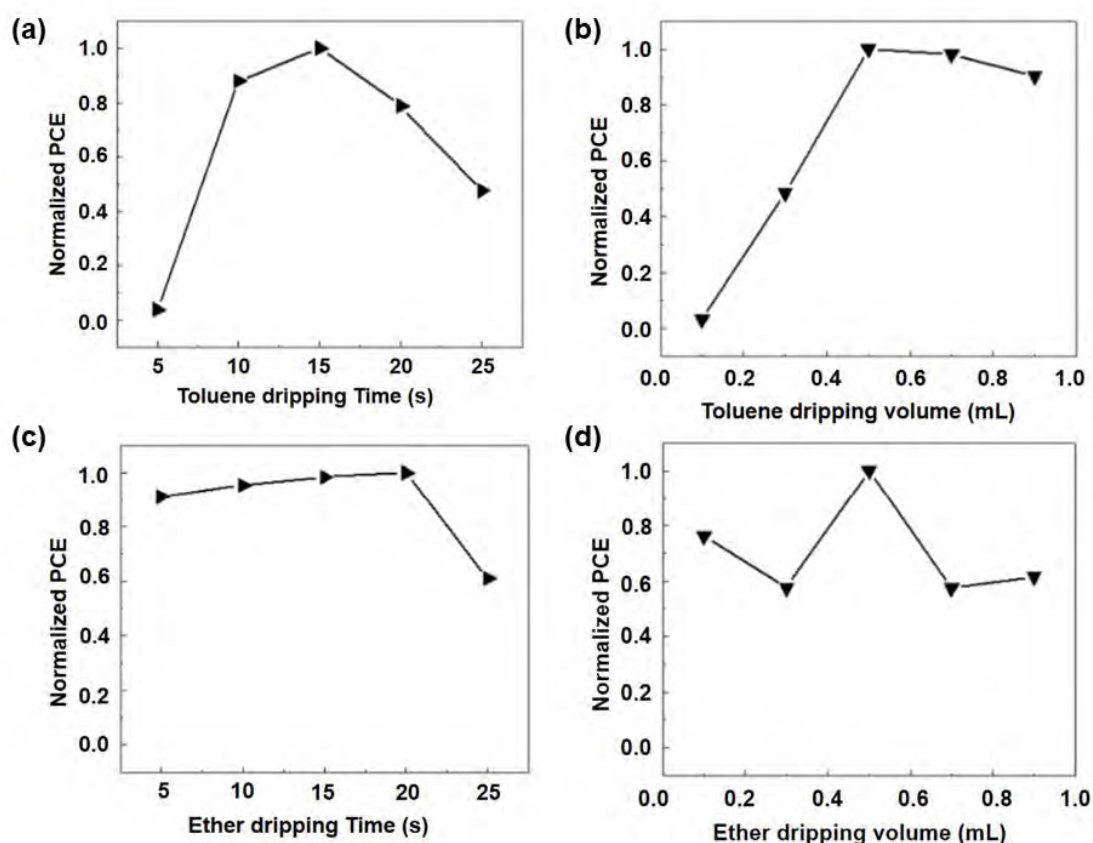
Fig. 5. Effect of adding (a) Tol and (b) ether at different dripping time on PCE of

FAMACs PSCs [52]. Effect of different volume of (c) Tol and (d) ether on PCE of

FAMACs PSCs [52]. Copyright 2018, Wiley-VCH.

Table 2. Dripping time of perovskite films prepared by antisolvent.

Antisolvent	Perovskites	Dripping condition	PCE (%)	Ref.
Tol	$CsPbI_3$	20 s in 1st spinning step	6.9	[53]
		15 s in 1st spinning step	11.4	[54]
	$FAPbBr_3$	25 s in 1st spinning step	5.7	[55]
	$MA_{0.5}FA_{0.5}Pb_{0.5}Sn_{0.5}I_3$	10 s in 1st spinning step	14.01	[56]
	FAMA-based perovskite	15 s in 2nd spinning step	18.1	[57]
	$Cs_{0.025}FA_{0.475}MA_{0.5}Sn_{0.5}Pb_{0.5}I_3$	11–15 s in 2nd spinning step	20.4	[58]
	$FA_{0.5}MA_{0.5}Sn_{0.5}Pb_{0.5}I_3$	11–15 s in 2nd spinning step	17.6	[59]
Ether	$MAPbI_3$	10 s in 1st spinning step	16.9	[60]
		26 s in 1st spinning step	18.47	[51]
	$FA_{0.75}Cs_{0.25}Sn_{0.4}Pb_{0.6}I_3$	18 s in 1st spinning step	15.4	[61]
	$FA_{0.5}MA_{0.5}Pb_{0.5}Sn_{0.5}I_3$	30 s in 1st spinning step	19.03	[62]
	$MAPbI_3$	4 s in 2nd spinning step	18.59	[41]
		10 s in 2nd spinning step	17.2	[63]
	CsFAMA-based perovskite	15 s in 2nd spinning step	19.5	[64]
CB	$MAPbI_3$	10 s in 1st spinning step	21.33	[65]
		20 s in 1st spinning step	19.19	[66]
		25 s in 1st spinning step	12.9	[28]
		5 s in 2nd spinning step	15.5	[67]
		6 s in 2nd spinning step	12.53	[68]
		20 s in 2nd spinning step	19.19	[69]
	$FA_{0.83}MA_{0.17}PbI_{2.49}Br_{0.51}$	15 s in 2nd spinning step	14.87	[70]
EA	$MAPbI_3$	20 s in 1st spinning step	14.5	[71]
	$CsPbI_2Br$	20 s in 1st spinning step	12.19	[72]
	$K_{0.03}Cs_{0.05}(FA_{0.85}MA_{0.15})_{0.92}Pb(I_{0.85}Br_{0.15})_3$	25 s in 1st spinning step	17.82	[45]
	$FA_{0.85}MA_{0.15}Pb(I_{0.85}Br_{0.15})_3$	27 s in 1st spinning step	19.43	[50]
	$(MAPbI_3)_{1-x}(FAPbIBr_2)_x$	7 s in 2nd spinning step	20.11	[73]
	$MA_{0.3}FA_{0.7}Pb_{0.5}Sn_{0.5}I_3$	20 s in 2nd spinning step	21.1	[74]

2.5. Dripping quantity effect

The quantity of antisolvent dripping also affects the device performance. A small

amount of antisolvent cannot completely cover the substrate, and a large volume of

antisolvent will cause cracks in the perovskite film [45]. The dripping quantity of

antisolvent affects the particle size distribution of perovskite [75] and the quality of

perovskite film [45]. Kara *et al.* [75] found that with the decrease of the quantity of

antisolvent (Tol), the grain size increased, which leads to enhancement of crystallinity.

For different antisolvent, the effect of their volumes on the PCE of the same PSCs is

also different. Fig. 5(c and d) shows the normalized PCE of FAMACs PSCs prepared

by Tol and ether, respectively. It can be seen that the effect of ether's quantity on PCE of FAMACs PSCs is less than that of Tol.

2.6. Classification of antisolvent

2.6.1. According to the toxicity of the antisolvent

The antisolvent is either toxic antisolvent or green antisolvent. Common antisolvent, such as CB [76], Tol [8], ether [44], and dichloromethane [63], can regulate the nucleation rate and crystallization of perovskite very well, but they are toxic antisolvents, which will have a negative impact on human body and environment. As halogenated hydrocarbons, CB has inhibitory and anaesthetic effects on the nervous system. Long term exposure to CB can cause liver and kidney lesions [77]. Tol can not only pollute the air and water, but also cause serious nerve damage. A large amount of Tol can even lead to coma or death [78,79]. Although ether is less harmful to the environment, long-term inhalation of ether can cause somnolence, headache, irregular breathing, depression and other symptoms, and even life-threatening [80]. Overall, the toxicity and volatility of these antisolvents will cause environmental pollution and threat to human body, which will limit the commercialization and large-scale production of PSCs.

In order to minimize or avoid the harm of toxic antisolvent to human body and the environment, fortunately there are green antisolvent, such as EA [50,71,72], anisole [52,81,82], IPA [83–85] and IB [30,31]. "Green" does not mean that there is no toxicity, but to minimize the harm to human body and negative effects on the environment [82,86]. Various toxic and green antisolvents and their structures are shown in Table 1.

2.6.1. According to the number of antisolvent used

2.6.1.1. Single antisolvent

Most of the antisolvent used by researchers is single antisolvent (*i.e.*, only containing one solvent), such as CB [28] or Tol [25]. Generally speaking, the antisolvent that can be used alone has moderate polarity and boiling point. Moderate polarity can ensure the perovskite precursor-solvent complex (precursor-solvent complex is related to the Lewis acid-base addition reactions. See Section 3 for details), which is an important factor for the preparation of high-quality perovskite thin films. The best nucleation process and the perovskite thin films with good morphology can be obtained using this antisolvent alone. For example, the polarity of Tol is about 2.3, and that of CB is about 2.6. Their polarities are in the middle range, which avoid harmful effects on PSCs due to too high or too low polarity. Antisolvent with high polarity can not only extract the solvent completely, but also dissolve the perovskite. Similarly, if the polarity of the antisolvent is too low, the extraction effect of the solvent will be weakened, resulting in too high intermediate product content. Either situation will have an adverse effect on the morphology of the perovskite film, such as the appearance of pinholes and excessive roughness. In 2014, Tol and CB were respectively used to prepare $MAPbI_3$ PSCs with good efficiency [8,27]. In addition to them, other antisolvents such as DCB, ether, trichloromethane and diisopropyl ether etc., can also be used alone (whose polarity can be obtained from Table 1). Table 3 lists the effects of various antisolvent on the photovoltaic performance of different PSCs, including single antisolvent, binary and ternary antisolvents.

2.6.1.2. Mixed antisolvents

The polarity of antisolvent such as ACN and PE is too high or too low to be used as a single antisolvent. In order to make better use of these antisolvents to prepare high-quality films, they can be mixed into binary or ternary antisolvents to achieve the purpose of neutralizing polarity. Gedamu *et al.* [87] mixed high polar EtOH with low polar CB and prepared $MAPbI_3$ thin film with high coverage of 99.97%. When sec-butyl alcohol (SBA) is used as antisolvent, the amount of intermediate is very low due to its high polarity, so the best nucleation process cannot be obtained, and the quality of the film is poor. Chen *et al.* [88] neutralized the polarity of SBA with CB and ether to form a ternary mixed antisolvent. The best nucleation process was obtained and the film quality and device performance were significantly improved (*i.e.*, the PCE of $MAPbI_3$ PSCs prepared by ternary mixed solvent was 16.5%, while the one prepared by single antisolvent was 15.06%).

The effect of different antisolvents on nucleation density and perovskite crystal growth differs. Some antisolvents can increase the nucleation density of perovskite, but higher nucleation density will lead to smaller grains in perovskite films, which increases GBs. Antisolvent, which can inhibit the growth of perovskite, are mixed into this kind of antisolvent to balance the nucleation density and crystal growth. Such mixed antisolvent can control the growth of perovskite crystal better. For example, both ether and PE can increase the nucleation density of perovskite, while *n*-hexane can delay the growth of perovskite. Therefore, mixing n-hexane with ether or PE is helpful to obtain the nucleation density of dense and smooth films [79,89].

Table 3. Summarized data (*i.e.*, perovskite type, device architecture, and the device performance) from literature of utilizing single antisolvent,

binary and ternary antisolvents on various PSCs.

Perovskite	Antisolvent	Device structure	V_{oc} (V)	J_{sc} (mA cm^{-2})	FF	PCE (%) without antisolvent	PCE (%) with antisolvent	Ref.
single antisolvent								
MAPb(I$_{1-x}$Br$_x$)$_3$ (x=0.1–0.15)	Tol	FTO/c-TiO$_2$/mp-TiO$_2$/perovskite/PTAA/Au	1.12	19.65	0.76	-	16.72	[8]
MAPbBr$_3$		FTO/c-TiO$_2$/perovskite/spiro/Au	1.42	7.55	0.77	-	8.29	[32]
MAPbI$_3$		FTO/c-TiO$_2$/perovskite/spiro/Metal contact layer	1.02	22.15	0.73	10.15	15.16	[90]
FAPbBr$_3$		FTO/c-TiO$_2$/perovskite/spiro/Au	1.32	6.3	0.69	1.1	5.7	[55]
CsPbI$_3$		FTO/c-TiO$_2$/mp-TiO$_2$/perovskite/CuSCN/carbon-graphite	0.94	13.8	0.52	-	6.9	[53]
Cs$_{0.05}$(MA$_{0.15}$FA$_{0.85}$)$_{0.95}$Pb(I$_{0.85}$Br$_{0.15}$)$_3$		FTO/c-TiO$_2$/mp-TiO$_2$/perovskite/spiro/Au	1.05	21.7	0.75		17.1	[91]
MA$_{0.9}$Cs$_{0.1}$Pb$_{0.75}$Sn$_{0.25}$I$_3$		ITO/PEDOT: PSS/perovskite/PCBM/Bis-C$_{60}$/Ag	0.84	22.8	0.76	-	14.55	[92]
FA$_{0.5}$MA$_{0.5}$Sn$_{0.5}$Pb$_0.5$I$_3$		ITO/PEDOT: PSS/perovskite/PCBM/C$_{60}$/BCP/Ag	0.75	30.56	0.76	-	17.6	[59]
Cs$_{0.025}$FA$_{0.475}$MA$_{0.5}$Sn$_{0.5}$Pb$_{0.5}$I$_3$		FTO/PEDOT: PSS/perovskite/PCBM/C$_{60}$/BCP/Ag	0.81	33.14	0.76	-	20.4	[58]
Cs$_3$Bi$_2$I$_9$- Ag$_3$Bi$_2$I$_9$ Bulk heterojunction		FTO/c-TiO$_2$/perovskite/PDBD-T/Au	0.78	7.65	0.60	-	3.59	[93]
MAPbI$_3$	CB	FTO/TiO$_2$/perovskite/spiro/Ag	1.04	21.1	0.63	1.8	13.8	[27]
MAPbI$_3$		FTO/TiO$_2$:CsCO$_3$/perovskite/spiro/MoO$_3$/Ag	1.11	23.68	0.73	-	19.19	[69]
CsPbBr$_3$		FTO/Ni-TiO$_2$/perovskite/CuPc/Carbon	1.362	7.92	0.79	6.94	8.55	[94]
FA$_{0.75}$MA$_{0.25}$SnI$_3$		ITO/PEDOT: PSS/perovskite/PCBM/Bis-C60/Ag	0.55	19.4	0.67	-	7.2	[95]
FAPb$_{0.75}$Sn$_{0.25}$I$_3$		ITO/NiO$_x$/perovskite/PCBM/BCP/Ag	0.81	28.23	0.75	-	17.25	[96]
MA$_3$Bi$_2$I$_9$		ITO/TiO$_2$/perovskite/spiro/Au	0.72	0.49	0.32	-	0.11	[97]
		FTO/c-TiO$_2$/mp-TiO$_2$/perovskite/spiro/Au	0.653	1.10	0.50	0.069	0.356	[98]
		FTO/c-TiO$_2$/mp-TiO$_2$/perovskite/PIF8-TAA/Au	0.85	1.15		0.73	0.71	[99]
MAPbI$_2$Br	Ether	FTO/c-TiO$_2$/perovskite/spiro/Ag	1.08	15.3	0.65	-	10.7	[49]
MAPbIBr$_2$		FTO/c-TiO$_2$/perovskite/spiro/Ag	0.985	8.26	0.55		4.46	[49]
MAPbI$_3$		FTO/c-TiO$_2$/perovskite/spiro/Au	1.13	21.8	0.78	-	18.6	[63]
(FASnI$_3$)$_{0.6}$(MAPbI$_3$)$_{0.4}$		ITO/PEDOT: PSS/perovskite/C$_{60}$/BCP/Ag	0.795	26.86	0.71	-	15.08	[100]
(FASnI$_3$)$_{0.6}$(MAPbI$_3$)$_{0.4}$		ITO/PEDOT: PSS/perovskite/C$_{60}$/BCP/Ag	0.853	28.5	0.73	-	17.6	[101]
Cs$_{0.05}$(MA$_{0.17}$FA$_{0.83}$)$_{0.95}$Pb(I$_{0.83}$Br$_{0.17}$)$_3$		FTO/c-TiO$_2$/perovskite/Spiro/Au	1.12	23.2	0.75	-	19.5	[64]
MAPbI$_3$	EA	FTO/NiO/perovskite/PCBM/BCP/Ag	0.78	17.9		-	14.5	[71]
		FTO/SnO$_2$/perovskite/spiro/Au	1.115	21.44	0.75	-	17.83	[102]

Perovskite	Antisolvent	Device structure	V_{oc}	J_{sc}	FF		PCE	Ref.
FA$_{0.85}$MA$_{0.15}$Pb(I$_{0.85}$Br$_{0.15}$)$_3$		FTO/TiO$_2$/perovskite/spiro/Au	1.123	22.89	0.756	-	19.43	[50]
(MAPbI$_3$)$_{0.952}$(FAPbIBr$_2$)$_{0.048}$		FTO/SnO$_2$/perovskite/spiro/Au	1.113	23.87	0.76	-	20.11	[73]
K$_{0.03}$Cs$_{0.05}$(FA$_{0.85}$MA$_{0.15}$)$_{0.92}$Pb(I$_{0.85}$Br$_{0.15}$)$_3$		FTO/SnO$_2$/perovskite/spiro/Au	13.56	1.014	0.70	-	17.82 (10×10 cm^2)	[45]
(FAPbI$_3$)$_{0.85}$ (MAPbBr$_3$)$_{0.15}$	Trifluorotoluene (TFT)	FTO/c-TiO$_2$/mp-TiO$_2$/perovskite/spiro/Ag	1.10	23.3	0.79	-	20.3	[29]
Cs$_{0.05}$(FA$_{0.85}$MA$_{0.15}$)$_{0.95}$Pb(I$_{0.85}$Br$_{0.15}$)$_3$	MB	FTO/SnO$_2$/perovskite/spiro/Au	1.22	24.46	0.75	-	22.37	[42]
Cs$_{0.05}$(MA$_{0.17}$FA$_{0.83}$)Pb(I$_{0.83}$Br$_{0.17}$)$_3$	Diisopropyl ether	FTO/c-TiO$_2$/mp-TiO$_2$/perovskite/spiro/Ag	1.16	23.19	0.79	-	21.26	[103]
CsPbI$_2$Br	EtOH	FTO/c-TiO$_2$/perovskite/Carbon	1.15	13.87	0.64	-	10.21	[104]
CsPbI$_3$	Methyl acetate	FTO/TiO$_2$/perovskite/PTAA/Au	1.11	18.31	0.78	3.94	15.91	[105]
CsPbI$_2$Br	IPA	ITO/c-TiO$_2$/perovskiter/spiro/Au	1.23	16.79	0.78	12.65	16.07	[106]
CsPbIBr$_2$		FTO/ZnO/perovskite/Carbon	1.03	11.6	0.63	-	7.6	[85]
(FASnI$_3$)$_{0.6}$(MAPbI$_3$)$_{0.4}$	Anisole	FTO/PEDOT:PSS/perovskite/PCBM/Ag	0.73	26.46	0.72	-	13.97	[107]
[CsPbI$_3$]$_{0.05}$[(FAPbI$_3$)$_{0.85}$(MAPbBr$_3$)$_{0.15}$]$_{0.95}$		FTO/c-TiO$_2$/mp-TiO$_2$/perovskite/spiro/Au	1.15	21.98	0.783	-	19.76	[82]
Cs$_{0.05}$(MA$_{0.17}$FA$_{0.83}$)$_{0.95}$Pb(I$_{0.83}$Br$_{0.17}$)$_3$		FTO/c-TiO$_2$/mp-TiO$_2$/perovskite/spiro/Ag	1.12	23.26	0.76	-	19.9	[81]
MAPbI$_3$	Iodobenzene	ITO/PEDOT: PSS/perovskite/PCBM/Ag	0.919	21.66	0.69	-	13.67	[31]
		ITO/PEDOT: PSS/perovskite/C$_{60}$-BCP/Ag	0.92	21.4	0.76	-	14.89	[30]

Binary antisolvent

Perovskite	Antisolvent	Device structure	V_{oc}	J_{sc}	FF		PCE	Ref.
MAPbI$_3$	Ether/n-hexane	FTO/mp-TiO$_2$/perovskite/spiro/Ag	1.091	22.06	0.71	15.74 (Ether);	17.08	[89]
	Chloroform/n-hexane		1.077	22.62	0.65	15.89 (n-hexane); 13.1(Chloroform)	16.77	
MAPbI$_{3-x}$Cl$_x$	CB/EtOH	FTO/c-TiO$_2$/perovskite/spiro/Au	0.91	24.3	0.62	-	14	[87]
MAPbI$_3$	ACN/CB	FTO/SnO$_2$/perovskite/spiro/Ag	1.13	22.3	0.75	16.2 (CB)	18.9	[108]
MAPbI$_3$	EA/CB (additive: PC$_{61}$BM)	FTO/TiO$_2$/perovskite/spiro/Ag	1.01	23	0.692	14.1 (CB)	16.1	[109]
(FAPbI$_3$)$_{0.85}$ (MAPbBr$_3$)$_{0.15}$	ACN/CB	FTO/c-TiO$_2$/mp-TiO$_2$/perovskite/spiro/Au	1.08	23.6	0.789	17.5 (CB)	20.1	[12]
Cs$_{0.05}$(FA$_{0.85}$MA$_{0.15}$)$_{0.95}$Pb(I$_{0.85}$Br$_{0.15}$)$_3$	EA/n-hexane	ITO/SnO$_2$/perovskite/spiro/Au	1.15	23.42	0.74	16.76 (EA)	20.06	[110]
MAPbI$_3$	SBA/CB	ITO/PEDOT: PSS/perovskite/PCBM/Bphen/Ag	0.976	21.25	0.793	15.06 (SBA); 14.69 (CB);	16.47	[88]
	SBA/ether		0.958	21.46	0.789	14.81 (ether)	16.24	

MAPbI$_3$	Tol/ Dichlorobenzene	FTO/c-TiO$_2$/mp-TiO$_2$/perovskite/spiro/Ag	1.05	23.07	0.737	16.39 (Tol)	18.01	[39]
	Tol/CB		1.04	22.46	0.728		17.06	
	Tol /Chloroform		1.06	21.4	0.657		15.1	
	Tol/ether		1.06	22.93	0.711		17.36	
MAPbI$_3$	EA /petroleum ether	FTO/c-TiO$_2$/perovskite/spiro/Ag	1.095	21.56	0.688	14.29 (EA); 8.11 (petroleum ether)	17.19	[79]
Cs$_{0.4}$(MA$_{0.17}$FA$_{0.83}$)$_{0.96}$Pb (I$_{0.83}$Br$_{0.17}$)$_3$	EA /n-hexane	ITO/NiO/perovskite/PCBM/ZnO/Ag	1.06	22.92	0.70	-	17.3	[111]
Ternary antisolvents								
MAPbI$_3$	SBA/CB/ether	ITO/PEDOT: PSS/perovskite/PCBM/Bphen/Ag	0.957	21.97	0.78	15.06 (SBA); 14.69 (CB); 14.81 (ether)	16.5	[88]

FTO: fluorine doped tin oxide, ITO: indium doped tin oxide, c-TiO$_2$: compact TiO$_2$, mp-TiO$_2$: mesoporous TiO$_2$, spiro: spiro-MeOTAD, BCP: bathocuproine, PCBM: [6,6]-phenyl-C$_{61}$-butyric acid methyl ester, BCP: 2,9-Dimethyl-4,7-diphenyl-1,10-phenanthroline, PTAA: poly[bis(4-phenyl)(2,4,6-trimethylphenyl) amine], CuPc: copper (II) phthalocyanine, Bphen: 7-diphenyl-1,10-phenanthroline, PIF8-TAA: Poly-indenofluoren-8-triarylamine, PDBD-T: poly[(2,6-(4,8-bis(5-(2-ethylhexyl)thiophen-2-yl)-benzo[1,2-b:4,5-b']dithiophene))-alt-(5,5-(1',3'-di-2-thienyl-5',7'-bis(2-ethylhexyl)benzo[1',2'-c:4',5'-c']dithiophene-4,8-dione))], PEDOT:PSS: poly(3,4-ethylenedioxythiophene)-poly(styrenesulfonate).

2.7. Antisolvent treatment window

2.7.1. Different antisolvents act on the same perovskite

The window of antisolvent here refers to the dripping time of antisolvent. Taking MAPbI$_3$ perovskite as an example, Xiao *et al.* found that the window for preparing MAPbI$_3$ perovskite by CB is less than 4 s [27]. Fig. 6(a) shows the SEM images of perovskite obtained by dripping CB at 2, 4 and 8 s respectively. Although the time interval is not long, the morphology of the films changes greatly. While, the window of preparing MAPbI$_3$ Perovskite with n-hexane and ether is 4–8 s and less than 5 s, respectively [112,113]. Therefore, for MAPbI$_3$, the window is different when using various antisolvent (CB, n-hexane and ether). This phenomenon also exists in FAMACs perovskite films. Zhao *et al.* [52] have studied the window of preparation of FAMACs perovskite with different antisolvent. Fig. 6(b) shows the variation of normalized PCE of FAMACs PSCs prepared by dripping CB and anisole at different times. It can be seen that anisole has a wider antisolvent window (about 20 s), while the window of CB is about 15 s. At the same time, the window for preparing FAMACs PCE by Tol and ether is about 5 s and 10 s, respectively, which can be seen from Fig. 5(a and c). Overall, for the same perovskite, the antisolvent window is different when adding different antisolvent.
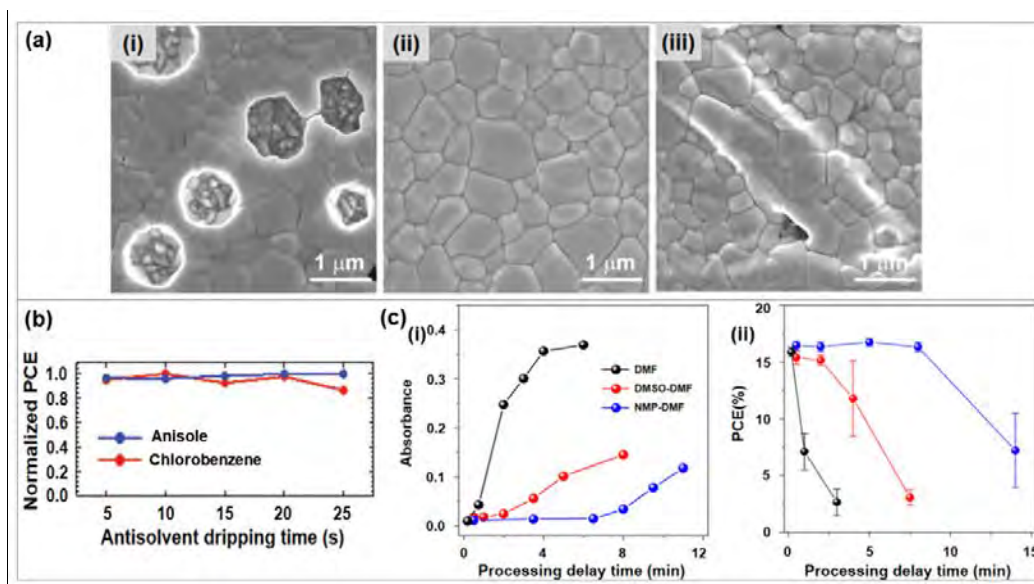
Fig. 6. (a) The SEM images of MAPbI$_3$ films prepared by dripping CB at (i) 2 s; (ii) 4 s; (iii) 8 s after the start of spin coating [27]. Copyright 2014, Wiley-VCH. (b) Antisolvent window for preparation of FAMACs perovskite from anisole and chlorobenzene (CB) [52]. Copyright 2018, Wiley-VCH. (c) When DMF, DMSO-DMF and NMP-DMF are used as solvents, the absorbance (i) of MAPbI$_3$ perovskite films varies with different delay time and the effect of different processing time on PCE (ii). Here, the "processing delay time" refers to the time from the completion of the blade coating of the precursor to the immersion in the antisolvent bathing [114]. Copyright 2017, Springer Nature.

2.7.2. The same antisolvent acts on different perovskites

For CB antisolvent, the window of MAPbI$_3$ perovskite film is narrow (about 4 s) [27], while that of FAMACs perovskite is about 15 s [52]. Similarly, the window of preparing MAPbBr$_3$ by Tol is about 20 s [32], while that of FAMACs is only 10 s [52]. Therefore, for different perovskites, although the antisolvent used is the same, the

antisolvent window is also distinct.

2.7.3. Strategies of broadening the dripping window of antisolvent

The wide antisolvent dripping window can increase for the repeatability of perovskite thin films fabrication. Therefore, broadening the window of antisolvent is of importance.

2.7.3.1. Choice of solvent

Firstly, in the preparation of perovskite, the choice of solvent determines the drying window of perovskite film, which has an important influence on the antisolvent window. The drying window of the film determines the window of antisolvent, because antisolvent must be dripped in the wet perovskite film and the evaporation rate of solvent affects the drying window of perovskite film [114]. DMF has a high vapor pressure, so that its rapid evaporation in the spin coating leads to a short drying window for perovskite thin films. However, other solvents, such as DMSO and NMP, have lower vapor pressure and are difficult to evaporate, thus greatly prolonging the drying window. Next, choice of solvent affects the amount of the solvent-precursor complexes, which can also control the antisolvent window. For example, the interaction between DMF and the perovskite precursor is too weak to form a stable DMF-precursor complexes [115], while other solvents like DMSO or NMP can [8] (see Section 3 for details). Therefore, considering the above two aspects, DMF is usually not used alone, but mixed with other solvents (such as DMSO, NMP) in order to widen the antisolvent window [116]. Fig. 6(c) shows the effects of DMF, DMF-DMSO and DMF-NMP on the antisolvent window of MAPbI$_3$ PSCs. When DMF is used as a solvent, the antisolvent

window is less than 1 min (panel i of Fig. 6c) because of its faster evaporation rate and unstable intermediates. When using DMSO or NMP mixed with DMF, the antisolvent window is widened to 2 min and 8 min (panel ii of Fig. 6c), respectively, because both DMSO and NMP have a smaller evaporation rate, and the intermediates they produce with the perovskite precursor are more stable. Wakamiya and coworkers used DMSO instead of DMF/DMSO mixed solvent to further expand the drying window of MAPbI$_3$ perovskite precursor wet film [117]. Then MAPbI$_3$·DMF was dissolved in DMSO. In this case, the solubility is increased (compared to the equivalent amounts of MAI and PbI$_2$ starting materials). The low volatility solvent (pure DMSO) greatly extends the drying window of the film, thereby broadening the window of antisolvent (Tol) for preparing MAPbI$_3$ PSCs from 5 s to 13 s, which can be seen in Fig. 7(a).
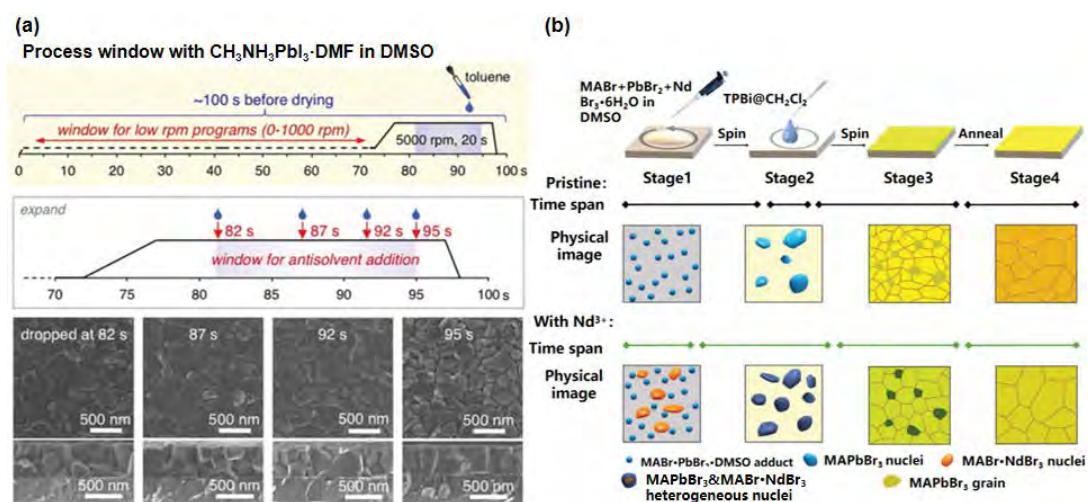
Fig. 7. (a) Schematic diagrams of the antisolvent window for dissolving MAPbI$_3$·DMF complex in a low-volatility solvent (DMSO) and SEM images of MAPbI$_3$ thin films prepared by dropping antisolvent in this window range [117]. Copyright 2019, Wiley-VCH. (b) Schematic diagrams of the process of preparing MAPbBr$_3$ perovskite film

with the introduction of Nd^{3+} additives in the antisolvent method, as well as a schematic diagram of the nucleation process and crystal growth [118]. Copyright 2020, Wiley-VCH.

2.7.3.2. Introduction of cations/halogens

The cations and halides in perovskite can also adjust the window of antisolvent. It is found that for single cation or single halide perovskite (such as $MAPbI_3$ and $FAPbBr_3$), their dripping window is about a few seconds [27,112,113], while mixed halide or mixed cation perovskites have a wider dripping window (about a few minutes) [129]. As we all know, perovskite will undergo sol-gel state in the process of precursor liquid to solid film. The duration of this sol-gel state determines the dripping window of the antisolvent. The introduction of cations/halogens into the single-cation/single-halogen perovskite increases the sol-gel time experienced during the formation of the perovskite film, which helps to widen the solvent dripping window [119].

The window of antisolvent can also be widened by introducing additives, ascribed to the promotion the heterogeneous nucleation of perovskite. It can separate crystal growth from the nucleation process, and helps to form crystals with higher phase purity and fewer defects. In the process of preparing $MAPbBr_3$ film with dichloromethane, Dong *et al.* [118] introduced Nd^{3+} additives to promote the heterogeneous nucleation of perovskite, which can be seen in Fig. 7(b). This work successfully widened the window from 3–5 s to 18 s by introducing Nd^{3+} in precursor.

2.8. Strategy of further improve morphology by adjusting the temperature of antisolvent

Sometimes the antisolvent method seems to be ineffective, *i.e.*, there are still pin holes or the film is in-continuous even though optimizing the spin time and quantity. This may not suggest the antisolvent's invalidity. Alternatively, the adjustment of the antisolvent temperature may change "invalid" to "validation" again. According to the classical nucleation theory, the nucleation rate of perovskite can be expressed by Eq. (1) [120,121]:

$$\frac{dN}{dt} = A\exp\left(-\frac{\Delta G_{crit}}{k_B T}\right), \tag{1}$$

$$\Delta G_{crit} = \frac{16\pi\gamma^3 V_M^2}{3(k_B T \ln S)^2}, \tag{2}$$

where N, A, k_B, and T are the number of nuclei, the pre-exponential factor, the Boltzmann constant, and temperature, respectively. ΔG_{crit} is the critical Gibbs free energy of nucleation, which is the energy barrier of nucleation, expressed by Eq. (2). γ is a function of the surface energy, V_M is molar volume of solute particles, and S represents supersaturation of the solution [121]. According to the Eq. (1), the nucleation rate of perovskite is inversely proportional to ΔG_{crit}, while ΔG_{crit} is related to supersaturation and temperature. With other conditions unchanged, ΔG_{crit} decreases with the increase of perovskite's temperature. The solubility of perovskite decreases with the increase of temperature, that is, the supersaturation increases with the increase of temperature [122]. When the perovskite is immersed in a hot antisolvent (compared to room temperature), the temperature and supersaturation of the perovskite increase. According to Eqs. (1) and (2), it can be found that the hot antisolvent bathing can

promote the nucleation of the perovskite. For example, Liu *et al.* prepared

$FA_{0.75}MA_{0.25}SnI_3$ perovskite thin film by hot CB antisolvent bathing (65 °C) [95]. Fig.

8(a and b) shows the growth diagrams of perovskite crystals immersed in an antisolvent

bathing at room temperature and 65 °C, respectively. The perovskite film prepared at

room temperature is not completely covered due to the lower nucleation density, and

there are pinholes on the surface (Fig. 8c), While a hot antisolvent bathing increased

the nucleation density of the perovskite and promoting full coverage of the perovskite

film (Fig. 8d). When the perovskite is immersed in a cold antisolvent (compared to

room temperature), the supersaturation of the perovskite also decreases due to the

decrease in temperature, which inhibits the nucleation of the perovskite. Jang *et al.*

immersed the $MAPbI_3$ perovskite precursor film in 0 °C antisolvent bathing to reduce

the temperature of the perovskite. By reducing the temperature of perovskite, the

nucleation of perovskite was inhibited and it promoted a preferential crystal orientation,

which can be seen from the X-ray diffraction spectra (Fig. 8e) [46]. In short, when using

an antisolvent bathing, you can adjust the nucleation rate of the perovskite or optimize

the crystal orientation of the perovskite by changing the temperature of the antisolvent.

In another case, when the antisolvent is added into the perovskite by dripping

instead of soaking, the effect of the antisolvent temperature adjustment on the

nucleation of the perovskite may be different from that of the soaking. For example,

Ren *et al.* prepared $(FAPbI_3)_{0.85}(MAPbBr_3)_{0.15}$ perovskite by dripping antisolvent (ether)

with different temperatures. It found that with the decrease of temperature, the

nucleation density of perovskite increased, which lead to uniform and compact film

[123].
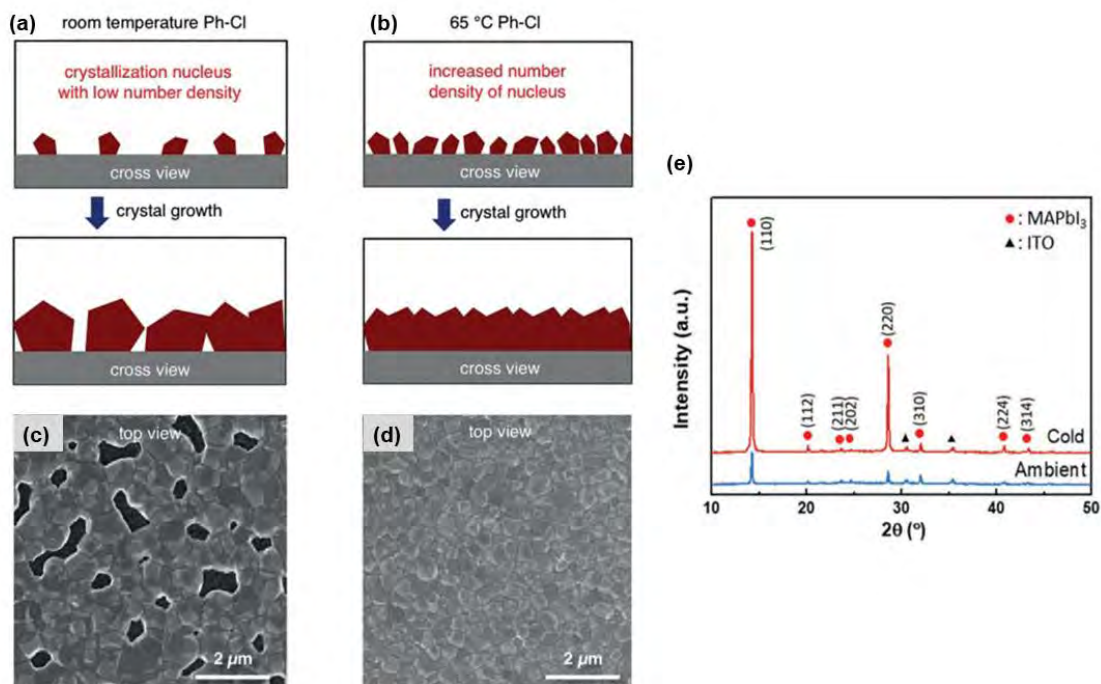
Fig. 8. Growth diagrams of $FA_{0.75}MA_{0.25}SnI_3$ thin films prepared by (a) room temperature antisolvent and (b) thermal antisolvent (Ph-Cl) [95]. Here, Ph-Cl is chlorobenzene (CB); (c, d) the corresponding SEM images of perovskite films [95]; Copyright 2018, Wiley-VCH. (e) XRD spectra of $MAPbI_3$ films prepared by 0 °C antisolvent bathing and ambient temperature antisolvent bathing [46]. Copyright 2019, Wiley-VCH.

2.9. The role of additives in antisolvent process

In order to improve the performance of PSCs, the antisolvent method is usually combined with additives. There are usually two ways to add additives, one is to add additives in the precursor of perovskite and the other is to add additives in the antisolvent. Table 4 shows the recent advances of additives added in different ways on

PSCs.

Table 4. Additives added to perovskite precursor or antisolvent.

Additive	Antisolvent	Perovskite	PCE without additive (%)	PCE with additive (%)	Function	Ref.
Added to perovskite precursor						
MACl	EA	$MAPbI_3$	13.97	17.22	Inhibition of too fast crystallization rate of antisolvent method	[124]
Meth-ylammonium formate (MAF)	CB	$MAPbI_3$	19.1	19.5	Controlling the distribution of grain size	[125]
CH_3NH_2 (MA)/EtOH	Ether	$MAPbI_3$	18.09	20.02	Passivate film defects	[126]
IT-4F	CB	$MAPbI_3$	16.78%	18.3%	Defect passivation	[127]
$PC_{70}BM$	CB	$MAPbI_3$	13.08	15.5	Minimizing grain boundaries (GBs) and reducing recombination	[67]
$NdBr_3 \cdot 6H_2O$	Dichloromethane	$MAPbBr_3$	-	-	Ultrawide processing window	[118]
Lanthanide ions ($Ln^{3+}= Sm^{3+}$, Tb^{3+}, Ho^{3+}, Er^{3+}, and Yb^{3+})	IPA	$CsPbBr_3$	6.99	10.14 (Sm^{3+})	Inhibition of charge recombination in thin films	[128]
HI	IPA	$CsPbI_3$	-	4.13	Phase stability	[129]
Sulfobetaine Zwitterions	Tol	$CsPbI_3$	-	11.4	Phase stability	[54]
FACl+ADAHCl (1-adamantylamine hydrochloride)	CB	FAMACs	19.43	21.2	Inhibition of too fast crystallization rate of antisolvent method	[130]
Sn metal	EA	$MA_{0.3}FA_{0.7}Pb_{0.5}Sn_{0.5}I_3$	-	21.1	Inhibition of Sn^{2+} oxidation	[74]
Ascorbic acid	Tol	$MA_{0.5}FA_{0.5}Pb_{0.5}Sn_{0.5}I_3$	-	14.01	Inhibition of Sn^{2+} oxidation	[56]
SnF_2			-	12.18		
NH_4SCN	Tol	$PEA_{0.15}FA_{0.85}SnI_3$	-	12.4	Defect passivation	[131]
SnF_2	Ether	$FASnI_3$	0.66	6.22	Inhibition of Sn^{2+} oxidation	[132]
N_2H_5Br	Tol	$FASnI_3$	5.6	7.81	Inhibition of Sn^{2+} oxidation	[133]
HCl	IPA	$Cs_3Sb_2I_9$	0.43	1.21	Stabilize layered phases of $Cs_3Sb_2I_9$	[83]
Added to antisolvent						
hexaazatrinaphthylene (HATNA)	Ether	$MAPbI_3$	7.2	8.66	Passivation electron trap	[134]
Bisthiadiazole-fused tetraazapentacenequinone (DCL97)	CB			8.4		
DMSO	CB	$MAPbI_3$	13.79	16.76	Controlling the crystallization of perovskite	[135]
I_2	CB	$MAPbI_3$	18.22	21.33	Inhibition of perovskite decomposition	[65]
p-type polymer with	CB	$MAPbI_3$	17.7	18.7	Surface	[136]

molecular fluorination (PF-1)					passivation and morphology modification	
C_{60}	Tol	$MAPbI_3$	17.5	19.8	Passivation film defects and prevent PbI_2 migration	[137]
HI	CB	$MAPbI_3$	15.65	17.32	Inhibition of perovskite decomposition	[66]
MAI	SBA	$MAPbI_3$	15.20	19.29	Passivation of excess PbI_2	[138]
Poly(α-methylstyrene)	Ether	$FASnI_3$	1.35	2.28	Suppression of nonradiative recombination carrier traps	[139]
$SnCl_2$	Ether	$FA_{0.5}MA_{0.5}Pb_{0.5}Sn_{0.5}I_3$	15.75	19.03	Passivation of grain boundaries	[62]
α-bis-PCBM	CB	$(FAPbI_3)_{0.85}(MAPbBr_3)_{0.15}$	18.8	20.8	Reducing defect density and improving stability	[140]
MABr	EtOH	$Cs_{0.15}FA_{0.85}PbI_3$	17.6	21.53	Passivation electron trap	[141]
Acetic Acid	CB	$Cs_{0.05}FA_{0.80}MA_{0.15}Pb(I_{0.85}Br_{0.15})_3$	19.1	22	Passivation of film defects and improvement of stability	[142]
MABr	IPA	FAMACs	13.37	15.38	Reducing trap density	[143]
Phthalocyanine nickel	CB	$Cs_{0.05}(MA_{0.17}FA_{0.83})_{0.95}Pb(I_{0.83}Br_{0.17})_3$	17.24	19.18	Improving interface contact between perovskite and HTL	[144]
PBDB-T	CB	$(CsPbI_3)_{0.04}(FAPbI_3)_{0.82}(MAPbBr_3)_{0.14}$	17.28	19.85	Passivation of defects and improvement of stability	[145]
Triphenylamine (TPA)	CB	FAMACs	17.78	19.84	Increase the stability and accelerate the crystallization of perovskite	[146]

2.9.1. Additives added to perovskite precursor

The additives added to the perovskite precursor must be soluble in DMF and other perovskite dissolving solvents. If they are insoluble in precursor solvent, the additives should be considered to be added into the antisolvent (where it should also be soluble) [134]. When additives are added to perovskite precursor, the aim is to stabilize the crystal structure [54,129], improve the uniformity of the film, and solve the problem of too fast crystallization of perovskite prepared by antisolvent method [124,130]. As we

all know, $CsPbI_3$ perovskite has the problem of phase instability, which will rapidly change into non-optically-active δ-phase in ambient air. In order to enhance the phase stability of $CsPbI_3$, additives, such as HI [129] and sulfobetaine zwitterion [54], are usually added to the perovskite precursor to achieve the goal. Chlorine ion additives are also used in antisolvent, which will be described in Section 4. Seo *et al.* used ionic liquid (methyl formate) as an additive in $MAPbI_3$ perovskite precursor, and the results show that the additive can delay the crystal growth and help to form dense perovskite films with larger grain size. The final PCE reaches 19.5% [125].

There is an inherent problem in tin-based perovskite, that is, Sn^{2+} is easy to be oxidized to Sn^{4+}, which will increase the defect density in the film and decrease the device performance. Additives (such as Sn metal [74] and SnF_2 [56]) are usually introduced into perovskite precursor to inhibit the oxidation. For example, Liao *et al.* added SnF_2 to the perovskite precursor to inhibit the oxidation of Sn^{2+} when preparing $FASnI_3$ perovskite thin films with ether as the antisolvent. Not only the stability of the devices is improved, but also the efficiency of $FASnI_3$ PSCs is increased to 6.22% [132]. Xu *et al.* compared the effect of SnF_2 and ascorbic acid on inhibiting Sn^{2+} oxidation. They found that ascorbic acid can much effectively inhibit the oxidation of Sn^{2+} and regulate the crystallization of perovskite. The PCE (14.01%) of $MA_{0.5}FA_{0.5}Pb_{0.5}Sn_{0.5}I_3$ PSC is higher than that of PSC prepared by SnF_2 (12.08%) [56]. Lin *et al.* inhibited the oxidation of Sn^{2+} by adding Sn powder into $MA_{0.3}FA_{0.7}Pb_{0.5}Sn_{0.5}I_3$ precursor, and the residual tin powder was removed by filtration. This method greatly reduces Sn vacancy and improves PCE greatly. The PCE of single junction PSC was up to 21.1% [74].

2.9.2. Additives added to antisolvent

When additives, such as I_2 [65], TPA [146] and conjugated polymer [136], are added to the antisolvent, they are generally used to control the nucleation and crystal growth of perovskite, improve the crystallinity and stability of perovskite, and reduce the defects in the film. For example, hexaazatrinaphthylene (HATNA) and bisthiadiazole-fused tetraazapentacenequinone (DCL97) were added to ether and CB respectively to synthesize $MAPbI_3$ perovskite thin films. It was found that the main role of the additives is to passivate the grain boundaries (GBs) and inhibit non-radiative recombination [134]. Han *et al.* added a small amount of DMSO solvent into CB. It is used to dissolve and recrystallize $MAPbI_3$ perovskite thin films. This method can reduce the GBs and trap states, and improve the crystallinity of the films. PCE was increased from 13.79% to 16.76% [135]. Take another example, Han *et al.* [143] found that during the annealing process, organic cationic components, such as MABr and FAI, could evaporate from the FAMACs perovskite film to form a defect state, especially on the surface of the film. A layer of MABr was spin-coated on the surface of the perovskite to compensate for the loss of organic cations and halogens, so as to reduce defects. Later, researchers discovered that the introduction of iodide ion additives (such as HI and I_2) in the antisolvent can stabilize organic cations and enhance the stability of the perovskite [65,66]. As mentioned above, tin ion additives (such as SnF_2) are added to the perovskite precursor to inhibit the oxidation of Sn^{2+}, while added to antisolvent, its role is to passivate GBs and extend the carrier lifetime [62].

3. Lewis acid-base adduct approach to fabricate perovskites

3.1. Lewis acid-base reaction

The existence of various defects (such as surface defects and GBs defects) in the structure of PSCs will lead to a large number of carrier non-radiative recombination, as well as hysteresis, which limit the PCE of PSCs. The uncontrollable crystallization in the preparation process also limits the improvement of PCE due to the unfavourable morphology of perovskite thin films and the generation of defects [147,148]. Lewis acid-base addition method can effectively control crystallization and passivate defect, and hence to prepare high-efficiency PSCs. A Lewis acid is a chemical species that contains an empty orbital which is capable of accepting an electron pair from a Lewis base to form a Lewis adduct [149,150]. A Lewis base, then, is any species that has a filled orbital containing an electron pair which is not involved in bonding but may form a dative bond with a Lewis acid to form a Lewis adduct. It is represented as follows:

$$\mathbf{A} + \mathbf{:B} \rightarrow \mathbf{A \cdot B}$$
$$\text{acid} \quad \text{base} \quad \text{adduct}$$

The coordination ability of Lewis base with Lewis acid can be measured by Lewis basicity, which is quantified by the value of Gutmann's donor number (D_N) [151]. If the Lewis base has high D_N, it indicates strong coordination ability with Lewis acid. Therefore, the higher the Lewis basicity is, the more stable Lewis base-acid adduct is formed [151–153]. On the contrary, the Lewis base with low D_N has weak coordination ability with Lewis acid, leading to unstable adduct. Lewis bases can be classified into O-donor, N-donor and S-donor according to their functional groups. Fig. 9 shows the

structures of commonly used Lewis bases. The formation of Lewis acid-base adducts can regulate the crystallization rate of perovskite and passivate defects, which will be described in detail in Section 3.3.
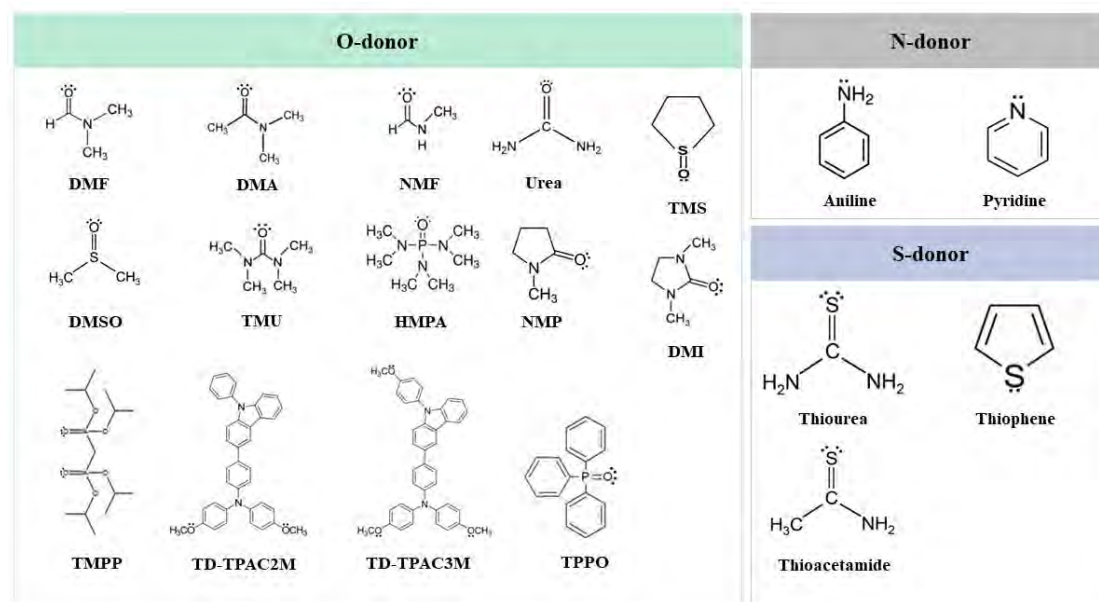
Fig. 9. Chemical structures of different Lewis bases commonly used in literature. **Note**: DMA: Dimethylacetamide; DMI: 1,3-dimethyl-2-imidazolidinone; TMU: Tetramethylurea; NMF: N-methylformamide; HMP: Hexamethylphosphoramide; HMPA: Hexamethylphosphoramide; TPPO: Triphenylphosphine oxide; TMPP: Tetraisopropyl methylenediphosphonate; TMS: Tetramethylene sulfoxide; TD-TPAC3M: Triarylamine derivatives-TPAC2M).

3.2. Different Lewis acid/base

3.2.1. Precursors and solvent acting as Lewis acid/base

In perovskite, metal cations (such as Pb^{2+}, Sn^{2+}, Bi^{3+}, Sb^{3+}) of perovskite have the properties of Lewis acid because they have empty orbitals and can accept electron pairs. The metal halides corresponding to these metal cations, such as PbX_2 (X = I, Br, Cl), SnI_2 and BiI_3 etc., also belong to Lewis acid. In the process of preparing perovskite thin

films by solution method, solvents (such as DMF, DMSO, NMP and thiourea) are the most common Lewis bases because their structures contain lone pair electrons. For example, DMF and DMSO have C=O and S=O bond respectively to provide electrons, so it has the characteristics of Lewis base.

DMF has weak coordination with PbI_2 due to its low basicity. It forms one-dimensional $PbI_2 \cdot DMF$ structure [154] with PbI_2 and this adduct ($PbI_2 \cdot DMF$) is metastable [115]. When pure DMF is used as solvent, due to the instability of the adduct, the crystallization of perovskite cannot be slowed down, resulting in the formation of perovskite thin films with pinholes (Fig. 10a). While DMSO has strong coordination ability with PbI_2 to form a stable $PbI_2 \cdot DMSO$ complex because of its high basicity. When MAI solution was added, the intermolecular exchange occurred between MAI and $PbI_2 \cdot DMSO$ complex, and part of Lewis base solvent was replaced by MAI to form $MAI \cdot PbI_2 \cdot DMSO$ intermediate [159]. Then $MAPbI_3$ films were formed after annealing [8,155]. The quality of the perovskite film is related to the amount of adduct because too many or too few adduct will result in uneven film or pinholes [155,156]. Therefore, the mixed solvent (diluting solvents with high Lewis basicity, such as DMSO, by DMF) is usually used to get the appropriate amount of intermediate to form uniform and dense perovskite films. Fig. 10(a) shows homogeneous and dense perovskite films prepared by mixed solvents (DMF/DMSO). Table 5 lists photovoltaic performance of PSCs prepared using precursors and solvent acting as Lewis acid/base.

Table 5. Photovoltaic performance of PSCs prepared using precursors and solvent acting as Lewis acid/base.

Perovskite	Solvent	Device structure	V_{oc} (V)	J_{sc} (mA/cm^2)	FF	PCE (%)	Ref.
MAPbI$_3$	DMF+DMSO	FTO/c-TiO$_2$/mp-TiO$_2$/perovskite/spiro/Ag	1.08	23.83	0.76	19.7	[24]
MAPbI$_3$	DMF	FTO/c-TiO$_2$/mp-TiO$_2$/perovskite/spiro/Au	0.96	19.1	0.72	13.3	[152]
	DMF+10%NMP		1.02	22.6	0.76	17.5	
MAPbI$_3$	DMF+DMA	FTO/c-TiO$_2$/mp-TiO$_2$/perovskite/spiro/Au	1.02	16.05	0.7	16.05	[157]
FAPbI$_3$	DMF+DMSO+thiourea	FTO/c-TiO$_2$/mp-TiO$_2$/perovskite/spiro/Au	0.95	21.9	0.66	13.6	[155]
FAPbI$_3$	DMF+NMP	ITO/SnO$_2$/perovskite/spiro/Ag	1.09	23.98	0.77	20.19	[26]
MAPbI$_3$	DMF+TMS	FTO/c-TiO$_2$/mp-TiO$_2$/perovskite/spiro/Au	1.02	21.5	0.74	16.2	[158]
MA$_{0.05}$Cs$_{0.12}$FA$_{0.83}$Pb(I$_{0.6}$Br$_{0.4}$)$_3$	DMF+DMSO DMF+NMP	ITO/SnO$_2$/perovskite/spiro/Au	1.04 1.10	16.17 20.52	0.55 0.61	9.29 13.89	[159]
(FAPbI$_3$)$_{0.875}$ (CsPbBr$_3$)$_{0.125}$	DMF+HMPA DMF+DMSO DMF	FTO/SnO$_2$/perovskite/spiro/Au	1.12 1.11 1.02	22.90 20.97 21.49	0.76 0.74 0.63	19.58 17.37 13.84	[160]
FA$_{0.85}$MA$_{0.15}$Pb(I$_{0.85}$Br$_{0.15}$)$_3$	DMF+DMSO	FTO/c-TiO$_2$/mp-TiO$_2$/perovskite/PTAA-LAD/Au	1.12	23.06	0.79	20.32	[161]
Cs$_3$Bi$_2$I$_9$	DMF+thiourea DMF	FTO/c-TiO$_2$/mp-TiO$_2$/perovskite/sprio/Au	0.62 0.64	4.61 2.41	0.59 0.58	1.69 0.88	[162]
Dimer-Cs$_3$Sb$_2$I$_9$	DMF+DMSO+thiourea	ITO/PEDOT:PSS/perovskite/PCBM/Al	0.83	3.62	0.54	1.59	[163]

3.2.2. Lewis acid/base additives except for the precursors and solvent

Lewis acid/base can be introduced into PSCs as additives in addition to precursor and Lewis basic solvent. The molecules containing Lewis acid/basic functional groups can play the role of Lewis acid/base and form complexes with defects like uncoordinated Pb^{2+}/X$^-$ in perovskite films, thus passivating defects [164]. Lewis acid additives are usually used to passivate negative ion defects such as uncoordinated halogen anions and Pb-I antistites, while Lewis base additives can passivate defects by coordination with uncoordinated Pb^{2+}/interstitial Pb^{2+} due to their non-volatile properties. Lewis acid/base additives can be added into the precursor or antisolvent to participate in the crystallization process of the perovskite by forming adduct with solvent or precursors. On the other hand, Lewis acid/base additives can also treat the surface of perovskite film, become an intermediate layer between the perovskite layer/HTL or the perovskite layer/ETL interfaces. In this case, they will not participate

in the crystallization process of the perovskite, but interact with defects so as to improve the photovoltaic properties of PSCs. Table 6 shows photovoltaic performance of PSCs prepared using Lewis acid/base additives.

Table 6. Photovoltaic performance of PSCs prepared using Lewis acid/base additives except for the precursors and solvent.

Perovskite	Solvent	Lewis acid/base additives	Device structure	V_{oc} (V)	J_{sc} (mA/ cm^2)	FF	PCE (%)	Ref.
MAPbI$_3$	DMF	Iodopentafluorobenzene -IPFB (Perovskite film is immersed in IPFB)	FTO/c-TiO$_2$/mp-Al$_2$O$_3$/perovskite/sprio/Ag	1.06	23.38	0.67	15.7	[165]
MAPbI$_3$	DMF	Pyridine (spin coated on the surface of perovskite)	FTO/c-TiO$_2$/ perovskite/sprio/Ag	1.05	24.1	0.72	16.5	[166]
		Thiophene (spin coated on the surface of perovskite)		1.02	21.3	0.68	15.3	
MAPbI$_3$	DMF	a conjugated Lewis base-IDIC	ITO/PTAA/perovskite/ IDIC/C$_{60}$/BCP/Cu	1.11	22.96	-	19.5	[167]
MAPbI$_3$	DMF+ DMSO	Urea (added into precursor)	ITO/SnO$_2$/perovskite/sp iro/Ag	1.09	21.68	0.78	18.55	[168]
(CsPbI$_3$)$_{0.04}$(FA PbI$_3$)$_{0.82}$(MAPb Br$_3$)$_{0.14}$	DMF+ DMSO	p-type-conjugated polymer (PBDB-T)	ITO/SnO$_2$/perovskite/sp iro/Au	1.11	22.39	0.78	19.38	[145]
Cs$_{0.05}$FA$_{0.8}$MA$_{0.}$ $_{15}$Pb(I$_{0.83}$Br$_{0.17}$)$_3$	DMF+ DMSO	triphenylphosphine oxide-TPPO (dripped on the surface of the perovskite film)	ITO/SnO$_2$/perovskite/sp iro/Au	1.14	23.37	0.72	19.10	[169]
	DMF+ DMSO	tetraisopropyl Methylenediphosphonat e-TMPP (dripped on the surface of the perovskite film)		1.13	23.58	0.72	19.13	
	DMF+ DMSO	tris(pentafluorophenyl)p hosphine-TPFP) (dripped on the surface of the perovskite film)		1.16	23.97	0.76	21.04	

3.2.3. Introduction of Lewis acid/base by solvent annealing

The perovskite films can be treated with the vapor of Lewis basic solvent. Sun *et al.* [170] treated PbI$_2$ wet film using tBP steam. After annealing to remove the PbI$_2$-tBP adduct, a porous PbI$_2$ film is obtained, which accelerated the reaction between PbI$_2$ and MAI, avoiding the problem of incomplete precursor reaction. By this way, a smooth, uniform and dense perovskite film was obtained.

3.3. The role of Lewis acid/base

3.3.1. Controlling the crystallization rate of perovskite

One of the most extensive functions of the Lewis acid-base reaction is to control the crystallization rate of the perovskite. The adduct can not only regulate the crystallization of perovskite crystal, but also increase the nucleation rate of perovskite during annealing, which is conducive to the formation of dense films [155]. For MAPbI$_3$, mixed solvents of DMF and DMSO have been widely used to adjust the amount of MAI-PbI$_2$-DMSO adducts, which can help to form high-quality perovskite films. In addition to DMSO, other solvents (such as NMP [152], DMA [157] and TMS [158]) can also be mixed with DMF to adjust the crystallization rate of MAPbI$_3$ perovskite.

When FAPbI$_3$ perovskite is prepared by Lewis acid-base reaction, solvent (such as thiourea, NMP and HMPA) rather than DMSO should be mixed with DMF [26,155,160]. This is mainly due to the unstable DMSO·PbI$_2$·FAI adduct formed by Lewis acid-base reaction, resulting in poor uniformity and poor repeatability of FAPbI$_3$ thin films. Fig. 10(b) shows the FTIR spectra of solvent-PbI$_2$ and solvent-PbI$_2$-FAI adducts prepared by DMSO and thiourea, respectively. After adding FAI, the peak position (indicated by arrows) of DMSO-PbI$_2$-FAI does not move compared with that of DMSO-PbI$_2$ complex, indicating the weak interaction between FAI and DMSO-PbI$_2$. While the peak position of thiourea-PbI$_2$-FAI has a significant shift compared with the thiourea-PbI$_2$ complex, it indicates that there is a clear interaction between FAI and thiourea-PbI$_2$ [155]. FA$^+$ is a softer Lewis acid compared with MA$^+$, while solvents

such as thiourea, NMP and HMPA is a softer base compared with DMSO. According to the principle that soft acid preferentially interacts with soft base, FA^+ preferentially interacts with these solvents instead of DMSO [26].

For lead-free perovskites (such as $MASnI_3$ [171], $Cs_3Bi_2I_9$ [97,99,162] and $Cs_3Sb_2I_9$ [163]), the reaction between their precursors is much faster than that of lead-based perovskites, which results in uncontrollable film morphology. The Lewis acid-base reaction between the Lewis base and the precursor can be used to slow down the crystallization rate. For example, DMSO (Lewis base) interacts with SnI_2 (Lewis acid) to form SnI_2-3DMSO adduct (Fig. 10c) [172], which adjusts the crystallization rate of $MASnI_3$ perovskite and is conducive to the preparation of highly uniform pinhole free perovskite films [173]. Take another example, Lewis base solvents (such as DMSO, NMP and thiourea) can interact with BiI_3 [97,99,162] or SbI_3 [163] to slow down the crystallization and promote preferred orientation growth of the $Cs_3Bi_2I_9$ and $Cs_3Sb_2I_9$ perovskite. In view of the fact that most of the solvents used in the preparation of other lead free perovskites (such as $Cs_2AgBiBr_6$ and Cs_2SnI_6) are hydrobromic acid [174] or IPA [175,176], which do not have the characteristics of Lewis base, Lewis acid-base reaction has not been widely used in these lead-free perovskites.
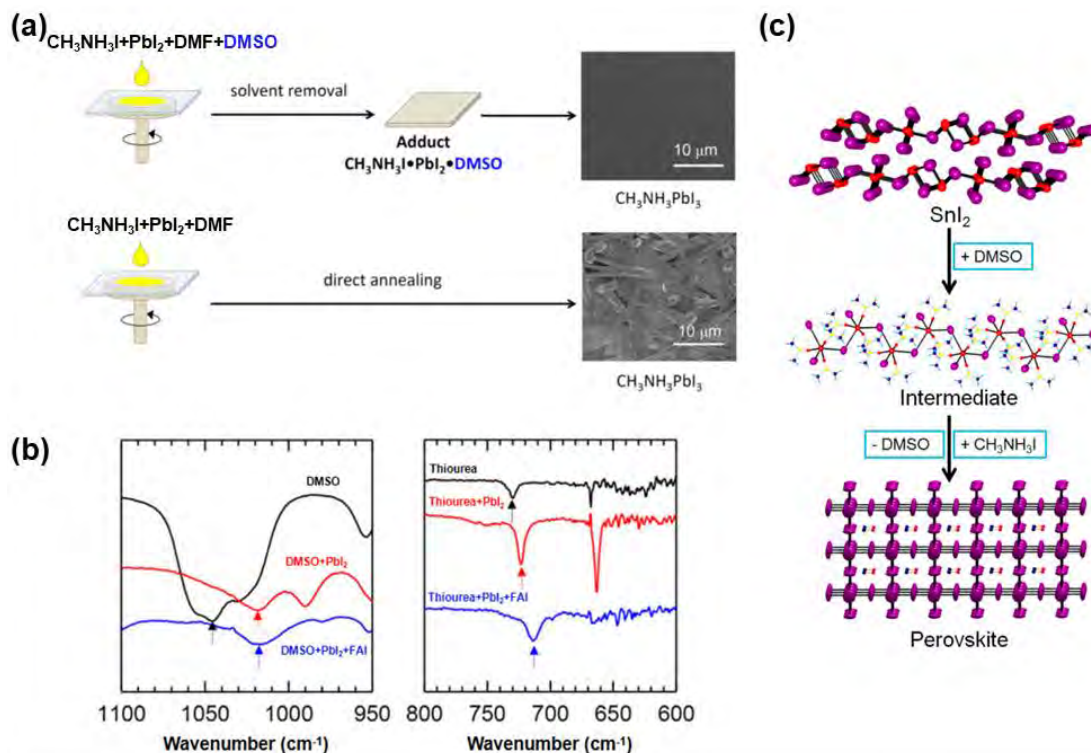
Fig. 10. (a) Schemes of preparing MAPbI$_3$ perovskite with and without DMSO, and the corresponding SEM images [155]. (b) FTIR spectra of the precursor-solvent adduct formed by Lewis acid-base reaction for preparing FAPbI$_3$ [155]. Copyright 2016, American Chemical Society. (c) Schematic diagrams of the formation of MASnI$_3$ perovskite (via SnI$_2$-3DMSO intermediate phase) [173]. Copyright 2015, American Chemical Society.

3.3.2. Passivation of defects

Lewis acid/base additives can be added to the preparation process of devices in different ways to coordinate with these defects. Directly, it can be added into the precursor or antisolvent during the process of preparing perovskite. Lee *et al.* added a non-volatile Lewis base additive (urea) into DMF/DMSO mixed solvent to regulate grain growth and passivate GBs. The growth of crystals can be delayed and there is a

preferential crystal orientation (Fig. 11a), which reduces the density of traps in the film and increases the PCE of the PSCs (from 16.8% to 18.55%) [168]. Qin *et al.* [145] introduced P-type π-conjugated polymer [(2,6-(4,8-bis(5-(2-ethylhexyl) thiophen-2-yl)-benzo[1,2-b:4,5-b']dithiophene))-alt-(5,5-(1',3'-di-2-thienyl-5',7'-bis(2-ethylhexyl) benzo[1',2'-c:4',5'-c']dithiophene-4,8-dione))] (PBDB-T) as Lewis base additive by dissolving it in CB and dropped it onto $(CsPbI_3)_{0.04}(FAPbI_3)_{0.82}(MAPbBr_3)_{0.14}$ perovskite during the spin coating. PBDB-T belongs to O-donor Lewis base, and oxygen atoms can form Lewis adduct with Pb^{2+}, which fills the GBs, passivates the traps at the crystal boundary, and improves the electron/hole transport. Therefore, the device performance was improved by Lewis base additive (*i.e.*, PBDB-T), along with the beneficial role of antisolvent.

Lewis acid/base additives can also be used to treat the surface of perovskite and become an intermediate layer between the perovskite layer/HTL or the perovskite layer/ETL. Yang *et al.* [169] used molecules containing phosphorous Lewis acid/base functional groups such as triphenylphosphine oxide (TPPO), tetraisopropylmethyl diphosphonic acid (TMPP) and tris(pentafluorophenyl) phosphine (TPFP) to treat perovskite. TPPO and TMPP belong to the O-donor Lewis base, and TPFP belongs to the Lewis acid. These three different passivators interact with different surface defects. Among these three Lewis acids/bases, TPFP-treated PSCs showed the optimical PCE (22.02%), indicating that there are more halide defects than Pb^{2+} related defects in PSCs. It also found that the passivation effects of different Lewis acids/bases can be used to distinguish the types of defects in perovskites, which provides guidance for selecting

appropriate Lewis acid/base additives. Noel *et al.* [166] spin-coated a layer of pyridine or thiophene on the top of the MAPbI$_{1-x}$Cl$_x$ perovskite layer. In this case, pyridine or thiophene does not participate in the formation of perovskite, and is completely used to passivate defects. The Lewis base functional groups in pyridine and thiophene interact with uncoordinated Pb^{2+}, which passivates the defect sites and greatly reduces the nonradiative recombination rate in perovskite films. Lin *et al.* [167] introduced π-Conjugated Lewis base IDIC (indacenodithiophene end-capped with 1.1-dicyanomethylene-3-indanone) between the MAPbI$_3$ perovskite layer and the ETL. Due to π-Conjugated Lewis base's n-type semiconductor characteristics, it can effectively extract electrons and passivate Lewis acid traps (such as uncoordinated Pb^{2+}), and ultimately increase the PCE of PSCs by 45% (Fig. 11b). Overall, the passivation of defects by the adduct inhibits the non-radiative recombination and hysteresis, meanwhile it greatly improves the PCE and environmental stability of PSCs.
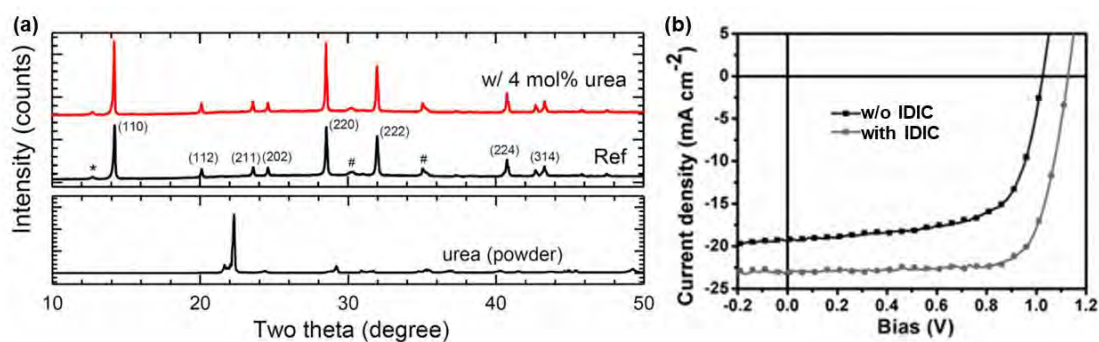
Fig. 11. (a) XRD spectra of perovskite film treated with or without urea and urea powder [168]. Copyright 2017, Elsevier. (b) *J-V* curves of PSCs with or without IDIC passivation layer [167]. Copyright 2017, Wiley-VCH.

4. Additive engineering

4.1. Cl-corporation additive

As we all know, additive engineering has made important contributions to the preparation of high-performance PSCs, especially chloride ion additives. It is found that chloride ions can control the nucleation of perovskite [177], increase the grain size [178] and charge transfer in the films [179]. Because the content of chloride in the additive is too small to be detected [180], it has little effect on the band gap of perovskite, but can significantly improve the quality of perovskite films [1,179,181,182]. Besides, density functional theory (DFT) calculation shows that chloride ions have a favorable interaction with TiO_2, which promotes the extraction of electrons from the device [183].

4.1.1. ACl (A= MA^+, FA^+, NH_4^+ and other organic cations)

The chloride additive used firstly was MACl, which has the function of increasing the grain size of perovskite, promoting preferential crystal orientation, enhancing carrier lifetime, and improving device efficiency [114,178,183]. Qi and his coworkers introduced MACl into $HPbI_3$ to obtain $HPbI_3(Cl)$ film by spin coating, so as to realize Cl doping [184]. After annealing, the $HPbI_3(Cl)$ film quickly reacts with CH_3NH_2 (*i.e.*, MA) to form $MAPbI_3(Cl)$ perovskite (*i.e.*, gas-solid reaction), as shown in Fig. 12(a). Using this technique, they successfully prepared thick $MAPbI_3(Cl)$ perovskite films (over 1 μm) with excellent opto-electronic properties. The 20% PCE of lab-based device and modules with high performance (15.3% PCE with 5×5 cm^2) were achieved (Fig. 12b) [184]. Cl additive (introduced by precursor) can also be combined with antisolvent to prepare $MAPbI_3$ thin films with (110) preferred crystalline orientation

[124]. However, there are several deficiencies when MACl is used as an additive mainly due to the evaporation of MACl during the annealing process, resulting in Cl loss and defects. FACl can replace MACl to avoid the defects caused by the evaporation of MACl [185]. In addition, FACl can also be used to solve the problems existing in the antisolvent method, such as small grains on the surface of the $(FAPbI_3)_{0.87}(MAPbBr_3)_{0.13}$ perovskite thin films due to rapid crystallization [130].
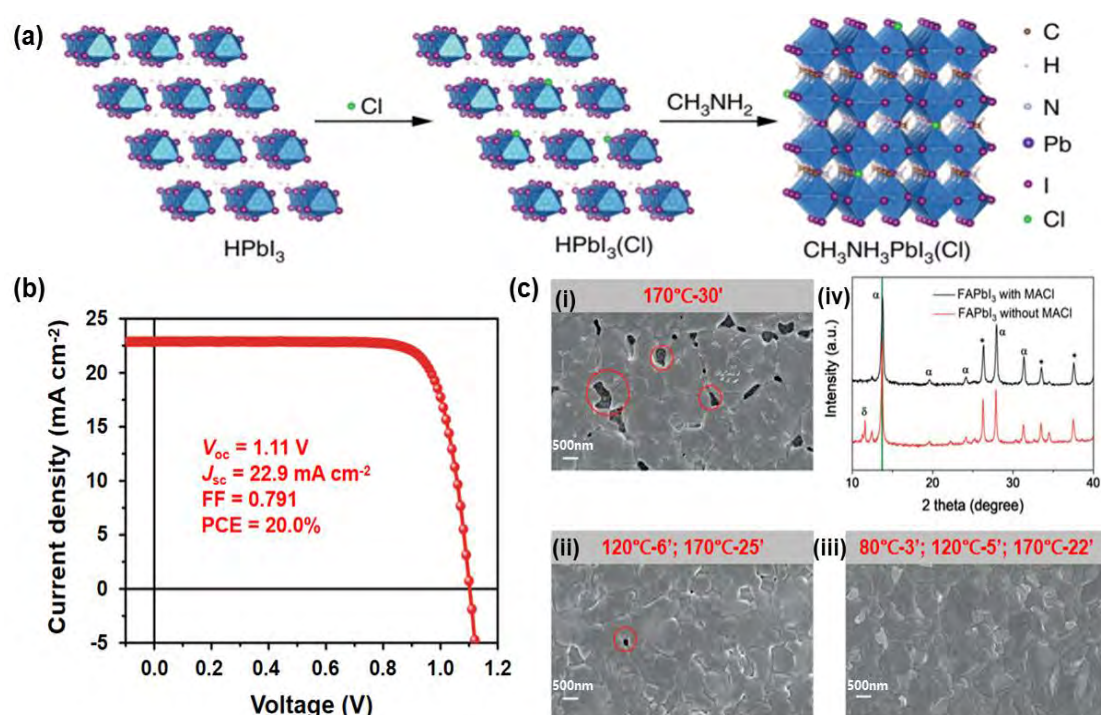
Fig. 12. Formation diagrams (a) and *J-V* curve (b) of MAPbI$_3$ perovskite prepared by gas-solid reaction [184]. Copyright 2018, Springer Nature. (c) Effect of different annealing treatments (i–iii) on the morphology of FAPbI$_3$ film treated by MACl and XRD pattern (iv) of FAPbI$_3$ perovskite thin film (with or without MACl treatment) [187]. Copyright 2020, Wiley-VCH.

Chloride ions additives can also stabilize the black phase of FAPbI$_3$. Three kinds

of chloride ion additives (NH$_4$Cl, MACl and FACl) were used to study their effects on the stability of black phase FAPbI$_3$ [188]. Among them, high volatile additives (NH$_4$Cl) cannot inhibit the formation of yellow δ-FAPbI$_3$, while low volatile additives (MACl or FACl) were helpful to form black phase FAPbI$_3$ in spin-coating stage. Moreover, MACl was proved to stabilize the intermediate, which can be converted into pure α-phase FAPbI$_3$ (*i.e.*, black phase) [186]. Based on the improvement of the phase stability of FAPbI$_3$ by MACl, the amount of MACl were studied. It was found that the PCE of FAPbI$_3$ PSCs can be improved to 24.02% by optimizing the amount of MACl (40 mol%) [186]. Liu *et al.* [187] combined the stepwise annealing process with the addition of MACl to stabilize α-phase FAPbI$_3$ perovskite; and meanwhile, the stepwise annealing process avoids the appearance of pinholes in the FAPbI$_3$ film due to the rapid evaporation of MACl during the annealing process (Fig. 12c). In a word, the phase stability of FAPbI$_3$ was greatly improved by adding MACl. Therefore, chloride additives have great potential in improving the stability of perovskite phase [189].

As organic compounds (such as Isatin-Cl), organic dyes contain a large number of carbonyls, which is conducive to improve the humidity stability of the device because of the hydrophobicity property [190]. In addition, hydrogen bonding and the coordination interaction between perovskite and the additives can passivate defects, such as halide vacancies and uncoordinated Pb^{2+}. For example, Isatin-Cl additive was introduced into perovskite precursor (Fig. 13a) [191] to passivate the defects in the interior and surface of the perovskite film (Fig. 13b) [191]. In addition, Isatin-Cl can make the Fermi level (E_F) closer to the conduction band, which helps to form more n-

type perovskites and improve the charge transfer. Therefore, Isatin-Cl treatment successfully increased the PCE of MAPbI₃ PSCs from 18.13% to 20.18% and suppressed the hysteresis [191].
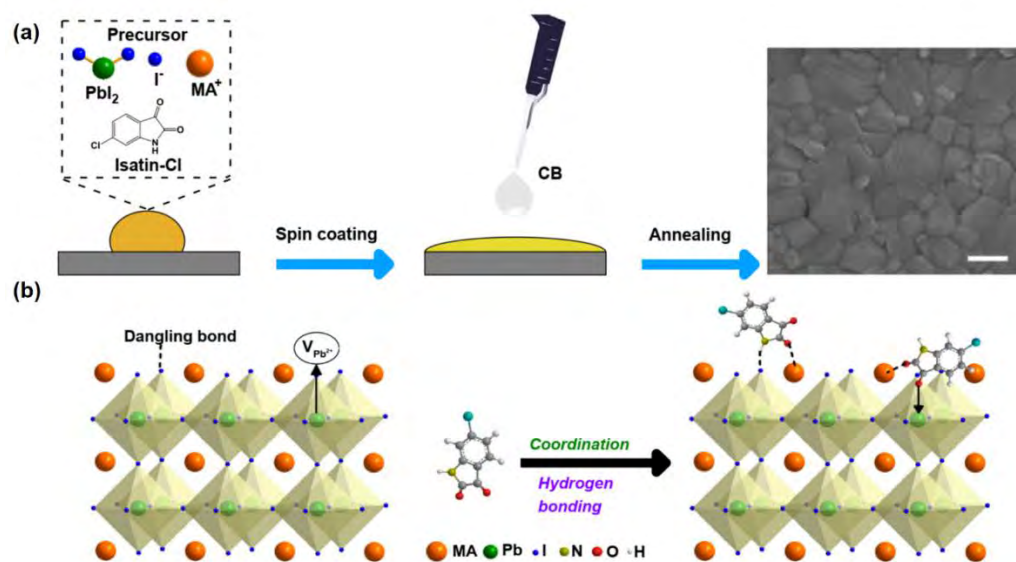
Fig. 13. (a) Processes of preparing MAPbI₃ perovskite thin films with Isatin-Cl, including the chemical structure of Isatin-Cl and the SEM image of the film (scale bar: 200 nm) [191]. (b) Schematic diagrams of the coordination and hydrogen bond interaction between Isatin-Cl and MAPbI₃ [191]. Copyright 2020, Wiley-VCH.

4.1.2. MCl (M= Li⁺, K⁺, Na⁺, Cs⁺, Rb⁺ and other metal ions)

MCl containing alkali metal, such as lithium (Li), potassium (K), sodium (Na), cesium (Cs) and rubidium (Rb), are widely used to improve the performance of PSCs. The role of chloride ions has been discussed in above section, while alkali metal ions have an effect on the tolerance factor, which determines the stability of perovskite. The tolerance factors of $APbI_3$ perovskite with alkali metal cations or organic cation (MA^+ and FA^+) as A-site is listed in Fig. 14(a) [192]. The appropriate range of tolerance factor for stable perovskite structure is 0.8–1. The ionic radius of Li^+, Na^+, K^+ is too small to

form stable perovskite. However, they can be used as additives to improve device performance. It was found that adding LiCl to MAPbI$_3$ precursor could improve the crystallinity of the film and accelerate the transport of electron in the perovskite layer. The device efficiency was increased from 10.0% to 14.5% [193]. When the perovskite film is prepared by two-step spin-coating method, the alkali metal chloride ion additives (NaCl, KCl and LiCl) can be added to the PbI$_2$ precursor to interact with Pb^{2+} ions, which can promote the improvement of the PbI$_2$ film quality (*i.e.*, better crystallinity and larger grain size). This could eventually promote the passivation of GBs in the perovskite film, which successfully increased the PCE of MAPbI$_3$ PSC from 11.4% to 15.08% (with 0.75% KCl). Besides, the stability of PSC was also improved [194]. MCl can also be introduced into the perovskite film by inserting a buffer layer into the interface layer between ETL and perovskite. For example, a KCl layer was inserted at the SnO$_2$/MAPbI$_{3-x}$Cl$_x$ interface enhanced the PCE to 19.44%, where K$^+$ and Cl$^-$ diffused into the perovskite film through thermal annealing, which passivated defects in the perovskite film [195].

On the other hand, CsCl is proven to improve the long-term stability of FAPbI$_3$ based perovskites. For example, Li *et al.* [196] introduced a small amount CsCl into PbI$_2$ solution to form MA$_{0.03}$FA$_{0.97}$Pb(I$_{0.97}$Br$_{0.03}$)$_3$ perovskite, which inhibited the nucleation of perovskite and increase the grain size. The PCE of PSCs was up to 22%, and the long-term stability of the FA-based PSC was greatly improved (panels i and ii of Fig. 14b) [196]. Similar to CsCl, RbCl can also be integrated into perovskite to form stable mixed cation perovskite, such as RbCsMAFA-based perovskite) [192]. Although

there is no stable black phase of $RbPbI_3$, Rb^+ can easily enter the lattice of perovskite to stabilize the black phase of FA-based perovskite because its tolerance factor is very close to that of stable black phase perovskite.

Besides, other chloride ion additives are also widely used to improve the performance of PSCs. For example, $PbCl_2$ plays a key role in the crystallization process of perovskite, which participates in the crystallization process and become the heterogeneous nucleation center of perovskite crystallization [2,7,23]. The good crystal orientation and charge carrier diffusion of perovskite films are promoted, combined with the subsequent annealing process (Cl^- is removed in the form of MACl vapor). The PCE of $MAPbBr_3$ PSCs was up to 5.4% by introducing $PbCl_2$, and V_{oc} was as high as 1.24 V [23]. Ren *et al.* [197] reported that by adding excessive amount of $PbCl_2$ into the perovskite precursor containing MACl, the non-radiation recombination in PSCs was significantly inhibited and therefore the V_{oc} loss was minimized (*i.e.*, from 0.116 V to 0.165 V). The hysteresis of *J-V* curve was also suppressed (Fig. 14c). The perovskite solar module prepared by this method obtained 17.88% of the PCE (area: 25.49 cm^2), and had a high fill factor (FF=78.6%) [197].
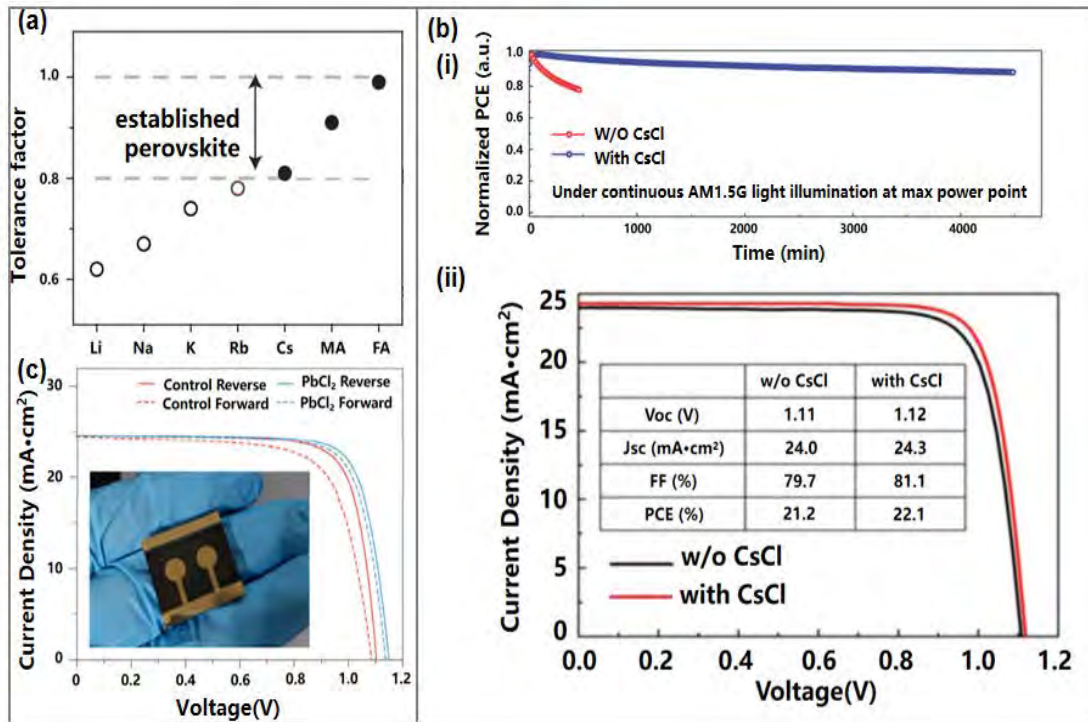
Fig. 14. (a) Tolerance factor of $APbI_3$ perovskite [192]. Copyright 2016, American Association for the Advancement of Science. (b) (i) Long term stability test of $MA_{0.03}FA_{0.97}Pb(I_{0.97}Br_{0.03})_3$ PSCs with or without CsCl additive treatment [196]. (ii) Forward and reverse *J-V* curves of PSCs with or without CsCl additive [196]. Copyright 2018, Wiley-VCH. (c) *J-V* curves of $(CsPbI_3)_{0.05}((FAPbI_3)_{1-x}(MAPbBr_3)_x)_{0.95}$ PSCs passivated with or without $PbCl_2$ additive (area: 0.188 cm^2) [197]. Copyright 2020, Elsevier.

4.2. Organic additives

4.2.1. Small molecule organic additives

4.2.1.1. Aromatics structure additives

In organic additives, different functional groups have different passivation effects. For example, benzene ring has the ability of electron donating, which can passivate

Lewis acid type defects (*i.e.*, halide defects, Pb^{2+}) [198]. Besides, Carboxyl and amine groups passivate charged defects (with positive or negative charges) through electrostatic interaction [198]. A passivator, d-4-tert-butylphenylalanine (D4TBP), which contains three passivation functional groups (*i.e.*, 4-tert-butylphenyl, amino and carboxyl groups) was developed to passivate the perovskite surface and GBs effectively in $Cs_{0.05}FA_{0.81}MA_{0.14}PbI_{2.55}Br_{0.45}$ perovskite. The molecular structure of D4TBP and its interaction with defects in perovskite can be seen in Fig. 15(a). It reduced the loss of V_{oc}, and the device PCE was up to 21.4% [198].
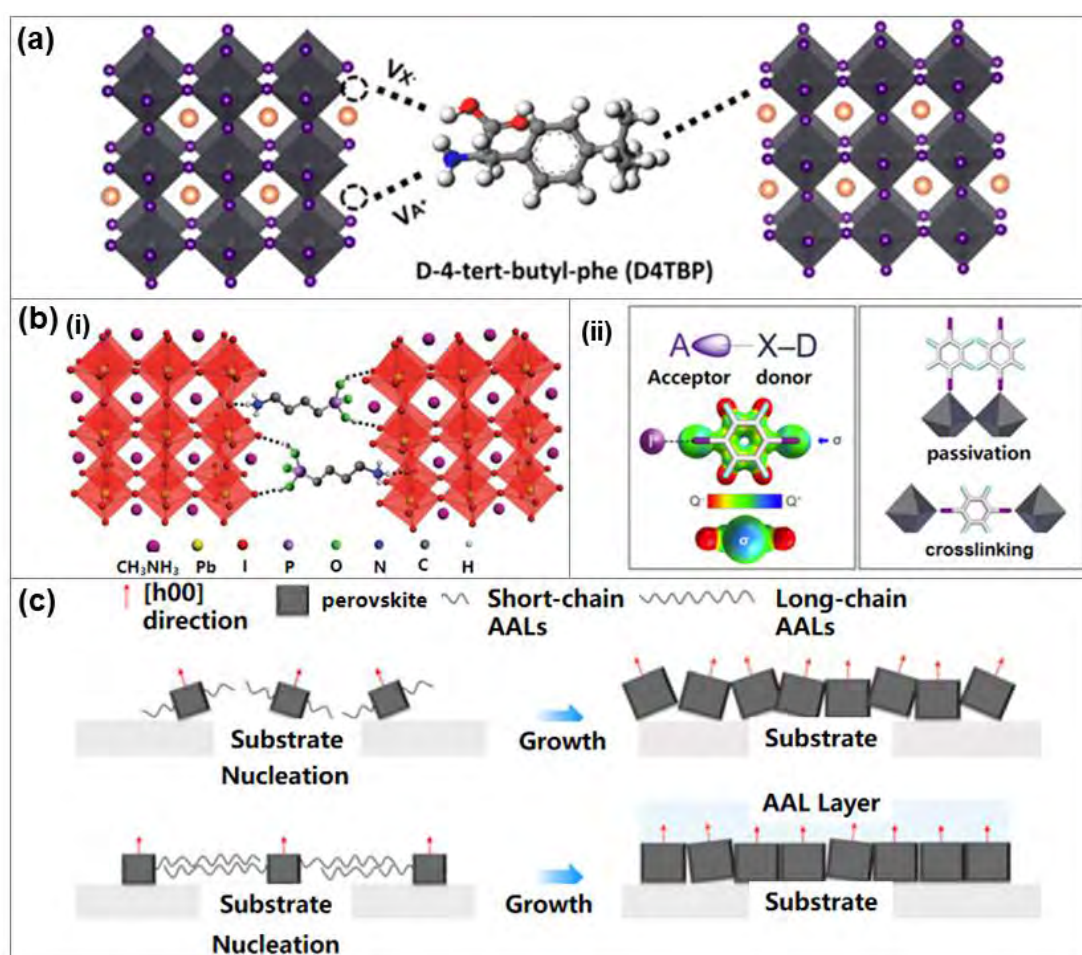
Fig. 15. (a) The molecular structure diagrams of D4TBP and its passivation principle

of different defects in perovskite structure [198]. Copyright 2019, American Chemical Society. (b) (i) Structure diagrams of two adjacent perovskite grains cross-linked by 4-ABPACl cross-linker [199]. Copyright 2015, Springer Nature. (ii) Left: Microscopic diagrams of halogen bond; right: the interaction mode (passivation and crosslinking) between TFDIB and perovskite [200]. Copyright 2020, American Chemical Society. (c) Schematic diagrams of the effect of short chain and long chain Alkyl amine ligands (AALs) on the growth and crystallization of FAMACs perovskite [201]. Copyright 2020, Springer Nature.

4.2.1.2. Alkyl-chain additives

The alkyl chain additives can not only passivate perovskite defects, but also crosslink perovskite crystals through functional groups. For example, Li *et al.* used butylphonic acid 4-ammonium chloride (4-ABPACl) with bi-functional groups ($-PO(OH)_2$ and $-NH_4^+$) to modify the surface of $MAPbI_3$ perovskite [199]. Phosphate group and ammonium ion form hydrogen bond with halide anion in perovskite, which can crosslink perovskite crystal and optimize the morphology of perovskite film (panel i of Fig. 15b). In addition, there is a strong interaction between the crosslinking additive and TiO_2, which contributes to the formation of a dense and fully covered perovskite film on the ETL. The photovoltaic performance (PCE=16.7%) and water stability of PSCs were significantly improved by this additive [199]. For another example, 2-aminoglycol (2-AET) can be introduced into $MAPbI_3$ perovskite precursor to form hydrogen bonds between ammonium groups in 2-AET and MAI. At the same time, thiocyanate in 2-AET can coordinate with PbI_2. Due to the above two interactions,

complexes such as $PbI_2 \cdot 2\text{-}AET \cdot MAI$ will be formed, which can greatly improve the long-term stability of $MAPbI_3$ PSCs [202]. Trimethylolpropane triacrylate (TMTA) additive can also be added into $MAPbI_3$ perovskite precursor to crosslink with perovskite through functional groups [203], which inhibits the ion migration at the GBs and improve the PCE from 19.08% to 20.22%. In addition to hydrogen bonding and coordination with perovskite, additives containing highly polar halogen atoms also interact with nucleophilic receptors (such as O and N). Ruiz-Preciado *et al.* [200] used 1,2,4,5-tetrafluoro-3,6-diiodobenzene (TFDIB) as additive, in which the highly polar fluorine would interact with $(FA_{0.9}MA_{0.1})_{0.95}Cs_{0.05}Pb(I_{0.93}Br_{0.1})_3$ perovskite materials (*i.e.*, crosslinking). This interaction requires highly polarized halogen atom (X) and nucleophilic halogen bond receptor (O, N) (panel ii of Fig. 15b). The cross-linking between TFDIB and perovskite is helpful to improve the photovoltaic performance (PCE=20.5%) and the device stability.

The alkyl chains mentioned above are all short chains. Long alkyl chain additives also have great potential for improving the photovoltaic performance and stability of PSCs. Zheng *et al.* [201] studied the effects of different lengths of alkyl amine ligands (AALs), including n-butylamine (BA), phenylethylamine (PEA), octylamine (OA) and oleylamine (OAm), on the quality of $Cs_{0.05}(FA_{0.92}MA_{0.08})_{0.95}Pb(I_{0.92}Br_{0.08})_3$ perovskite films. The interactions of short chain AAL and long chain AAL with FAMACs perovskite are shown in Fig. 15(c). The perovskite with short chain AALs has more defects due to the random grain orientation, while the long chain AALs limits the inclination of perovskite grains during the growth process to form perovskite films with

(100) preferred orientation, which helps to reduce defects. Besides, the long-chain alkyl group shows greater hydrophobicity than short-chain alkyl group. Therefore, the addition of long-chain AAL improved photovoltaic performance from 20.5% to 23%, accompanied with the enhanced stability.

4.2.1.3. Non-fullerene electron acceptor

Non-fullerene electron acceptors, such as 3,9-bis(2-methylene-(3-(1,1-dicyanomethylene)-indanone))-5,5,11,11-tetrakis(4-hexylphenyl)-dithieno[2,3-d:2',3'-d']-s-indaceno[1,2-b:5,6-b']dithiophene (ITIC) has caused widespread concern in organic solar cells. The utilizaition of non-fullerene electron acceptors in perovskite was also explored. It was found that non-fullerene electron acceptor can inhibit the influence of precursor aging (*i.e.*, the degradation of precursor with time evolution) on device performance. The aging time of precursor solution affects the nucleation rate, crystal growth, crystallinity and coverage rate of the films, which determine the quality of the perovskite films [204,205]. In addition, the aged precursor will affect long-term stability of perovskite films. Qin *et al.* stabilized the perovskite precursor solution by adding an organic non-fullerene fused ring electron acceptor (3,9-bis(2-meth-ylene-(3-(1,1-dicyanomethylene)-indanone))-5,5,11,11-tetrakis(5-hexylthienyl)-dithieno[2,3-d:2',3'-d']-s-indaceno[1,2-b:5,6-b']dithiophene) (ITIC-Th) to inhibit the degradation of the precursor [20]. In addition, ITIC-Th can inhibit the formation of non-optically active phase (*i.e.*, yellow phase or δ-phase) in the films prepared by aged precursor solution. Singh *et al.* added small molecule 3,9-bis(2-methylene-(3-(1,1-dicyanomethylene)-indanone))-5,5,11,11-tetrakis(4-hexylphenyl)-dithieno[2,3-

d:2',3'-d']-s-indaceno[1,2-b:5,6-b']dithiophene (ITIC) into perovskite precursor and prepared bulk heterojunction $MAPbI_3$: ITIC perovskite film by a two-step spin coating method. The film with ITIC showed better morphology. The device shows the optimized PCE of 17.6%, and the *J-V* hysteresis can be ignored [206].

4.2.2. Organic polymer additives
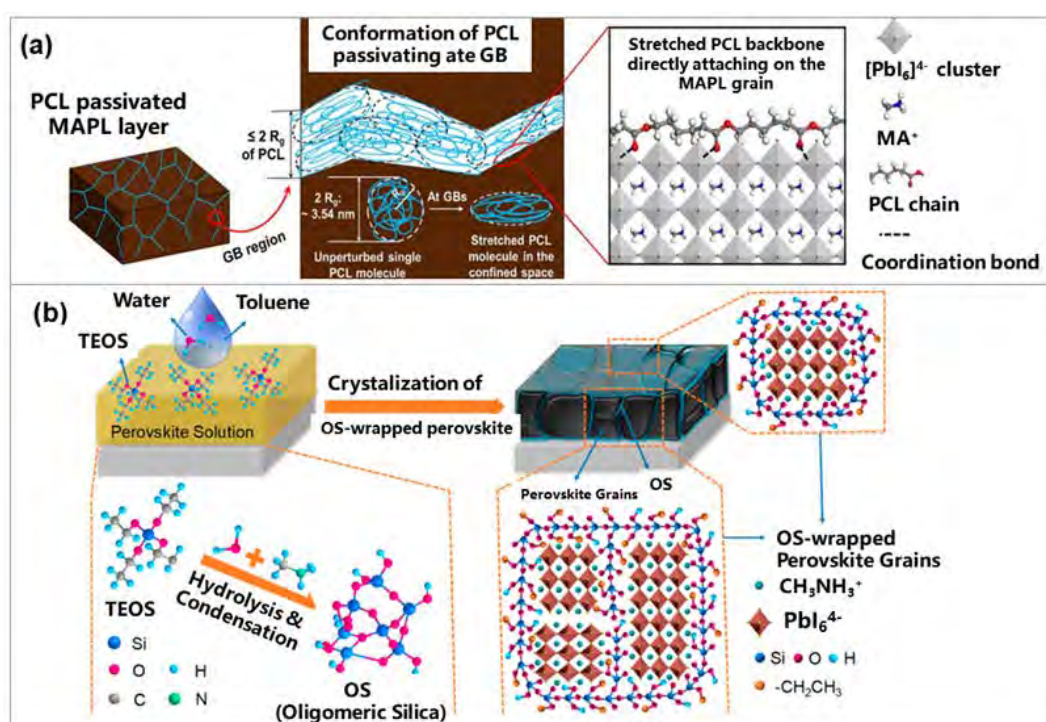
Fig. 16. (a) Micro-diagrams of PCL passivation $MAPbI_3$ perovskite [207]. Copyright 2020, American Chemical Society. (b) Schematic diagrams of formation process of OS-coated perovskite films [208]. Copyright 2019, American Chemical Society.

Organic polymer additives can also be used to passivate defects in perovskite. Qin *et al.* [209] introduced Ethyl cellulose (EC) into the perovskite layer to produce a perovskite film with large grains and low defect density. There is a hydrogen bond between EC and perovskite, which can passivate the charge defects at GBs. In addition,

the long chain in EC can be used as the support of perovskite structure, which can eliminate the lattice strain caused by annealing. The PCE of PSCs with EC additives increased from 17.11% to 19.27%. Zhou *et al.* [207] introduced Polycaprolactone (PCL) into perovskite to passivate GBs, which is due to the coordination between Pb^{2+} and C=O existing in the main chain of PCL. (Fig. 16a). Finally, PCL successfully inhibited the migration of ions to the ETL and HTL and improved the photovoltaic performance of PSCs from 17.5% to 20.1%.

4.2.3. Organic additives for hydrolytic polycondensation

Additives that can hydrolyze and polycondensate tend to form a thin coating layer on grains to passivate and stabilize perovskite. Bai *et al.* [208] introduced tetraethyl orthosilicate (TEOS), which will be hydrolyzed and condensed in contact with water, into the MAPbI$_3$ perovskite precursor. At the same time a small amount of water was introduced to form oligomeric silica (OS) matrix coated with perovskite crystal particles. The mechanism process is shown in Fig. 16b. There is $-OCH_2CH_3$ group in OS, which is a Lewis base and can passivate Pb^{2+} defect. The OS shell can cover the surface of perovskite thin films and the GBs, which reduce the trapped states in the films and inhibit the migration of ions. Finally, the introduction of TEOSreduced the hysteresis of MAPbI$_3$ PSCs and improved the environmental stability of PSCs, accompanied with the improvement of PCE (from 19.1% to 21.5%).

5. Methods for preparing large-area PSCs

5.1. Evaporation method

Besides the solution method, vacuum thermal evaporation method, *i.e.*, dual-

source [210,211] and multi-source co-evaporation (including three-source [212] and four-source [213,214]) could also prepare high-quality perovskite thin films and high-efficiency PSCs. In a certain vacuum environment, the source materials (*i.e.*, the precursors) are heated and evaporated. The vaporized materials get deposited on the substrate, and then react to form perovskite. Vacuum thermal evaporation has various advantages, such as avoiding the usage of toxic solvent, easy deposition of a film from precursor salts with low solubility (such as CsX), precisely controlled film thickness and being compatible with large-scale industrial production [210–212,215–217]. The photovoltaic parameters of PSCs based on different perovskite materials prepared by vacuum deposition are listed in Table 7.

Table 7. High photovoltaic performance of PSCs prepared by evaporation methods.

Perovskite	Number of sources	V_{oc} (V)	J_{sc} (mA cm^{-2})	FF	PCE (%)	Year	Ref.
$MAPbI_3$	2	1.12	23.3	0.78	20.28	2020	[210]
$FAPbI_3$	2	1.01	22.1	-	15.8	2017	[218]
$MA_{0.77}Cs_{0.23}PbI_3$	2	1.10	23.17	0.79	20.13	2017	[219]
$CsSn_{0.5}Ge_{0.5}I_3$	1	0.63	18.61	0.61	7.11	2019	[220]
$FAPb_{0.5}Sn_{0.5}I_3$	4	0.72	24.5	0.72	13.98	2019	[213]
$FA_{0.7}Cs_{0.3}Pb(I_{0.9}Br_{0.1})_3$	3	-	23.0	0.75	18.2	2020	[212]
$Cs_{0.5}FA_{0.4}MA_{0.1}Pb(I_{0.83}Br_{0.17})_3$	4	1.15	17.0	0.82	16	2018	[214]

Single source evaporation usually results in relatively low efficiency (such as 7.73% [11] and 9.92% [221] for $MAPbI_3$ PSCs) because of the ease decomposition of MA-based perovskite. However, for inorganic lead-free perovskite, it may not be a problem. For example, $CsSn_{0.5}Ge_{0.5}I_3$ perovskite film was fabricated by single source evaporation and the PCE of the corresponding PSC reached 7.11%, which is the record efficiency for Sn-Ge perovskite with 50% Sn in molar ratio [220]. Dual source evaporation is the most common method in the preparation of perovskite films by

evaporation. The schematic diagram of dual-source thermal evaporation to prepare MAPbI$_3$ perovskite film is shown in panel i of Fig. 17(a) [210]. The device structure and statistical distribution of PCE in MAPbI$_3$ PSCs (which were treated by different treatments) are also shown in panels (i) and (ii) of Fig. 17(a). The optimized PCE was 20.28% (0.16 cm^2). Moreover, the potential of prepare large-area PSCs (21 cm^2 modules) with a PCE of 18.13% was demonstrated [210]. This suggests that vacuum evaporation can indeed fabricate high efficiency PSCs (over 20% with small area). Although PCE of this method is still lower than solution method, the merit of large area by evaporation method is clear. For Cs containing halide perovskite, the solubility of the precursor CsX in solution method is poor, resulting in poor quality of the corresponding perovskite films. Howerer, evaporation method can solve this problem. For example, the film of CsCl-PbCl$_2$ mixture can be obtained by dual-source evaporation of PbCl$_2$ and CsCl powder [219]. Then, the mixture film reacted with MAI layer (a layer of MAI powder with a thickness of about 0.5mm) to obtain MA$_{1-x}$Cs$_x$PbI$_3$ film. The PCE of the corresponding MA$_{1-x}$Cs$_x$PbI$_3$ PSC was up to 20.13%. It should be noted that the dual-evaporation method is also facing certain difficulties, such as the need to balance the evaporation rates of the two precursors to deposit a perovskite film that meets the stoichiometric ratio.

Similarly, three-source evaporation and four-source evaporation have also been developed. The schematic diagram of fabricating FA$_{0.7}$Cs$_{0.3}$Pb(I$_{0.9}$Br$_{0.1}$)$_3$ perovskite film by three-source thermal evaporation (precursors: PbI$_2$, CsBr and FAI powder) is shown in panel (i) of Fig. 17(b) [212]. After adjusting the processing conditions, a stable

power output (SPO) of 18.2% was obtained (panel ii of Fig. 17b) [212]. Besides, $Cs_{0.5}FA_{0.4}MA_{0.1}Pb(I_{0.83}Br_{0.17})_3$ could be fabricated by four-source evaporation of used MAI, CsBr, FAI, and PbI_2 precursors [214]. The corresponding PCE reached 16%. Evaporation method is not only suitable for the evaporation of perovskite precursors, but also is suitable for the evaporation of additives (powders). For example, $FAPb_{0.5}Sn_{0.5}I_3$ film was deposited by four-source evaporation of FAI, SnI_2, SnF_2 and PbI_2 power, where SnF_2 was used as an additive to prevent the oxidation of Sn^{2+} (panel i of Fig. 17c) [213]. The PCE of the prepared PSCs reached 13.98% (panel ii of Fig. 17c) [213]. When using multi-source evaporation methods (such as three-source and four-source) to prepare perovskite films, the main obstacle comes from the precise control of the deposition rate of each source *in situ*.

For the PSCs mentioned above, other layers (such as carrier transport layers; except for perovskite layer) were prepared using the solution method. Vacuum deposition method can be used not only for the preparation of perovskite layer, but also for other layers of devices of PSCs. The thickness and composition of each layer can be precisely controlled by evaporation method [222]. Momblona *et al.* [223] prepared all-vacuum $MAPbI_{3-x}Cl_x$ PSCs with p-i-n and n-i-p structures, and the average efficiency they achieved of 15% (for p-i-n) and 18% (for n-i-p), respectively.
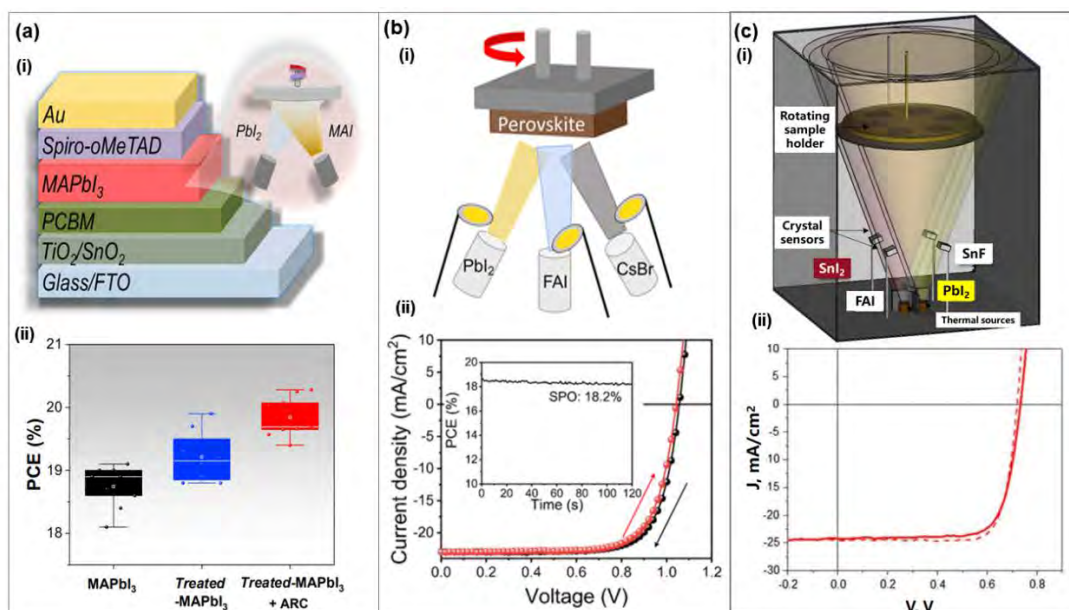
Fig. 17. (a) (i) Schematic diagram to show the process to deposit perovskite thin films by co-evaporation (dual-source) and the corresponding device structure [210]. (ii) Statistical distribution of PCE in MAPbI$_3$ PSCs treated by different treatments. Here, Treated-MAPbI$_3$ refers to the treatment of MAPbI$_3$ perovskite layer with KAc (CH$_3$COOK). Treated-MAPbI$_3$+ARC (antireflective coating) refers to introducing a layer of LIF (100 nm) as antireflective coating on the basis of treated-MAPbI$_3$ [210]. Copyright 2020, Elsevier. (b) (i) Schematic diagram to show the process to deposit perovskite thin films by three-source evaporation [212]. (ii) The forward (red) and backward (black) *J-V* curves of PSCs. The inset is a SPO (*i.e.*, stable power output) measurement [212]. Copyright 2020, American Chemical Society. (c) (i) Schematic diagram to show the process to deposit perovskite thin films by four-source evaporation [213]. (ii) The forward (solide line) and backward (dotted line) *J-V* curves of PSCs [213]. Copyright 2019, Wiley-VCH.

5.2. Blading coating

To realize the commercialization of perovskite solar cells, large-area thin film preparation methods are desirable. Blade coating is a simple, low-cost and efficient method for preparing large-scale perovskite films. Schematic diagrams of blade coating were in panel (i) of Fig. 18(a) [224]. During the coating process, the perovskite precursor solution is dropped onto the substrate, and the blade linearly scrubs the solution at a constant speed. With the simultaneous heating of the substrate in the blade coating process, direct crystallization occurs. Too low a temperature of the substrate may cause the drying time of the film to be too long and therefore produce a rough and pinhole film; while a too high temperature may cause the decomposition of $MAPbI_3$ perovskite. Therefore, the substrate temperature need be optimized for obtaining a dense high quality perovskite film. The optimized PCE of the $MAPbI_3$ perovskite solar cell prepared by this method reached 18.74% (panel ii of Fig. 18a) [224]. Similar to spin coating, blade coating can also be combined with additive (bilateral alkylamine) to improve the PCE of PSCs from 18.3% to 21.7% [225].
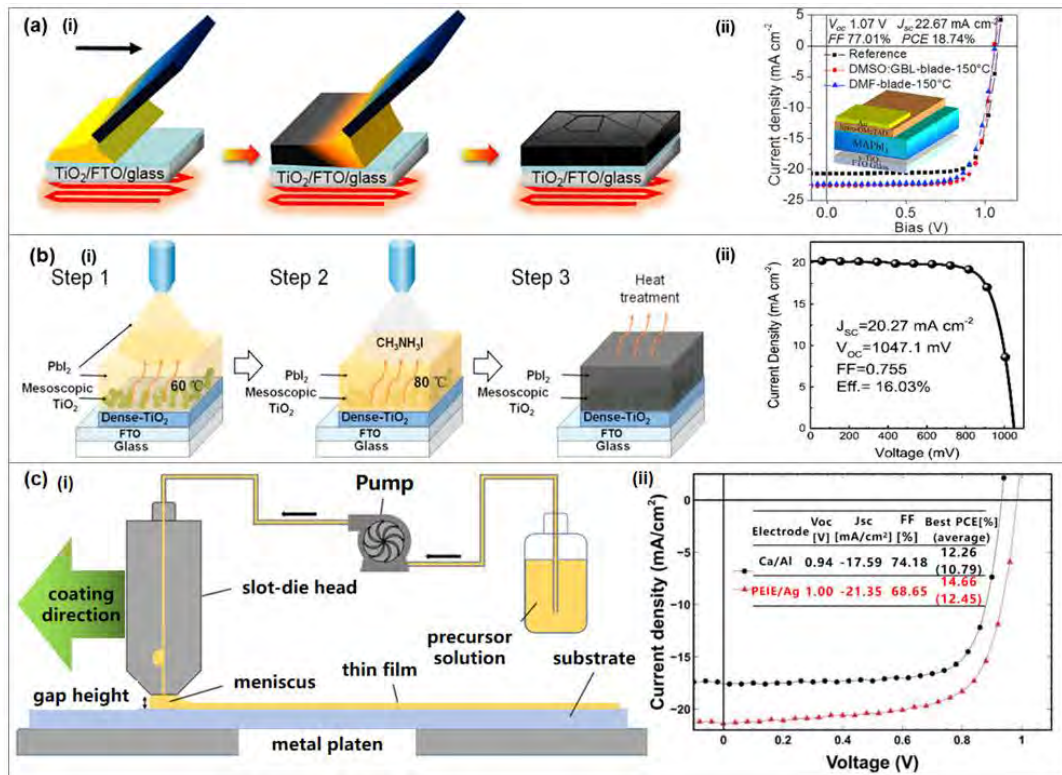
Fig. 18. (a) (i) Schematic diagram to show the process to deposit MAPbI₃ perovskite film by blade coating [224]. (ii) *J-V* curves of MAPbI₃ PSCs prepared under different conditions (*i.e.*, solvent and annealing temperature). Reference here refers to DMSO: GBL-blade-25 °C with antisolvent drip [224]. Copyright 2018, Elsevier. (b) (i) Schematic diagram of the process to deposit MAPbI₃ perovskite films by two-step spraying [226]. (ii) *J-V* curve of the corresponding device [226]. Copyright 2016, Elsevier. (c) (i) Schematic diagram to show the process to deposit MAPbI₃ perovskite films by slot die coating [227]. Copyright 2018, Royal Society of Chemistry. (ii) *J-V* curves of MA$_{0.6}$FA$_{0.38}$Cs$_{0.02}$PbI$_{2.975}$Br$_{0.025}$ PSCs with different electrode prepared by slot die coating. Here, PEIE is polyethyleneimine ethoxylate [228]. Copyright 2018, Wiley-VCH.

5.3. Spray coating

Spray coating is a promising method to deposit large area PSCs at low cost [229]. Preparation of perovskite thin films by spray coating consists of the following steps. First, the precursor droplets of perovskite are atomized by ultrasonic spraying, which can increase the uniformity of droplet size. Then the atomized droplets reach the surface of the substrate. After that, the droplets aggregate to form a wet perovskite film. Finally, the solvent gets evaporated and the wet film becomes dry gradually [230,231]. Solvent, precursor concentration, fluid velocity, nozzle height/velocity, and substrate temperature are all critical for the quality of the film. For example, Qi and co-workers used a spray method to first prepare a PbI_2 wet film, which was then immersed in a MAI precursor solution to obtain a $MAPbI_3$ film [232]. It was found that the higher solvent evaporation rate during the spraying process caused macroscopically visible inhomogeneity of the perovskite film, while the thicker wet film (PbI_2) resulted in low surface coverage of the $MAPbI_3$ film. The Ref. [232] above is just for PbI_2 deposition by spray method. Two-step ultrasonic spray methods shown in panel i of Fig. 18(b) [226]. After depositing PbI_2 layer by ultrasonic spraying, then MAI was sprayed on the PbI_2 film. The PCEs of the PSCs with 0.1 and 1 cm^2 were 16.03% (panel ii of Fig. 18b) and 13.09%, respectively. Continuous high current ultrasonic spraying can reduce the droplet size, which is helpful for the preparation of large-area PSCs with good photovoltaic performance, such as the PCEs of the $MAPbI_3$ PSCs with were 16.9% and 14.2% for 0.0754 cm^2 and 1 cm^2 areas, respectively. Similar to spin coating, ultrasonic spraying can also be combined with antisolvent to prepare large area PSCs. For example, Hest *et al.* [233] prepared a chlorine-containing $MAPbI_3$ perovskite thin film using

ultrasonic spraying, combined with antisolvent (ether) bathing under ambient conditions. Although the surface roughness of the film prepared by this method was higher than that of spin coating, the corresponding PSCs still reached 17.3% (active area: 0.06 cm^2). Bishop *et al.* [234] exposed the trication perovskite wet film prepared by the ultrasonic spraying method to vacuum conditions for a short while, which helped to control the crystallization process of perovskite, hence improving the surface morphology of the film. The efficiency of PSCs with 2.6 mm^2 and 16 mm^2 areas obtained by this method is as high as 17.8% and 15%, respectively. In a follow-up work, they used the same method to prepare charge transport layers, and the PCE of the corresponding PSC achieved 19.4% (2.5 mm^2). At the same time, the PCE of the corresponding large-area PSC reached 16.3% (15.4 mm^2) [235]. Ultrasonic spraying can also be combined with chemical vapor deposition (CVD) to prepare large-area and high-efficiency PSCs, meanwhile reducing lead waste. For example, Qi and co-workers succesfully prepared large-area (10 cm × 10 cm) FAPbI$_x$Br$_{3-x}$ perovskite films and the device acheved high performance [236]. Firstly, PbI$_2$ thin films were prepared by ultrasonic spraying. The move of the spray head in X and Y directions is conducive to deposit a uniform PbI$_2$ wet film across large areas. Then, PbI$_2$ is converted into FAPbI$_x$Br$_{3-x}$ in FAI, FABr and MACl steam by CVD. The PSCs prepared based on this method exhibited a PCE of 14.7% (active area: 12 cm^2). Although the efficiency of PSCs prepared by spray coating is still lower than that prepared by spin coating method, it shows clear potential in fabricating large area and scalable PSCs.

5.4. Slot die coating

Slot die coating is an effective process for manufacturing large-area roll-to-roll printed perovskite solar cells. It has the characteristics of high flux and high material utilization. In the slot die coating process, the perovskite precursor solution is added to the die with slits, and the die head passes through the substrate at a fixed coating speed to obtain the precursor wet film (panel i of Fig. 18c) [227]. The thickness of the wet film prepared in this way can be controlled by adjusting the concentration of the precursor solution, the coating speed, and the distance between the slit of the die and the substrate [227,228]. Blowing and heating (60 °C) can be introduced to accelerate the evaporation of the solvent to improve the morphology of the slot die coated perovskite films. The PCE of the MAPbI$_3$ PSC prepared in this way was up to 12.7% (10 mm^2) [237]. Kim *et al.* prepared MA$_{0.6}$FA$_{0.38}$Cs$_{0.02}$PbI$_{2.975}$Br$_{0.025}$ perovskite in air using slot die coating combined with heating assisted deposition (>100 °C), and the corresponding device efficiency reached 14.7% (panel ii of Fig. 18c) [228]. For MAPbI$_{3-x}$Cl$_x$, the PCE prepared by slot die coating can reach 18% (active area: 0.06 cm^2) [227]. In order to further improve the high-throughput characteristics of PSCs prepared by slot die coating, Qi and co-workers replaced the ultraviolet ozone treatment with corona treatment to achieve the purpose of high throughput, which successfully reduced the time of surface treatment from 15 min (ultraviolet ozone) to 0.1 s (corona) [238]. Although slot die coating has the potential to produce roll-to-roll PSCs with a large area, its PCE is still lower than that of PSCs prepared by spin coating. The other layers in the above PSCs (except the perovskite layer) are all prepared by the traditional solution methods.

Slot coating can be used not only to prepare perovskite layers, but also to prepare other layers in PSCs, which is helpful for high-throughput production of PSCs. However, because the PCE of the entire PSCs prepared by slot die coating is low (such as 5.73% [239] and 11.7% [228]), the preparation conditions need to be further optimized.

6. Strain engineering

6.1. Origin of strain

Strains may exist in perovskite films. Strain includes internal strain and external strain, which can be characterized by the shift of XRD peak due to the change of lattice parameters [240]. Internal strain generally refers to the lattice strain caused by crystal defects in perovskite crystal [241] and composition inhomogeneity [242]. The external strain is generally caused by the gradient thermal stress during film processing [243]. During the annealing (*i.e.*, upon heating on a hot plate), there is thermal gradient from the bottom (near the substrate) and the surface. Upon cooling, the surface of the perovskite film is cooled faster than the bottom, so the surface of the perovskite film is subject to tensile strain, while the bottom is relatively compressed strain. The combined effect of these two strains results in a gradient residual tensile strain in the perovskite film [242]. Furthermore, the external strain can be also formed due to the different thermal expansion coefficient between the perovskite layer and the adjacent layer (ETL and/or HTL) [244]. Fig. 19(a) shows the coefficient of thermal expansion of materials commonly used in each layer of PSCs. It can be seen that the thermal expansion coefficients of the substrate and ETLs are smaller than those of perovskite, except for

very few ETL (such as PC). On the other hand, the coefficients of thermal expansion for HTLs (PDCBT and commonly used P3HT) are higher than that for perovskite materials.
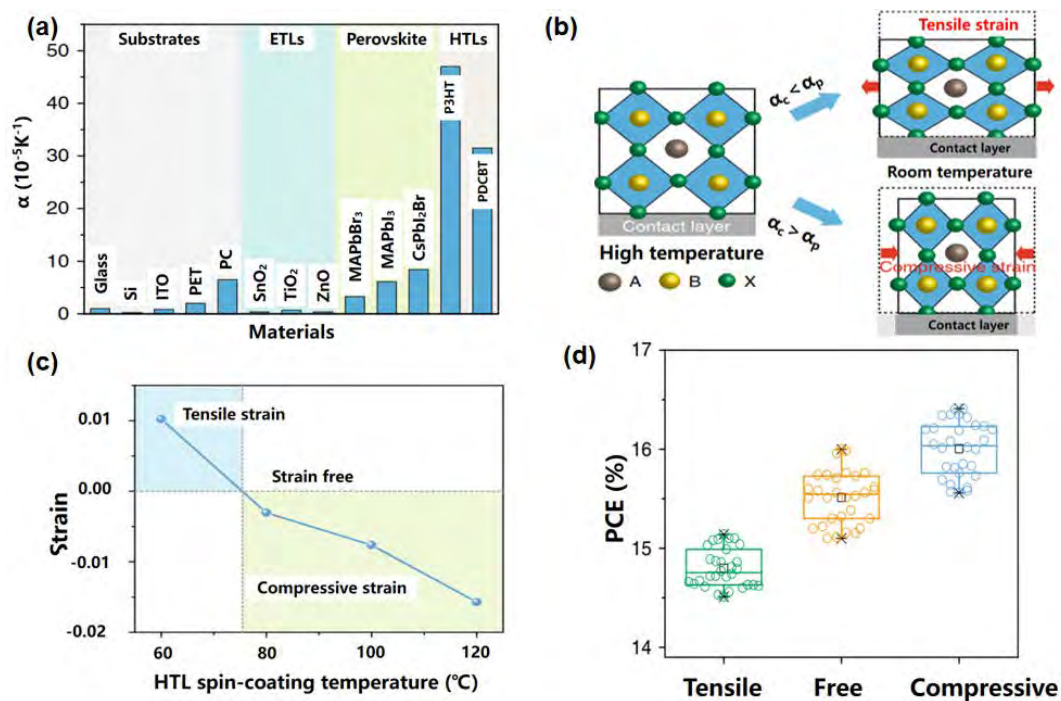
Fig. 19. (a) Thermal expansion coefficients (α) of different layers in PSCs [243]. (b) Schematic diagrams of tensile strain and compressive strain in perovskite layer. The α_c and α_p refer to the thermal expansion coefficient of contact layer (such as HTL) and perovskite respectively [243]. (c) Effect of HTL annealing temperature on strain of CsPbI$_2$Br perovskite thin films [243]. (d) Statistical distribution of PCE of CsPbI$_2$Br PSCs under different strain conditions [243]. Copyright 2020, Springer Nature.

6.2. Strain adjustment

6.2.1. Reducing harmful tensile strain

In the perovskite film, the existence of tensile strain will reduce the activation energy of ion migration and accelerate the degradation of perovskite. The tensile strain

can be relaxed in the following ways. First, lowering the formation temperature can reduce the tensile strain in perovskite [245]. Besides, the A-site doping can improve the thermal and light instability of perovskite, which is due to the strain release, accompanied by lattice shrinkage [219,246]. In addition, the ion substitution will change lattice constant of perovskite by affecting the [BX$_6$] octahedral framework to adjust the lattice strain. For example, Shai *et al.* [247] introduced Zn into the MAPbI$_3$ perovskite and obtained an ordered and stable MA(Zn:Pb)I$_{3-x}$Cl$_x$ crystal, where Zn doping produced lattice shrinkage in the [BX$_6$] octahedral framework and therefore released the lattice strain. The resultant PCE of PSC was up to 20.06%, and the stability was greatly improved.

6.2.2. Introducing compressive strain

By introducing compressive strain (*i.e.*, stress compensation), the harmful tensile strain can be reduced. The simplest way to adjust strain is to apply external stress to perovskite. Bending the film into a convex shape will increase the lattice strain, while bending it into a concave shape can reduce the residual strain in the film [244]. Secondly, it is possible to adjust the thermal expansion coefficient (higher or lower) of the adjacent layer (ETL/HTL) to adjust the strain in the perovskite layer. When the adjacent layers of perovskite (ETL or HTL) with higher coefficient of thermal expansion is used, the perovskite film will produce compressive strain. Otherwise, tensile strain will be produced (Fig. 19b). Based on such principle, poly[5,5-bis(2-butenyl)-(2,2-dithiophene)-4,4-dicarboxylate-alt-5,5-2,2-di-Thiophene] (PDCBT) was used as HTL [243] , because that thermal expansion coefficient of PDCBT (*i.e.*, α_c) is higher than

that of CsPbI$_2$Br perovskite (*i.e.*, α_p), to produce compressive strain. Besides, PDCBT

has rich carbonyl groups, which has strong interaction with perovskite so as to achieve

strain compensation. The temperature for preparing HTL will also affect the strain (Fig.

19c) [243], *i.e.*, relatively high temperature causes compressive strain, while relatively

low temperature causes tensile strain. The optimized condition of HTL improve the

photovoltaic performance and the optimal PCE of CsPbI$_2$Br PSCs is up to 16.4% (Fig.

19d) [243]. On the other hand, HTL with lower treatment temperature (60–80 °C) will

lead to tensile strain, which leads to the decrease of PCE (Fig. 19c and d). For another

example, Chen *et al.* [248] epitaxially grown α-FAPbI$_3$ single crystal film on a

MAPbCl$_x$Br$_{3-x}$ perovskite substrate with mismatched lattice. By adjusting x and

changing the lattice parameters of the substrate, strain is adjusted. The strong ionic bond

between the α-FAPbI$_3$ and the substrate (MAPbCl$_x$Br$_{3-x}$) can prevent the phase

transition of FAPbI$_3$. At the same time, the α-FAPbI$_3$ thin film is compressed due to the

lower interface energy of cubic α-FAPbI$_3$/cubic substrate compared with that of

hexagonal δ-FAPbI$_3$/cubic substrate. Therefore, the phase stability of α-FAPbI$_3$ was

greatly improved.

7. Adjusting the band gap of perovskite

Through the continuous efforts of scientific researchers, the efficiency of

perovskite solar cells is constantly approaching the Shockley-Queisser limit [249]. Fig.

20(a) shows the influence of the perovskite band gap of each sub-cell in single junction

and multi-junction PSCs on the theoretical maximum efficiency [250]. The maximum

efficiency of single-junction solar cell can be achieved when the band gap is 1.4 eV.

Fig. 20(a) also lists the band gap range of each sub-cell of the multi-junction PSCs, as well as the optimal band gap of the perovskite in each sub-cell to achieve the best theoretical efficiency [250]. Simultaneously, with the increase of the number of sub cells, the influence of the perovskite's bandgap of the bottom sub-cell on the maximum efficiency of the multi-junction PSCs gradually decreases. Fortunately, perovskite has the advantage of tunable bandgap. In the following section, we will discuss the composition engineering to tune the bandgap of perovskite.

7.1. Composition engineering

7.1.1. X-site anion

The choice of halogen element X in ABX_3 metal halide perovskite materials has strong impact on its optical band gap. When other elements remain unchanged, the band gap of perovskite increases with the decrease of halogen ion size [251]. The content of Br in $MAPb(I_{1-x}Br_x)_3$ affects the band gap of perovskite. By adjusting the content of bromine, the band gap of perovskite can be continuously adjusted (*i.e.*, 1.55~2.3 eV) (Fig. 20b) [252]. Similarly, in tin-based perovskite, such as $MASnI_3$ and $CsSnI_3$, the incorporation of bromine to replace iodine will enlarge the band gap [253,254]. For example, its band gap of $CsSnI_3$ is about 1.27 eV. When I is replaced by Br, its band gap will gradually increase to 1.37, 1.65 and 1.75 eV for $CsSnI_2Br$, $CsSnIBr_2$ and $CsSnBr_3$, respectively [254]. The increase of band gap will lead to the decrease of J_{sc}, but the V_{oc} will rise. Similar to Br, doping Cl in lead iodide perovskite can also increase the band gap, which is not conducive to the photovoltaic performance of single junction PSCs [255].

The low-dimensional $Cs_3Bi_2I_9$ perovskite shows excellent air stability, but it limits the application in solar cells due to its large band gap (~2 eV). The substitution of I by Br in $Cs_3Bi_2I_9$ could reduce the band gap of $Cs_3Bi_2I_9$ from 2.2 eV (for $Cs_3Bi_2I_9$) to 2.03 eV (for $Cs_3Bi_2I_6Br_3$) [256]. It seems that halogen is effective in regulating the band gap of $Cs_3Bi_2I_9$. However, McCall *et al.* [257] partially replaced I in 0D $Cs_3Bi_2I_9$ with Cl to form 2D $Cs_3Bi_2I_6Cl_3$ perovskite. Cl in $Cs_3Bi_2I_6Cl_3$ occupies the bilayer's bridging position, while I occupies the terminal site, which results in the (111) oriented two-dimensional bilayer structure. The Cl does not affect the band gap, but introduces a direct band gap, which enhances the photoelectric performance of the PSC. The discussions above indicate that the effect of Br and Cl replacement for I in low-dimensional $Cs_3Bi_2I_9$ is different from of that in both lead-based perovskites and tin-based perovskites.
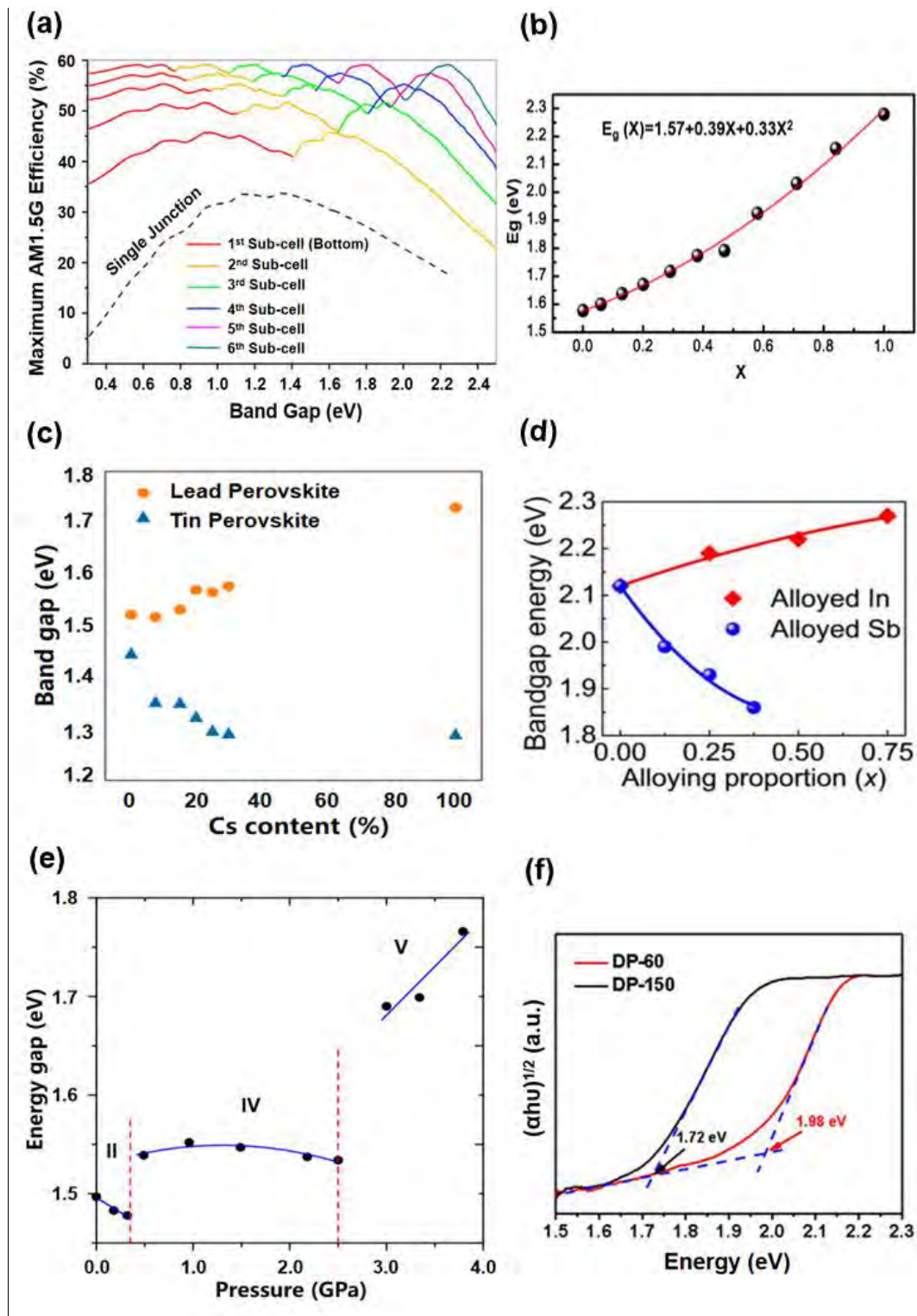
Fig. 20. (a) The band gap and theoretical maximum efficiency of perovskite in each sub-cell of single junction and multi-junction PSCs [250]. Copyright 2016, Elsevier. (b) The relationship between the band gap (E_g) of MAPbI$_{3-x}$Br$_x$ (pseudo cubic or cubic)

and Br content (x) [252]. Copyright 2013, American Chemical Society. (c) Effect of A-site cation composition engineering on the band gap of $FA_{1-x}Cs_xMI_3$ (M = Pb, Sn) [258]. Copyright 2017, American Chemical Society. (d) The influence of alloyed In and Sb on the indirect band gap of $Cs_2AgBiBr_6$, respectively [259]. Copyright 2017, Wiley-VCH. (e) Dependence of band gap of $MAPbI_3$ on pressure applied on perovskite. Here, II, IV and V refer to the tetragonal phase, cubic phase and isostructural cubic phase, respectively [260]. Copyright 2016, American Chemical Society. (f) Tauc plots of the indirect band gap of $Cs_2AgBiBr_6$ perovskite single crystals. Here, DP-60 and DP-150 refer to the evaporation of perovskite precursor solution at 60 °C and 150 °C, respectively [261]. Copyright 2020, Wiley-VCH.

7.1.2. A-site cation

The band gap of perovskite can also be adjusted by changing the A-site cation. In lead-based perovskite, the band gap increases when A-site cation is replaced by a smaller A-site cation. For example, when the larger FA (2.53 Å) was replaced by a smaller Cs (1.88 Å) atom, the band gap increased due to the inclination of octahedron (Fig. 20c) [258]. For another example, the band gaps of $Cs_{0.10}MA_{0.90}PbI_3$, $Cs_{0.20}MA_{0.80}PbI_3$ and $Cs_{0.30}MA_{0.70}PbI_3$ formed by partially replacing MA (2.17 Å) with Cs are 1.54, 1.57 and 1.58 eV [262], respectively, which shows an increase in the band gap compared to $MAPbI_3$ (1.52 eV). When substituting larger cations for smaller cations, the band gap will be reduced. For example, partial replacement of MA by FA in $MAPbI_3$ (~1.57 eV) formed the mixed cation perovskite (such as $MA_{0.6}FA_{0.4}PbI_3$) and reduced the band gap (1.53 eV), which is due to the isotropic shrinkage of the

crystal lattice [258]. Finally, it resulted in the increased light absorption range and the excellent photovoltaic performance [263]. While in tin-based perovskite, the substitution of Cs for FA reduce the band gap due to the lattice shrinkage (Fig. 20c) [258]. It is worth noting that different preparation processes will cause a slight change in the band gap of the same perovskite such as $MAPbI_3$. Therefore, the selection of the A-site cation plays an important role in adjusting the band gap.

7.1.3. B-site metal cation

For $MAPbI_3$, partial replacement of Pb with Sn can reduce the band gap of perovskite as much as possible to the band gap most suitable for single-junction PSC [264,265]. Although lead-free double perovskites (such as $Cs_2AgBiBr_6$) avoid the toxic Pb, their application in PSCs is still limited mainly because of the large band gap. Alloying trivalent metal elements (In or Sb) can adjust the band gap of $Cs_2AgBiBr_6$ [259]. In and Sb show different effects on band gap adjustment. The band gap of $Cs_2AgBiBr_6$ perovskite increased with the addition of alloyed In. When Bi is partially replaced by In, the ordering of $[BiBr_6]$ octahedron reduced, leading to the downward shift of valence band and the increase of band gap. On the contrary, the band gap of $Cs_2AgBiBr_6$ perovskite decreases with the addition of alloyed Sb, as shown in Fig. 20(d) [259]. Sb alloying can reduce the band gap because that the energy level of the 5s states of Sb is higher than that of the 6s states of Bi, which leads to the increase of the valence band (V_B) of perovskite after Sb alloying [259].

7.2. Pressure regulation

Pressure can adjust the crystal structure, electronic structure and energy gap of

semiconductor to realize band gap adjustment [266,267]. The pressure exerted on the MAPbI$_3$ causes a phase change in the perovskite, as shown in Fig. 20(e) [260]. When the applied pressure is less than 0.35 GPa, the MAPbI$_3$ perovskite is in the tetragonal phase (II). In this range, as the pressure increases, the band gap decreases from 1.5 to 1.475 eV. When the pressure reaches 0.35 GPa, MAPbI$_3$ undergoes a phase change, changing from a tetragonal phase to a cubic phase (IV). At this time, the band gap (1.54 eV) of MAPbI$_3$ changes slightly with increasing the pressure. When the pressure reaches 2.5 GPa, the perovskite becomes isostructural cubic phase (V), and the band gap sharply increases. With further increasing pressure, the band gap increase more. Pressure will distort the inorganic framework in the perovskite and cause structural distortion, which affects the electronic state of the absorption edge, and ultimately manifests as a change in the band gap.

Pressure can also change the band gap of lead-free perovskites by affecting the crystal lattice. For example, the band gap of the Cs$_2$AgBiBr$_6$ can be reduced from 2.2 eV at environmental condition to 1.7 eV at 15 GPa [268]. Taking another example, the band gap of Cs$_3$Bi$_2$I$_9$ can be adjusted from 2.06 eV at atmospheric pressure to 1.12 eV at 12.1 GPa [269]. However, this adjustment of band gap is limited. Once the pressure is removed, the perovskite will recrystallize and return to its original state. So the pressure regulation for band gap is not applicable to solar cell fabrication, but help to understand the basic physical property.

7.3. Temperature

The change of temperature will lead to the thermal expansion of the lattice, which

will change the electronic structure and optical properties. In lead-based perovskites, such as MAPbI$_3$, the band gap is slightly increasing, and the change value is about 80–90 meV with the increase of temperature from 15 K to 300 K [270,271]. Although temperature has almost no effect on the band gap of lead-based perovskites, its effect on the band gap of lead-free perovskites seems to be a bit greater compared to lead-based perovskites. For example, in Cs$_2$AgBiBr$_6$, when the temperature was increased from 25 °C to 200 °C, the band gap was reduced (the maximum reduction is about 0.07 eV) [272]. This is mainly because the change of temperature will cause the bond length of Ag−Br and Bi−Br to change, which is manifested as a reversible thermos-chromic phenomenon. Later, it is discovered that the growth of lead-free perovskite crystals through temperature adjustment seems to have a relatively large effect on the band gap of lead-free perovskite. For example, by slowly evaporating the precursor solution at different temperatures, Cs$_2$AgBiBr$_6$ single crystals with different band gaps can be synthesized [261]. As the evaporation temperature increased from 60 °C to 150 °C, the color of Cs$_2$AgBiBr$_6$ single crystal changed from red to black, corresponding to the reduction of the band gap. By controlling the crystal growth temperature and rate, the reduction of band gap is about 0.26 eV (from 1.98 eV to 1.72 eV) (Fig. 20f) [261]. The authors proposed that increasing the disorder of Ag−Bi can reduce the band gap, which is verified by first-principle calculation. Overall, the influence of temperature on band gap is negligible for Pb based perovskites, but it seems more effective to adjust the band gap of lead free perovskites.

8. Perspectives

We reviewed the common strategies (including antisolvent, Lewis acid-base addition reaction, chloride ion additive, scaleable fabrication, strain engineering and bandgap adjustment)for fabricating high-quality perovskite films, and therefore for fabricating PSCs with high performance (*i.e.*, both high PCE and high stability). The quality of thin films prepared by traditional solution method usually is poor, which is characterized by uneven grain size, voids, low coverage and high roughness. The utilization of antisolvent method largely addressed these problems. The antisolvent can control the crystallization of perovskite by extracting solvent, so as to improve the quality of perovskite thin films. In this process, the choice of suitable antisolvent is particularly important. The polarity and boiling point of the selected antisolvent should not be too high or too low, otherwise it will lead to poor film morphology. Of course, the polarity of the antisolvent with higher or lower polarity can be adjusted by mixing the antisolvent to achieve the optimal crystallization rate. The miscibility of the antisolvent to the solvent depends on the polarity of the antisolvent. They regulate the crystallization rate of perovskite by influencing the intermediates. In addition to the physicochemical properties of the antisolvent itself, the time (or window) and volume of the antisolvent also affect the film quality, so as to the device performance. Although the antisolvent method has made an important contribution to the preparation of high-quality thin films, the processing window is narrow. The window of antisolvent is first affected by the composition of perovskite. The antisolvent window of mixed cation/halide perovskite is wider than that of single cation/halide perovskite. For the same antisolvent, the windows are also different for perovskites with different cations

and halides. Secondly, different solvents also lead to wide or narrow windows. In some preparation processes, the advantage of antisolvent is not obvious or even negative. At this time, adjusting the temperature of the antisolvent may optimize the application of antisolvent and made antisolvent effective again. The ultimate goal of applying antisolvent is to optimize the nucleation and growth of perovskite, and improve the repeatability of preparation. A large number of antisolvent are combined with additives to solve the problems of perovskite itself, or to solve the disadvantages of antisolvent method. There are two ways to add additives, one is to add the additive (s) to perovskite precursor, the other is to add it to the antisolvent. The solubility of additive and solvent is the prerequisite for additive to be added into perovskite precursor or antisolvent. If one wants to stabilize the crystal structure or passivate the perovskite, the additive should be added to the perovskite precursor; if the purpose is to control the nucleation and crystal growth of perovskite, then the additive should be added to the antisolvent.

Lewis acid-base addition reaction is also a common strategy in the preparation of perovskite thin films by solution method. Lewis acid is usually the metal cation in the perovskite precursor. The Lewis base generally includes a Lewis base solvent (such as DMSO, DMF and thiourea) and molecules containing Lewis base functional groups. When Lewis bases are added to the process of preparing perovskite films (such as added to precursor/antisolvents), they participate in the formation of perovskites and form Lewis acid-base adducts with metal cations, which can regulate crystallization and growth of perovskite. Generally speaking, the effect on the crystallization process will also affect the defects in the perovskite film, and there is no obvious boundary between

them. After the perovskite film is formed (after thermal annealing), when the surface of the perovskite film is treated with Lewis base/acid molecules, they can only play a role in passivating defects. Some people also use Lewis acid/base additives to passivate the defects in perovskite and improve the hole extraction effect of HTL, which is beneficial to improve the performance of PSCs.

The applications of chloride ion additives (such as MACl, FACl, and CsCl) are mainly used to suppress the loss of non-radiative recombination due to defects (such as interstitial Pb^{2+} and halide vacancies). These additives also improve the stability of the perovskite phase. Other additives, such as small molecule additives containing various functional groups (*e.g.*, aromatics structure, alkyl-chain and non-fullerene electron acceptor), organic polymer additives and hydrolytic polycondensable additives (such as TEOS) can also be used to inactivate the bulk and surface defects of the perovskite, and therefore to enhance the device performance and the stability.

Besides, in order to provide guidance for the large area perovskite module fabrication, the methods for preparing scaleable perovskite films are described (including evaporation method, blading coating, spray coating and slot die coating). Although the PCE of PSCs prepared by evaporation method is still lower than that by solution method, the advantages of large area compatibility can not be ignored. Blade coating, spray coating and slot die coating are not only compatible with the preparation of large area perovskite film, but also can reduce the waste of precursor compared with spin-coating.

Strain is ubiquitous in perovskite. The defects and composition inhomogeneity in

perovskite lead to lattice strain, which has a negative effect on the stability of perovskite and the performance of the device. The [BX$_6$] octahedral framework can be affected by ion substitution (such as A-site doping or partially replacement by other ions) to achieve the purpose of strain release or strain compensation. On the other hand, due to the mismatch of thermal expansion coefficient between the perovskite layer and other layers in PSCs, tensile strain exists widely in perovskite films during the high temperature annealing process, which is harmful to the intrinsic stability of perovskite. In order to improve its internal stability, the harmful tensile strain in perovskite can be adjusted by performaning the annealing at relatively low temperature (note: the crystalizaion should not be considerably sacrificed; the opto-elctronic property of the perovskite film should be not compromized), introducing external compressive strain and adjusting the thermal expansion coefficients of adjacent layers and perovskite.

The band gap of perovskite can be adjusted through component engineering (including A-site, B-site and X-site), imposing high pressure to perovskite crystal and temperature adjustment. Component adjustment should be considered in the premise of target device (*i.e.*, single junction solar cell or tandem solar cell). The high pressure can adjust the band gap in a wide range. However, once the pressure is removed, the band gap of perovskite will recover. For Pb-based perovskite, the temperature has little effect on the band gap, while temperature can adjust the band gap in a certain range in the lead-free perovskite (such as $Cs_2AgBiBr_6$).

Thanks to the tremendous efforts on perovskite from perovskite community, impressive progress has been made for PSCs. However, there still remain several

challenges for the commercialization of this technologyas follows.

(1) The optimized composition and the structure of perovskite with best performance need be studied extensively. Currently, lots of compositions are reported, and different fabrication methods, as well as treatment methods (such as normal annealing, vapor annealing, ramping annealing, and different additives) are used for fabricating PSCs. However, there is no one method that is almighty because of the versatile compositions and the corresponding various physiochemicial properties of them. Therefore, the role of each strategy or the mechanism of it should be understand deeply in order to find the protocol or the best condition for controllably fabricating PSCs with the highest PCEs.

(2) The fabrication environment should be controlled. Perovskite is very sensitive to the environment both during the fabrication process and during the usage. For example, in summer, high humidity will hinder obtaining high PCE when fabrication PSCs. Usage in air or under the environment with thermal stress also lead to the performance degradation. Therefore, strict encapsulation methods should be exploited to avoid the degradation during the usage.

(3) Intrinsic stability should be focused more. Even applying the encapsulation, the perovskite still degrades, because of the weak binding, ion migration and intrinsic defects. Therefore, encapsulation is just considered as a supplementary method, and the priority for solving the stability issues is to search for perovskite materials with enhanced intrinsic stability.

(4) PSCs, especially lead-based PSCs, have excellent photoelectric properties, and have made remarkable progress. However, their commercial development can be hindered

by the safety concerns regarding the toxic element (lead in these PSCs). Lead is harmful to environment and human body. Rainwater may cause irreversible decomposition of the perovskite layer in PSCs, and Pb can be dissolved in rainwater, thus polluting the environment [273]. Besides, Pb can cause serious damage to human body such as nervous system and reproductive system, especially to children [274]. Therefore, in order to expand the commercial application of PSCs, it is necessary to prevent the harmful effects of Pb on the environment and human body while ensuring the high efficiency and stability of PSCs.

The problem of lead toxicity can be solved from the following aspects. Firstly, more effective encapsulation technology can be developed to minimize Pb leakage into environment in case PSCs are damaged under extreme weather conditions [275]. Secondly, strategies should be developed to recycle PSCs that have reached their service life [276]. In addition to the above two methods focusing on reduction of the harmful effects of Pb-based PSCs to the environment, it is also beneficial to develop Pb-free PSCs. At present, many nontoxic elements (such as Sn, Ge, Bi and Sb) have been used to replace Pb. However, the development of lead-free perovskite is facing several challenges For example, most of the lead-free perovskite films prepared by low-cost solution methods have the problem of fast crystallization rates, which leads to poor film morphology [97,99,162,171]. In addition, the air stability of tin-based or germanium-based perovskites is poor [277,278]. Besides, the band gap of bismuth-based perovskite is too large (~2 eV) to prepare single junction perovskite solar cells with high PCE. Therefore, more efforts are needed in the development of lead-free

perovskites.

(5) The technology of large area with high efficiency is needed. If we compare the technologies of PSCs and the silicon-based solar cells, their PCEs of lab-based devices are very similar, but the large area device (or modules) of perovskite photovoltaic is fall behind of Si-based photovoltaic. As we know, with increasing the area, the film quality gradually faces challenges. For example, the spin-coating method is incompatible with large area fabrication. Take another example, the film uniformity become challenging when expanding the area in vacuum method and pinholes may appear. Therefore, it is necessary to develop reliable fabrication methods for fabricating large area PSCs and modules.

References:

[1]   G. Xing, N. Mathews, S. Sun, S.S. Lim, Y. M. Lam, M. Grätzel, S. Mhaisalkar,T.C. Sum, Science 342 (2013) 344-347.
[2]   S.D. Stranks, G.E. Eperon, G. Grancini, C. Menelaou, M.J. Alcocer, T. Leijtens, L.M. Herz, A. Petrozza, H.J. Snaith, Science 342 (2013) 341-344.

[3] J. Berry, T. Buonassisi, D.A. Egger, G. Hodes, L. Kronik, Y.L. Loo, I. Lubomirsky, S.R. Marder, Y. Mastai, J.S. Miller, D.B. Mitzi, Y. Paz, A.M. Rappe, I. Riess, B. Rybtchinski, O. Stafsudd, V. Stevanovic, M.F. Toney, D. Zitoun, A. Kahn, D. Ginley, D. Cahen, Adv. Mater. 27 (2015) 5102-5112.

[4] K.T.A. Kojima, Y. Shirai, T. Miyasaka, J. Am. Chem. Soc. 131 (2009) 6050.

[5] A.M.A. Leguy, J.M. Frost, A.P. McMahon, V.G. Sakai, W. Kockelmann, C. Law, X. Li, F. Foglia, A. Walsh, B.C. O'Regan, J. Nelson, J.T. Cabral, P.R.F. Barnes, Nat. Commun. 6 (2015) 7124.

[6] W.E.I. Sha, X. Ren, L. Chen, W.C.H. Choy, Appl. Phys. Lett. 106 (2015) 221104.

[7] G.E. Eperon, V.M. Burlakov, P. Docampo, A. Goriely, H.J. Snaith, Adv. Funct. Mater. 24 (2014) 151-157.

[8] N.J. Jeon, J.H. Noh, Y.C. Kim, W.S. Yang, S. Ryu, S.I. Seok, Nat. Mater. 13 (2014) 897-903.

[9] H. Ying, Y. Liu, Y. Dou, J. Zhang, Z. Wu, Q. Zhang, Y.-B. Cheng, J. Zhong, Front. Optoelectron. 13 (2020) 272–281.

[10] M. Liu, M.B. Johnston, H.J. Snaith, Nature 501 (2013) 395-398.

[11] G. Liang, H. Lan, P. Fan, C. Lan, Z. Zheng, H. Peng, J. Luo, Coatings 8 (2018) 256.

[12] D.S. Lee, J. Bing, J. Kim, M.A. Green, S. Huang, A.W.Y. Ho-Baillie, Sol. RRL 4 (2019) 1900397.

[13] S. Ghosh, S. Mishra, T. Singh, Adv. Mater. Interfaces 7 (2020) 104362.

[14] S. Wang, A. Wang, X. Deng, L. Xie, A. Xiao, C. Li, Y. Xiang, T. Li, L. Ding, F. Hao, J. Mater. Chem. A 8 (2020) 12201-12225.

[15] A. Mahapatra, D. Prochowicz, M.M. Tavakoli, S. Trivedi, P. Kumar, P. Yadav, J. Mater. Chem. A 8 (2020) 27-54.

[16] K. Wang, Z. Jin, L. Liang, H. Bian, D. Bai, H. Wang, J. Zhang, Q. Wang, S. Liu, Nat. Commun. 9 (2018) 4544.

[17] S. Wang, Y. Jiang, E.J. Juarez-Perez, L.K. Ono, Y.B. Qi, Nat. Energy 2 (2016) 16195.

[18] Y. Wang, T. Zhang, M. Kan, Y. Zhao, J. Am. Chem. Soc. 140 (2018) 12345-12348.

[19] S.D. Stranks, V.M. Burlakov, T. Leijtens, J.M. Ball, A. Goriely, H.J. Snaith, Phys. Rev. Appl. 2 (2014) 034007.

[20] M. Qin, J. Cao, T. Zhang, J. Mai, T.-K. Lau, S. Zhou, Y. Zhou, J. Wang, Y.-J. Hsu, N. Zhao, J. Xu, X. Zhan, X. Lu, Adv. Energy Mater. 8 (2018) 1703399.

[21] F. Lamberti, T. Gatti, E. Cescon, R. Sorrentino, A. Rizzo, E. Menna, G. Meneghesso, M. Meneghetti, A. Petrozza, L. Franco, Chem 5 (2019) 1806-1817.

[22] L. Caliò, M. Salado, S. Kazim, S. Ahmad, Joule 2 (2018) 1800-1815.

[23] Y. Tidhar, E. Edri, H. Weissman, D. Zohar, G. Hodes, D. Cahen, B. Rybtchinski, S. Kirmayer, J. Am. Chem. Soc. 136 (2014) 13249-13256.

[24] N. Ahn, D.Y. Son, I.H. Jang, S.M. Kang, M. Choi, N.G. Park, J. Am. Chem. Soc. 137 (2015) 8696-8699.

[25] C.-C. Chen, S.H. Chang, L.-C. Chen, H.-M. Cheng, Z.-L. Tseng, C.-G. Wu, Sol. Energy 139 (2016) 518-523.

[26] J.W. Lee, Z. Dai, C. Lee, H.M. Lee, T.H. Han, N.D. Marco, O. Lin, C.S. Choi, B. Dunn, J. Koh, D. Di Carlo, J.H. Ko, H.D. Maynard, Y. Yang, J. Am. Chem. Soc. 140 (2018) 6317-6324.

[27] M. Xiao, F. Huang, W. Huang, Y. Dkhissi, Y. Zhu, J. Etheridge, A. Gray-Weale, U. Bach, Y.B. Cheng, L. Spiccia, Angew. Chem. Int. Ed. 53 (2014) 9898-9903.

[28] J.W. Jung, S.T. Williams, A.K.Y. Jen, RSC Adv. 4 (2014) 62971-62977.

[29] S. Paek, P. Schouwink, E.N. Athanasopoulou, K.T. Cho, G. Grancini, Y. Lee, Y. Zhang, F. Stellacci, M.K. Nazeeruddin, P. Gao, Chem. Mater. 29 (2017) 3490-3498.

[30] S.H. Chang, W.-C. Huang, C.-C. Chen, S.-H. Chen, C.-G. Wu, Appl. Surf. Sci. 445 (2018) 24-29.

[31] C.-C. Chen, S.H. Chang, L.-C. Chen, C.-L. Tsai, H.-M. Cheng, W.-C. Huang, W.-N. Chen, Y.-C. Lu, Z.-L. Tseng, K.Y. Chiu, S.-H. Chen, C.-G. Wu, Sol. Energy Mater. Sol. Cells 159 (2017) 583-589.

[32] X. Zheng, B. Chen, C. Wu, S. Priya, Nano Energy 17 (2015) 269-278.

[33] J.S. Yun, A. Ho-Baillie, S. Huang, S.H. Woo, Y. Heo, J. Seidel, F. Huang, Y.B. Cheng, M.A. Green, J. Phys. Chem. Lett. 6 (2015) 875-880.

[34] Q. Chen, H. Zhou, T.-B. Song, S. Luo, Z. Hong, H.-S. Duan, L. Dou, Y. Liu, Y. Yang, Nano Lett. 14 (2014) 4158–4163.

[35] D.-Y. Son, J.-W. Lee, Y.J. Choi, I.-H. Jang, S. Lee, P.J. Yoo, H. Shin, N. Ahn, M. Choi, D. Kim, N.-G. Park, Nat. Energy 1 (2016) 16081.

[36] W. Nie, H. Tsai, R. Asadpour, A.J. Neukirch, G. Gupta, J.J. Crochet, M. Chhowalla, S. Tretiak, M.A. Alam, H. Wang, J.-C. Blancon, A.J. Neukirch, G. Gupta, J.J. Crochet, M. Chhowalla, S. Tretiak, M. Alam, H. Wang, A.D. Mohite, Science 347 (2015) 522.

[37] Z. Yuan, Y. Yang, Z. Wu, S. Bai, W. Xu, T. Song, X. Gao, F. Gao, B. Sun, ACS Appl. Mater. Interfaces 8 (2016) 34446-34454.

[38] R. Yang, L. Zhang, Y. Cao, Y. Miao, Y. Ke, Y. Wei, Q. Guo, Y. Wang, Z. Rong, N. Wang, R. Li, J. Wang, W. Huang, F. Gao, Appl. Phys. Lett. 111 (2017) 073302.

[39] K.-M. Lee, C.-J. Lin, B.-Y. Liou, S.-M. Yu, C.-C. Hsu, V. Suryanarayanan, Org. Electron. 65 (2019) 266-274.

[40] D.D. Girolamo, N. Phung, F.U. Kosasih, F.D. Giacomo, F. Matteocci, J.A. Smith, M.A. Flatken, H. Köbler, S.H.T. Cruz, A. Mattoni, L. Cinà, B. Rech, A. Latini, G. Divitini, C. Ducati, A.D. Carlo, D. Dini, A. Abate, Adv. Energy Mater. 10 (2020) 2000310.

[41] Z. Ren, N. Wang, P. Wei, M. Cui, X. Li, C. Qin, Chem. Eng. J. 393 (2020) 124731.

[42] Y. Yun, F. Wang, H. Huang, Y. Fang, S. Liu, W. Huang, Z. Cheng, Y. Liu, Y. Cao, M. Gao, L. Zhu, L. Wang, T. Qin, W. Huang, Adv. Mater. 32 (2020) 1907123.

[43] F. Zhang, C. Xiao, X. Chen, B.W. Larson, S.P. Harvey, J.J. Berry, K. Zhu, Joule 3 (2019) 1452-1463.

[44] Y. Zhou, M. Yang, W. Wu, A.L. Vasiliev, K. Zhu, N.P. Padture, J. Mater. Chem. A 3 (2015) 8178-8184.

[45] T. Bu, X. Liu, J. Li, W. Huang, Z. Wu, F. Huang, Y.-B. Cheng, J. Zhong, Sol. RRL 4 (2019) 1900263.

[46] G. Jang, H.C. Kwon, S. Ma, S.C. Yun, H. Yang, J. Moon, Adv. Energy Mater. 9 (2019) 1901719.

[47] G. Murugadoss, R. Thangamuthu, M.R. Kumar, S.K.S. Murugesan, V. Prabu, Mater. Lett. 205 (2017) 130-133.

[48] T. Gotanda, H. Oooka, S. Mori, H. Nakao, A. Amano, K. Todori, Y. Nakai, K. Mizuguchi, J. Power Sources 430 (2019) 145-149.

[49] Y. Zhou, M. Yang, O.S. Game, W. Wu, J. Kwun, M.A. Strauss, Y. Yan, J. Huang, K. Zhu, N.P. Padture, ACS Appl. Mater. Interfaces 8 (2016) 2232-2237.

[50] T. Bu, L. Wu, X. Liu, X. Yang, P. Zhou, X. Yu, T. Qin, J. Shi, S. Wang, S. Li, Z. Ku, Y. Peng, F.

Huang, Q. Meng, Y.-B. Cheng, J. Zhong, Adv. Energy Mater. 7 (2017) 1700576.

[51]   J. Li, R. Yang, L. Que, Y. Wang, F. Wang, J. Wu, S. Li, J. Mater. Res. 34 (2019) 2416-2424.

[52]   P. Zhao, B.J. Kim, X. Ren, D.G. Lee, G.J. Bang, J.B. Jeon, W.B. Kim, H.S. Jung, Adv. Mater. 30 (2018) 1802763.

[53]   G. Murugadoss, R. Thangamuthu, S.M.S. Kumar, N. Anandhan, M.R. Kumar, A. Rathishkumar, J. Alloys Compd. 787 (2019) 17-26.

[54]   Q. Wang, X. Zheng, Y. Deng, J. Zhao, Z. Chen, J. Huang, Joule 1 (2017) 371-382.

[55]   J. Das, A.S. Subbiah, N. Mahuli, R. Singh, S.K. Sarkar, Energy Technol. 5 (2017) 1807-1813.

[56]   X. Xu, C.-C. Chueh, Z. Yang, A. Rajagopal, J. Xu, S.B. Jo, A.K.Y. Jen, Nano Energy 34 (2017) 392-398.

[57]   C. Bi, B. Chen, H. Wei, S. DeLuca, J. Huang, Adv. Mater. 29 (2017) 1605900.

[58]   G. Kapil, T. Bessho, C.H. Ng, K. Hamada, M. Pandey, M.A. Kamarudin, D. Hirotani, T. Kinoshita, T. Minemoto, Q. Shen, T. Toyoda, T.N. Murakami, H. Segawa, S. Hayase, ACS Energy Lett. 4 (2019) 1991-1998.

[59]   G. Kapil, T.S. Ripolles, K. Hamada, Y. Ogomi, T. Bessho, T. Kinoshita, J. Chantana, K. Yoshino, Q. Shen, T. Toyoda, T. Minemoto, T.N. Murakami, H. Segawa, S. Hayase, Nano Lett. 18 (2018) 3600-3607.

[60]   F. Wang, Z. Ye, H. Sarvari, S.M. Park, A. Abtahi, K. Graham, Y. Zhao, Y. Wang, Z.D. Chen, S. Li, J. Power Sources 412 (2019) 359-365.

[61]   R. Prasanna, T. Leijtens, S.P. Dunfield, J.A. Raiford, E.J. Wolf, S.A. Swifter, J. Werner, G.E. Eperon, C. de Paula, A.F. Palmstrom, C.C. Boyd, M.F.A.M. van Hest, S.F. Bent, G. Teeter, J.J. Berry, M.D. McGehee, Nat. Energy 4 (2019) 939-947.

[62]   C. Li, R. Ma, X. He, T. Yang, Z. Zhou, S. Yang, Y. Liang, X.W. Sun, J. Wang, Y. Yan, W.C.H. Choy, Adv. Energy Mater. 10 (2020) 1903013.

[63]   Y. Li, J. Wang, Y. Yuan, X. Dong, P. Wang, Sustain. Energy Fuels 1 (2017) 1041-1048.

[64]   M.M. Byranvand, S. Song, L. Pyeon, G. Kang, G.-Y. Lee, T. Park, Nano Energy 34 (2017) 181–187.

[65]   F. Wang, M. Yang, S. Yang, X. Qu, L. Yang, L. Fan, J. Yang, F. Rosei, Nano Energy 67 (2020) 104224.

[66]   Y. Yang, S. Feng, M. Li, F. Li, C. Zhang, Y. Han, L. Li, J. Yuan, L. Cao, Z. Wang, B. Sun, X. Gao, Nano Energy 48 (2018) 10-19.

[67]   R. Ranjan, B. Usmani, S. Ranjan, H.C. Weerasinghe, A. Singh, A. Garg, R.K. Gupta, Sol. Energy Mater. Sol. Cells 202 (2019) 110130.

[68]   Y. Cao, H. Wu, W. Li, Z. Zhao, Z. Xiao, W. Zi, N. Cheng, J. Liu, Y. Tu, Org. Electron. 76 (2020) 105455.

[69]   H. Zong, Y.-H. Lou, M. Li, K.-L. Wang, S.M. Jain, Z.-K. Wang, Org. Electron. 77 (2020) 105495.

[70]   Y. Lv, Y. Jin, W. Cai, Z. Zhang, X. Zhou, H. Chen, J. Alloys Compd. 821 (2020) 153272.

[71]   J. Troughton, K. Hooper, T.M. Watson, Nano Energy 39 (2017) 60-68.

[72]   C. Liu, M. Wu, Y. Wu, D. Wang, T. Zhang, J. Power Sources 447 (2020) 227389.

[73]   S. Kim, I. Jeong, C. Park, G. Kang, I.K. Han, W. Kim, M. Park, Sol. Energy Mater. Sol. Cells 203 (2019) 110197.

[74]   R. Lin, K. Xiao, Z. Qin, Q. Han, C. Zhang, M. Wei, M.I. Saidaminov, Y. Gao, J. Xu, M. Xiao, A. Li, J. Zhu, E.H. Sargent, H. Tan, Nat. Energy 4 (2019) 864-873.

[75] K. Kara, D.A. Kara, C. Kırbıyık, M. Ersoz, O. Usluer, A.L. Briseno, M. Kus, RSC Adv. 6 (2016) 26606-26611.

[76] G. Niu, H. Yu, J. Li, D. Wang, L. Wang, Nano Energy 27 (2016) 87-94.

[77] S. Michael, M. Taisuke, D. Konrad, S. Ji-Youn, U. Amita, M.Z. Shaik, C.-B. Juan-Pablo, R.T. Wolfgang, A. Antonio, H. Anders, G. Michael, Science 354 (2016) 206.

[78] C.-C. Chueh, K. Yao, H.-L. Yip, C.-Y. Chang, Y.-X. Xu, K.-S. Chen, C.-Z. Li, P. Liu, F. Huang, Y. Chen, W.-C. Chen, A.K.Y. Jen, Energy Environ. Sci. 6 (2013) 3241.

[79] J. Yi, J. Zhuang, Z. Ma, Z. Guo, W. Zhou, S. Zhao, H. Zhang, X. Luo, H. Li, Org. Electron. 69 (2019) 69-76.

[80] J.L. Shea, Clin. Chem. Lab. Med. 51 (2013) 205-212.

[81] M. Yavari, M. Mazloum-Ardakani, S. Gholipour, M.M. Tavakoli, S.-H. Turren-Cruz, N. Taghavinia, M. Grätzel, A. Hagfeldt, M. Saliba, Adv. Energy Mater. 8 (2018) 1800177.

[82] M. Zhang, Z. Wang, B. Zhou, X. Jia, Q. Ma, N. Yuan, X. Zheng, J. Ding, W.H. Zhang, Sol. RRL 2 (2018) 1700213.

[83] F. Umar, J. Zhang, Z. Jin, I. Muhammad, X. Yang, H. Deng, K. Jahangeer, Q. Hu, H. Song, J. Tang, Adv. Opt. Mater. 7 (2019) 1801368.

[84] Q. Li, Y. Zhao, W. Zhou, Z. Han, R. Fu, F. Lin, D. Yu, Q. Zhao, Adv. Energy Mater. 9 (2019) 1902239.

[85] C. Wang, J. Zhang, L. Jiang, L. Gong, H. Xie, Y. Gao, H. He, Z. Fang, J. Fan, Z. Chao, J. Alloys Compd. 817 (2020) 152768.

[86] C. Capello, U. Fischer, K. Hungerbühler, Green Chem. 9 (2007) 927.

[87] D. Gedamu, I.M. Asuo, D. Benetti, M. Basti, I. Ka, S.G. Cloutier, F. Rosei, R. Nechache, Sci. Rep. 8 (2018) 12885.

[88] J. Chen, J. Ren, Z. Li, H. Wang, Y. Hao, Org. Electron. 56 (2018) 59-67.

[89] Y. Yu, S. Yang, L. Lei, Q. Cao, J. Shao, S. Zhang, Y. Liu, ACS Appl. Mater. Interfaces 9 (2017) 3667-3676.

[90] N. Sakai, S. Pathak, H.-W. Chen, A.A. Haghighirad, S.D. Stranks, T. Miyasaka, H.J. Snaith, J. Mater. Chem. A 4 (2016) 4464-4471.

[91] M. Deepa, M. Salado, L. Calio, S. Kazim, S.M. Shivaprasad, S. Ahmad, Phys. Chem. Chem. Phys. 19 (2017) 4069-4077.

[92] X. Liu, Z. Yang, C.-C. Chueh, A. Rajagopal, S.T. Williams, Y. Sun, A.K.Y. Jen, J. Mater. Chem. A 4 (2016) 17939-17945.

[93] W. Hu, X. He, Z. Fang, W. Lian, Y. Shang, X. Li, W. Zhou, M. Zhang, T. Chen, Y. Lu, L. Zhang, L. Ding, S. Yang, Nano Energy 68 (2020) 104362.

[94] X. Liu, Z. Liu, X. Tan, H. Ye, B. Sun, S. Xi, T. Shi, Z. Tang, G. Liao, J. Power Sources 439 (2019) 227092.

[95] J. Liu, M. Ozaki, S. Yakumaru, T. Handa, R. Nishikubo, Y. Kanemitsu, A. Saeki, Y. Murata, R. Murdey, A. Wakamiya, Angew. Chem. Int. Ed. 57 (2018) 13221-13225.

[96] D. Chi, S. Huang, M. Zhang, S. Mu, Y. Zhao, Y. Chen, J. You, Adv. Funct. Mater. 28 (2018) 1804603.

[97] M. Abulikemu, S. Ould-Chikh, X. Miao, E. Alarousu, B. Murali, G.O.N. Ndjawa, J. Barbé, A.E. Labban, A. Amassian, S.D. Gobbo, J. Mater. Chem. A 4 (2016) 12504-12515.

[98] S.S. Mali, H. Kim, D.-H. Kim, C.K. Hong, ChemistrySelect 2 (2017) 1578-1585.

[99]   S.S. Shin, J.P.C. Baena, R.C. Kurchin, A. Polizzotti, J.J. Yoo, S. Wieghold, M.G. Bawendi, T. Buonassisi, Chem. Mater. 30 (2018) 336-343.

[100] W. Liao, D. Zhao, Y. Yu, N. Shrestha, K. Ghimire, C.R. Grice, C. Wang, Y. Xiao, A.J. Cimaroli, R.J. Ellingson, N.J. Podraza, K. Zhu, R.G. Xiong, Y. Yan, J. Am. Chem. Soc. 138 (2016) 12360-12363.

[101] D. Zhao, Y. Yu, C. Wang, W. Liao, N. Shrestha, C.R. Grice, A.J. Cimaroli, L. Guan, R.J. Ellingson, K. Zhu, X. Zhao, R.-G. Xiong, Y. Yan, Nat. Energy 2 (2017) 17018.

[102] W. Zhang, Y. Li, X. Liu, D. Tang, X. Li, X. Yuan, Chem. Eng. J. 379 (2020) 122298.

[103] L. Wang, X. Wang, L.-L. Deng, S. Leng, X. Guo, C.-H. Tan, W.C.H. Choy, C.-C. Chen, Mater. Horizons (2020)

[104] C. Dong, X. Han, W. Li, Q. Qiu, J. Wang, Nano Energy 59 (2019) 553-559.

[105] L. Liang, Z. Li, F. Zhou, Q. Wang, H. Zhang, Z. Xu, L. Ding, S. Liu, Z. Jin, J. Mater. Chem. A 7 (2019) 26776-26784.

[106] W. Chen, H. Chen, G. Xu, R. Xue, S. Wang, Y. Li, Y. Li, Joule 3 (2019) 191-204.

[107] X. Du, R. Qiu, T. Zou, X. Chen, H. Chen, H. Zhou, Adv. Mater. Interfaces 6 (2019) 1900413.

[108] H. Li, Y. Xia, C. Wang, G. Wang, Y. Chen, L. Guo, D. Luo, S. Wen, ACS Appl. Mater. Interfaces 11 (2019) 34989-34996.

[109] H. Mao, Y. Huang, Z. Ma, L. Jin, L. Tian, Y. Li, H. Yu, C. Peng, J. Mater. Sci. - Mater. Electron. 30 (2019) 3511-3520.

[110] H.B. Lee, M.K. Jeon, N. Kumar, B. Tyagi, J.W. Kang, Adv. Funct. Mater. 29 (2019) 1903213.

[111] N. Kumar, H.B. Lee, S. Hwang, J.-W. Kang, J. Mater. Chem. A 8 (2020) 3357-3368.

[112] N. Lin, J. Qiao, H. Dong, F. Ma, L. Wang, J. Mater. Chem. A 3 (2015) 22839-22845.

[113] S. Sidhik, D. Esparza, T. López-Luke, E. De la Rosa, Sol. Energy Mater. Sol. Cells 163 (2017) 224-230.

[114] M. Yang, Z. Li, M.O. Reese, O.G. Reid, D.H. Kim, S. Siol, T.R. Klein, Y. Yan, J.J. Berry, M.F.A.M. van Hest, K. Zhu, Nat. Energy 2 (2017) 17038.

[115] J.-H. Im, H.-S. Kim, N.-G. Park, APL Mater. 2 (2014) 081510.

[116] Y. Rong, Z. Tang, Y. Zhao, X. Zhong, S. Venkatesan, H. Graham, M. Patton, Y. Jing, A.M. Guloy, Y. Yao, Nanoscale 7 (2015) 10595-10599.

[117] M. Ozaki, A. Shimazaki, M. Jung, Y. Nakaike, N. Maruyama, S. Yakumaru, A.I. Rafieh, T. Sasamori, N. Tokitoh, P. Ekanayake, Y. Murata, R. Murdey, A. Wakamiya, Angew. Chem. Int. Ed. 58 (2019) 9389-9393.

[118] Y. Dong, P. Zeng, Y. Yu, Y. Xie, B. Yang, R. Liang, Q. Ou, S. Zhang, Adv. Electron. Mater. 6 (2020) 1901162.

[119] K. Wang, M.-C. Tang, H.X. Dang, R. Munir, D. Barrit, M.D. Bastiani, E. Aydin, D.-M. Smilgies, S.D. Wolf, A. Amassian, Adv. Mater. 31 (2019) 1808357.

[120] S.G. Kwon, T. Hyeon, Small 7 (2011) 2685-2702.

[121] N.T. Thanh, N. Maclean, S. Mahiddine, Chem. Rev. 114 (2014) 7610-7630.

[122] M.I. Saidaminov, A.L. Abdelhady, B. Murali, E. Alarousu, V.M. Burlakov, W. Peng, I. Dursun, L. Wang, Y. He, G. Maculan, A. Goriely, T. Wu, O.F. Mohammed, O.M. Bakr, Nat. Commun. 6 (2015) 7586.

[123] Y.-K. Ren, X.-H. Ding, Y.-H. Wu, J. Zhu, T. Hayat, A. Alsaedi, Y.-F. Xu, Z.-Q. Li, S.-F. Yang, S.-Y. Dai, J. Mater. Chem. A 5 (2017) 20327-20333.

[124] C. Fei, L. Guo, B. Li, R. Zhang, H. Fu, J. Tian, G. Cao, Nano Energy 27 (2016) 17-26.

[125] J.-Y. Seo, T. Matsui, J. Luo, J.-P. Correa-Baena, F. Giordano, M. Saliba, K. Schenk, A. Ummadisingu, K. Domanski, M. Hadadian, A. Hagfeldt, S.M. Zakeeruddin, U. Steiner, M. Grätzel, A. Abate, Adv. Energy Mater. 6 (2016) 1600767.

[126] Z. Liu, J. Hu, H. Jiao, L. Li, G. Zheng, Y. Chen, Y. Huang, Q. Zhang, C. Shen, Q. Chen, H. Zhou, Adv. Mater. 29 (2017) 1606774.

[127] Y. Guo, J. Ma, H. Lei, F. Yao, B. Li, L. Xiong, G. Fang, J. Mater. Chem. A 6 (2018) 5919-5925.

[128] J. Duan, Y. Zhao, X. Yang, Y. Wang, B. He, Q. Tang, Adv. Energy Mater. 8 (2018) 1802346.

[129] P. Luo, W. Xia, S. Zhou, L. Sun, J. Cheng, C. Xu, Y. Lu, J. Phys. Chem. Lett. 7 (2016) 3603-3608.

[130] M.M. Tavakoli, P. Yadav, D. Prochowicz, M. Sponseller, A. Osherov, V. Bulović, J. Kong, Adv. Energy Mater. 9 (2019) 1803587.

[131] X. Jiang, F. Wang, Q. Wei, H. Li, Y. Shang, W. Zhou, C. Wang, P. Cheng, Q. Chen, L. Chen, Z. Ning, Nat. Commun. 11 (2020) 1245.

[132] W. Liao, D. Zhao, Y. Yu, C.R. Grice, C. Wang, A.J. Cimaroli, P. Schulz, W. Meng, K. Zhu, R.-G. Xiong, Y. Yan, Adv. Mater. 28 (2016) 9333-9340.

[133] D. Wu, P. Jia, W. Bi, Y. Tang, J. Zhang, B. Song, L. Qin, Z. Lou, Y. Hu, F. Teng, Y. Hou, Org. Electron. 82 (2020) 105728.

[134] T.T. Ngo, I. Suarez, G. Antonicelli, D. Cortizo-Lacalle, J.P. Martinez-Pastor, A. Mateo-Alonso, I. Mora-Sero, Adv. Mater. 29 (2017) 1604056.

[135] F. Han, J. Luo, Z. Wan, X. Liu, C. Jia, Appl. Surf. Sci. 408 (2017) 34-37.

[136] F. Li, J. Yuan, X. Ling, Y. Zhang, Y. Yang, S.H. Cheung, C.H.Y. Ho, X. Gao, W. Ma, Adv. Funct. Mater. 28 (2018) 1706377.

[137] C. Ji, C. Liang, H. Zhang, M. Sun, F. Sun, Q. Song, X. Zhang, D. Li, F. You, Z. He, Org. Electron. 63 (2018) 276-282.

[138] L. Qiu, L. Dong, D. Mei, W.-H. Chen, L. Song, J. Wang, J. Zou, P.-C. Jiang, P. Du, J. Xiong, J. Mater. Chem. C 8 (2020) 12560-12567.

[139] W. Zeng, D. Cui, Z. Li, Y. Tang, X. Yu, Y. Li, Y. Deng, R. Ye, Q. Niu, R. Xia, Y. Min, Sol. Energy 194 (2019) 272-278.

[140] F. Zhang, W. Shi, J. Luo, N. Pellet, C. Yi, X. Li, X. Zhao, T.J.S. Dennis, X. Li, S. Wang, Y. Xiao, S.M. Zakeeruddin, D. Bi, M. Grätzel, Adv. Mater. 29 (2017) 1606806.

[141] W. Xu, Y. Gao, W. Ming, F. He, J. Li, X.H. Zhu, F. Kang, J. Li, G. Wei, Adv. Mater. 32 (2020) 2003965.

[142] Y. Li, J. Shi, J. Zheng, J. Bing, J. Yuan, Y. Cho, S. Tang, M. Zhang, Y. Yao, C.F.J. Lau, D.S. Lee, C. Liao, M.A. Green, S. Huang, W. Ma, A.W.Y. Ho-Baillie, Adv. Sci. 7 (2020) 1903368.

[143] G. Han, T.M. Koh, S.S. Lim, T.W. Goh, X. Guo, S.W. Leow, R. Begum, T.C. Sum, N. Mathews, and S. Mhaisalkar, ACS Appl. Mater. Interfaces 9 (2017) 21292–21297.

[144] S. Jin, Y. Wei, F. Huang, X. Yang, D. Luo, Y. Fang, Y. Zhao, Q. Guo, Y. Huang, J. Wu, J. Power Sources 404 (2018) 64-72.

[145] P.L. Qin, G. Yang, Z.W. Ren, S.H. Cheung, S.K. So, L. Chen, J. Hao, J. Hou, G. Li, Adv. Mater. 30 (2018) e1706126.

[146] J. Yi, J. Zhuang, X. Liu, H. Wang, Z. Ma, D. Huang, Z. Guo, H. Li, J. Alloys Compd. 830 (2020) 154710.

[147]   C.V. Thompson, Annu. Rev. Mater. Sci. 42 (2012) 399-434.

[148]   J. Burschka, N. Pellet, S.J. Moon, R. Humphry-Baker, P. Gao, M.K. Nazeeruddin, M. Grätzel, Nature 499 (2013) 316-319.

[149]   H. Krautscheid, F. Vielsack, J. Chem. Soc., Dalton Trans. 16 (1999) 2731–2735.

[150]   I. Wharf, T. Gramstad, R. Makhija, M. Onyszchuk, ChemInform 54 (1976) 3431-3438.

[151]   J.C. Hamill, J. Schwartz, Y.-L. Loo, ACS Energy Lett. 3 (2017) 92-97.

[152]   X. Cao, C. Li, Y. Li, F. Fang, X. Cui, Y. Yao, J. Wei, Nanoscale 8 (2016) 19804-19810.

[153]   S. Rahimnejad, A. Kovalenko, S.M. Fores, C. Aranda, A. Guerrero, ChemPhysChem 17 (2016) 2795-2798.

[154]   A. Wakamiya, M. Endo, T. Sasamori, N. Tokitoh, Y. Ogomi, S. Hayase, Y. Murata, Chem. Lett. 43 (2014) 711-713.

[155]   J.-W. Lee, H.-S. Kim, N.-G. Park, Acc. Chem. Res. 49 (2016) 311-319.

[156]   L. Lou, T. Liu, J. Xiao, S. Xiao, X. Long, S. Zheng, S. Yang, Energy Technol. 8 (2020) 1900972.

[157]   X. Cao, L. Zhi, Y. Li, F. Fang, X. Cui, Y. Yao, L. Ci, K. Ding, J. Wei, ACS Appl. Mater. Interfaces 9 (2017) 32868-32875.

[158]   Y. Ren, X. Ding, J. Zhu, T. Hayat, A. Alsaedi, Z. Li, X. Xu, Y. Ding, S. Yang, M. Kong, S. Dai, J. Alloys Compd. 758 (2018) 171-176.

[159]   Y. Li, D. Song, J. Meng, J. Dong, Y. Lu, X. Huo, A. Maqsood, Y. Song, S. Zhao, B. Qiao, Z. Xu, J. Mater. Sci. 55 (2020) 9787-9794.

[160]   K.-S. Lim, D.-K. Lee, J.-W. Lee, N.-G. Park, J. Mater. Chem. A 8 (2020) 9345-9354.

[161]   J. Luo, J. Xia, H. Yang, H.A. Malik, F. Han, H. Shu, X. Yao, Z. Wan, C. Jia, Nano Energy 70 (2020) 104509.

[162]   Q. Jia, C. Li, W. Tian, M.B. Johansson, E.M.J. Johansson, R. Yang, ACS Appl. Mater. Interfaces 12 (2020) 43876-43884.

[163]   A. Singh, S. Najman, A. Mohapatra, Y.J. Lu, C. Hanmandlu, C.W. Pao, Y.F. Chen, C.S. Lai, C.W. Chu, ACS Appl. Mater. Interfaces 12 (2020) 32649-32657.

[164]   T. Niu, J. Lu, R. Munir, J. Li, D. Barrit, X. Zhang, H. Hu, Z. Yang, A. Amassian, K. Zhao, S.F. Liu, Adv. Mater. 30 (2018) 1706576.

[165]   A. Abate, M. Saliba, D.J. Hollman, S.D. Stranks, K. Wojciechowski, R. Avolio, G. Grancini, A. Petrozza, H.J. Snaith, Nano Lett. 14 (2014) 3247-3254.

[166]   N. K. Noel, A. Abate, S.D. Stranks, E.S. Parrott, V.M. Burlakov, A. Goriely, H.J. Snaith, ACS Nano 8 (2014) 9815.

[167]   Y. Lin, L. Shen, J. Dai, Y. Deng, Y. Wu, Y. Bai, X. Zheng, J. Wang, Y. Fang, H. Wei, W. Ma, X.C. Zeng, X. Zhan, J. Huang, Adv. Mater. 29 (2017) 1604545.

[168]   J.-W. Lee, S.-H. Bae, Y.-T. Hsieh, N.D. Marco, M. Wang, P. Sun, Y. Yang, Chem 3 (2017) 290-302.

[169]   Z. Yang, J. Dou, S. Kou, J. Dang, Y. Ji, G. Yang, W.Q. Wu, D.B. Kuang, M. Wang, Adv. Funct. Mater. 30 (2020) 1910710.

[170]   K. Sun, Z. Hu, B. Shen, C. Lu, L. Huang, J. Zhang, J. Zhang, Y. Zhu, ACS Appl. Energy Mater. 1 (2018) 2114-2122.

[171]   T. Yokoyama, D.H. Cao, C.C. Stoumpos, T.-B. Song, Y. Sato, S. Aramaki, M.G. Kanatzidis, J. Phys. Chem. Lett. 7 (2016) 776-782.

[172]   S.J. Lee, S.S. Shin, Y.C. Kim, D. Kim, T.K. Ahn, J.H. Noh, J. Seo, S.I. Seok, J. Am. Chem. Soc.

138 (2016) 3974-3977.

[173] F. Hao, C.C. Stoumpos, P. Guo, N. Zhou, T.J. Marks, R.P. Chang, M.G. Kanatzidis, J. Am. Chem. Soc. 137 (2015) 11445-11452.

[174] J. Su, Y.-q. Huang, H. Chen, J. Huang, Cryst. Res. Technol. 55 (2020) 1900222.

[175] B. Lee, A. Krenselewski, S.I. Baik, D.N. Seidman, R.P.H. Chang, Sustain. Energy Fuels 1 (2017) 710-724.

[176] Y. Jiang, H. Zhang, X. Qiu, B. Cao, Mater. Lett. 199 (2017) 50-52.

[177] J. Qing, H.T. Chandran, Y.H. Cheng, X.K. Liu, H.W. Li, S.W. Tsang, M.F. Lo, C.S. Lee, ACS Appl. Mater. Interfaces 7 (2015) 23110-23116.

[178] Q. Dong, Y. Yuan, Y. Shao, Y. Fang, Q. Wang, J. Huang, Energy Environ. Sci. 8 (2015) 2464-2470.

[179] Q. Chen, H. Zhou, Y. Fang, A.Z. Stieg, T.B. Song, H.H. Wang, X. Xu, Y. Liu, S. Lu, J. You, P. Sun, J. McKay, M.S. Goorsky, Y. Yang, Nat. Commun. 6 (2015) 7269.

[180] P. Docampo, F.C. Hanusch, S.D. Stranks, M. Döblinger, J.M. Feckl, M. Ehrensperger, N.K. Minar, M.B. Johnston, H.J. Snaith, T. Bein, Adv. Energy Mater. 4 (2014) 1400355.

[181] Y. Zhao, K. Zhu, J. Phys. Chem. C 118 (2014) 9412-9418.

[182] S. Colella, E. Mosconi, P. Fedeli, A. Listorti, A. Rizzo, F. Gazza, F. Orlandi, P. Ferro, T. Besagni, G. Calestani, F.D. Angelis, R. Mosca, G. Gigli, Chem. Mater. 1667 (2014) 4613–4618.

[183] S. Colella, E. Mosconi, G. Pellegrino, A. Alberti, V.L. Guerra, S. Masi, A. Listorti, A. Rizzo, G.G. Condorelli, F.D. Angelis, G. Gigli, J. Phys. Chem. Lett. 5 (2014) 3532-3538.

[184] Z. Liu, L. Qiu, E.J. Juarez-Perez, Z. Hawash, T. Kim, Y. Jiang, Z. Wu, S.R. Raga, L.K. Ono, S. F. Liu, Y.B. Qi, Nat. Commun. 9 (2018) 3880.

[185] Y. Wu, X. Li, S. Fu, L. Wan, J. Fang, J. Mater. Chem. A 7 (2019) 8078-8084.

[186] M. Kim, G.-H. Kim, T.K. Lee, I.W. Choi, H.W. Choi, Y. Jo, Y.J. Yoon, J.W. Kim, J. Lee, D. Huh, H. Lee, S.K. Kwak, J.Y. Kim, D.S. Kim, Joule 3 (2019) 2179-2192.

[187] Y. Liu, S. Akin, A. Hinderhofer, F.T. Eickemeyer, H. Zhu, J.Y. Seo, J. Zhang, F. Schreiber, H. Zhang, S.M. Zakeeruddin, A. Hagfeldt, M.I. Dar, M. Grätzel, Angew. Chem. Int. Ed. 59 (2020) 15688-15694.

[188] Z. Wang, Y. Zhou, S. Pang, Z. Xiao, J. Zhang, W. Chai, H. Xu, Z. Liu, N.P. Padture, G. Cui, Chem. Mater. 27 (2015) 7149-7155.

[189] M. Lyu, N.-G. Park, Sol. RRL 4 (2020) 2000331.

[190] T.-H. Han, J.-W. Lee, C. Choi, S. Tan, C. Lee, Y. Zhao, Z. Dai, N.D. Marco, S.-J. Lee, S.-H. Bae, Nat. Commun. 10 (2019) 520.

[191] S. Xiong, J. Song, J. Yang, J. Xu, M. Zhang, R. Ma, D. Li, X. Liu, F. Liu, C. Duan, M. Fahlman, Q. Bao, Sol. RRL 4 (2020) 1900529.

[192] M. Saliba, T. Matsui, K. Domanski, J.-Y. Seo, A. Ummadisingu, S.M. Zakeeruddin, J.-P. Correa-Baena, W.R. Tress, A. Abate, A. Hagfeldt, M. Grätzel, Science 354 (2016) 206.

[193] Y. Sheng, Y. Hu, A. Mei, P. Jiang, X. Hou, M. Duan, L. Hong, Y. Guan, Y. Rong, Y. Xiong, H. Han, J. Mater. Chem. A 4 (2016) 16731-16736.

[194] K.M. Boopathi, R. Mohan, T.-Y. Huang, W. Budiawan, M.-Y. Lin, C.-H. Lee, K.-C. Ho, C.-W. Chu, J. Mater. Chem. A 4 (2016) 1591-1597.

[195] P. Wang, J. Wang, X. Zhang, H. Wang, X. Cui, S. Yuan, H. Lu, L. Tu, Y. Zhan, L. Zheng, J. Mater. Chem. A 6 (2018) 15853-15858.

[196] Q. Li, Y. Zhao, R. Fu, W. Zhou, Y. Zhao, X. Liu, D. Yu, Q. Zhao, Adv. Mater. 30 (2018) 1803095.

[197] A. Ren, H. Lai, X. Hao, Z. Tang, H. Xu, B.M.F.Y. Jeco, K. Watanabe, L. Wu, J. Zhang, M. Sugiyama, J. Wu, D. Zhao, Joule 4 (2020) 1263-1277.

[198] S. Yang, J. Dai, Z. Yu, Y. Shao, Y. Zhou, X. Xiao, X.C. Zeng, J. Huang, J. Am. Chem. Soc. 141 (2019) 5781-5787.

[199] X. Li, M.I. Dar, C. Yi, J. Luo, M. Tschumi, S.M. Zakeeruddin, M.K. Nazeeruddin, H. Han, M. Grätzel, Nat. Chem. 7 (2015) 703-711.

[200] M.A. Ruiz-Preciado, D.J. Kubicki, A. Hofstetter, L. McGovern, M.H. Futscher, A. Ummadisingu, R. Gershoni-Poranne, S.M. Zakeeruddin, B. Ehrler, L. Emsley, J.V. Milic, M. Grätzel, J. Am. Chem. Soc. 142 (2020) 1645-1654.

[201] X. Zheng, Y. Hou, C. Bao, J. Yin, F. Yuan, Z. Huang, K. Song, J. Liu, J. Troughton, N. Gasparini, C. Zhou, Y. Lin, D.-J. Xue, B. Chen, A.K. Johnston, N. Wei, M.N. Hedhili, M. Wei, A.Y. Alsalloum, P. Maity, B. Turedi, C. Yang, D. Baran, T.D. Anthopoulos, Y. Han, Z.-H. Lu, O.F. Mohammed, F. Gao, E.H. Sargent, O.M. Bakr, Nat. Energy 5 (2020) 131-140.

[202] B. Li, C. Fei, K. Zheng, X. Qu, T. Pullerits, G. Cao, J. Tian, J. Mater. Chem. A 4 (2016) 17018-17024.

[203] X. Li, W. Zhang, Y.C. Wang, W. Zhang, H.Q. Wang, J. Fang, Nat. Commun. 9 (2018) 3806.

[204] D.P. McMeekin, Z. Wang, W. Rehman, F. Pulvirenti, J.B. Patel, N.K. Noel, M.B. Johnston, S.R. Marder, L.M. Herz, H.J. Snaith, Adv. Mater. 29 (2017) 1607039.

[205] H. Tsai, W. Nie, Y.-H. Lin, J.C. Blancon, S. Tretiak, J. Even, G. Gupta, P.M. Ajayan, A.D. Mohite, Adv. Energy Mater. 7 (2017) 1602159.

[206] R. Singh, V.K. Shukla, Sol. Energy 178 (2019) 90-97.

[207] Y. Zhou, Y. Yin, X. Zuo, L. Wang, T.-D. Li, Y. Zhou, N.P. Padture, Z. Yang, Y. Guo, Y. Xue, K. Kisslinger, M. Cotlet, C.-Y. Nam, M.H. Rafailovich, Chem. Mater. 32 (2020) 5104-5117.

[208] Y. Bai, Y. Lin, L. Ren, X. Shi, E. Strounina, Y. Deng, Q. Wang, Y. Fang, X. Zheng, Y. Lin, Z.-G. Chen, Y. Du, L. Wang, J. Huang, ACS Energy Lett. 4 (2019) 1231-1240.

[209] J. Yang, S. Xiong, T. Qu, Y. Zhang, X. He, X. Guo, Q. Zhao, S. Braun, J. Chen, J. Xu, Y. Li, X. Liu, C. Duan, J. Tang, M. Fahlman, Q. Bao, ACS Appl. Mater. Interfaces 11 (2019) 13491-13498.

[210] J. Li, H. Wang, X.Y. Chin, H.A. Dewi, K. Vergeer, T.W. Goh, J.W.M. Lim, J.H. Lew, K.P. Loh, C. Soci, T.C. Sum, H.J. Bolink, N. Mathews, S. Mhaisalkar, A. Bruno, Joule 4 (2020) 1035-1053.

[211] X. Zhu, D. Yang, R. Yang, B. Yang, Z. Yang, X. Ren, J. Zhang, J. Niu, J. Feng, S. Liu, Nanoscale 9 (2017) 12316-12323.

[212] Y.H. Chiang, M. Anaya, S.D. Stranks, ACS Energy Lett. 5 (2020) 2498-2504.

[213] A.M. Igual-Muñoz, J. Ávila, P.P. Boix, H.J. Bolink, Sol. RRL 4 (2019) 1900283.

[214] L. Gil-Escrig, C. Momblona, M.-G. La-Placa, P.P. Boix, M. Sessolo, H.J. Bolink, Adv. Energy Mater. 8 (2018) 1703506.

[215] L.K. Ono, S. Wang, Y. Kato, Y.B. Qi, Energy Environ. Sci. 7 (2014) 3989.

[216] S. Wang, L.K. Ono, M.R. Leyden, Y. Kato, S.R. Raga, M.V. Lee, Y.B. Qi, J. Mater. Chem. A 3 (2015) 14631.

[217] S. Wang, X. Li, J. Wu, W. Wen, Y.B. Qi, Curr. Opin. Electrochem. 11 (2018) 130.

[218] J. Borchert, R.L. Milot, J.B. Patel, C.L. Davies, A.D. Wright, L.M. Maestro, H.J. Snaith, L.M. Herz, M.B. Johnston, ACS Energy Lett. 2 (2017) 2799-2804.

[219] X. Zhu, D. Yang, R. Yang, B. Yang, Z. Yang, X. Ren, J. Zhang, J. Niu, J. Feng, S.F. Liu, Nanoscale 9 (2017) 12316-12323.

[220] M. Chen, M.-G. Ju, H.F. Garces, A.D. Carl, L.K. Ono, Z. Hawash, Y. Zhang, T. Shen, Y.B. Qi, R.L. Grimm, D. Pacifici, X.C. Zeng, Y. Zhou, N.P. Padture, Nat. Commun. 10 (2019) 16.

[221] H. Peng, Z. Su, Z. Zheng, H. Lan, J. Luo, P. Fan, G. Liang, Materials 12 (2019) 1237.

[222] M. Kaltenbrunner, G. Adam, E.D. Glowacki, M. Drack, R. Schwodiauer, L. Leonat, D.H. Apaydin, H. Groiss, M.C. Scharber, M.S. White, N.S. Sariciftci, S. Bauer, Nat. Mater. 14 (2015) 1032-1039.

[223] C. Momblona, L. Gil-Escrig, E. Bandiello, E.M. Hutter, M. Sessolo, K. Lederer, J. Blochwitz-Nimoth, H.J. Bolink, Energy Environ. Sci. 9 (2016) 3456-3463.

[224] J. Li, R. Munir, Y. Fan, T. Niu, Y. Liu, Y. Zhong, Z. Yang, Y. Tian, B. Liu, J. Sun, D.-M. Smilgies, S. Thoroddsen, A. Amassian, K. Zhao, S. Liu, Joule 2 (2018) 1313-1330.

[225] W.-Q. Wu, Z. Yang, P.N. Rudd, Y. Shao, X. Dai, H. Wei, J. Zhao, Y. Fang, Q. Wang, Y. Liu, Y. Deng, X. Xiao, Y. Feng, J. Huang, Sci. Adv. 5 (2019) eaav8925.

[226] H. Huang, J. Shi, L. Zhu, D. Li, Y. Luo, Q. Meng, Nano Energy 27 (2016) 352-358.

[227] J.B. Whitaker, D.H. Kim, B.W. Larson, F. Zhang, J.J. Berry, M.F.A.M. van Hest, K. Zhu, Sustain. Energy Fuels 2 (2018) 2442-2449.

[228] J.E. Kim, S.S. Kim, C. Zuo, M. Gao, D. Vak, D.Y. Kim, Adv. Funct. Mater. 29 (2019) 1809194.

[229] M. Remeika, Y.B. Qi, J. Energy Chem. 27 (2018) 1101-1110.

[230] J.E. Bishop, T.J. Routledge, D.G. Lidzey, J. Phys. Chem. Lett. 9 (2018) 1977-1984.

[231] J.E. Bishop, J.A. Smith, D.G. Lidzey, ACS Appl. Mater. Interfaces 12 (2020) 48237-48245.

[232] M. Remeika, S.R. Raga, S. Zhang, Y.B. Qi, J. Mater. Chem. A 5 (2017) 5709-5718.

[233] S. Uličná, B. Dou, D.H. Kim, K. Zhu, J.M. Walls, J.W. Bowers, M.F.A.M. van Hest, ACS Appl. Energy Mater. 1 (2018) 1853-1857.

[234] J.E. Bishop, J.A. Smith, C. Greenland, V. Kumar, N. Vaenas, O.S. Game, T.J. Routledge, M. Wong-Stringer, C. Rodenburg, D.G. Lidzey, ACS Appl. Mater. Interfaces 10 (2018) 39428-39434.

[235] J.E. Bishop, C.D. Read, J.A. Smith, T.J. Routledge, D.G. Lidzey, Sci. Rep. 10 (2020) 6610.

[236] Y. Jiang, M. Remeika, Z. Hu, E.J. Juarez-Perez, L. Qiu, Z. Liu, T. Kim, L.K. Ono, D.Y. Son, Z. Hawash, M.R. Leyden, Z. Wu, L. Meng, J. Hu, Y.B. Qi, Adv. Energy Mater. 9 (2019) 1803047.

[237] J.-E. Kim, Y.-S. Jung, Y.-J. Heo, K. Hwang, T. Qin, D.-Y. Kim, D. Vak, Sol. Energy Mater Sol. Cells 179 (2018) 80-86.

[238] M. Remeika, L.K. Ono, M. Maeda, Z. Hu, Y.B. Qi, Org. Electron. 54 (2018) 72-79.

[239] D. Burkitt, J. Searle, T. Watson, Roy. Soc. Open Sci. 5 (2018) 172158.

[240] A.K. Zak, W.H. Abd. Majid, M.E. Abrishami, R. Yousefi, Solid State Sci. 13 (2011) 251-256.

[241] J.T.-W. Wang, Z. Wang, S. Pathak, W. Zhang, D.W. deQuilettes, F. Wisnivesky-Rocca-Rivarola, J. Huang, P.K. Nayak, J.B. Patel, H.A.M. Yusof, Y. Vaynzof, R. Zhu, I. Ramirez, J. Zhang, C. Ducati, C. Grovenor, M.B. Johnston, D.S. Ginger, R.J. Nicholas, H.J. Snaith, Energy Environ. Sci. 9 (2016) 2892-2901.

[242] D.J. Xue, Y. Hou, S.C. Liu, M. Wei, B. Chen, Z. Huang, Z. Li, B. Sun, A.H. Proppe, Y. Dong, M.I. Saidaminov, S.O. Kelley, J.S. Hu, E.H. Sargent, Nat. Commun. 11 (2020) 1514.

[243] J. Zhao, Y. Deng, H. Wei, X. Zheng, Z. Yu, Y. Shao, J.E. Shield, J. Huang, Sci. Adv. 3 (2017) eaao5616.

[244] C. Zhu, X. Niu, Y. Fu, N. Li, C. Hu, Y. Chen, X. He, G. Na, P. Liu, H. Zai, Y. Ge, Y. Lu, X. Ke, Y. Bai, S. Yang, P. Chen, Y. Li, M. Sui, L. Zhang, H. Zhou, Q. Chen, Nat. Commun. 10 (2019) 815.

[245] N. Rolston, K.A. Bush, A.D. Printz, A. Gold-Parker, Y. Ding, M.F. Toney, M.D. McGehee, R.H. Dauskardt, Adv. Energy Mater. 8 (2018) 1802139.

[246] W. Rehman, D.P. McMeekin, J.B. Patel, R.L. Milot, M.B. Johnston, H.J. Snaith, L.M. Herz, Energy Environ. Sci. 10 (2017) 361-369.

[247] X. Shai, J. Wang, P. Sun, W. Huang, P. Liao, F. Cheng, B. Zhu, S.-Y. Chang, E.-P. Yao, Y. Shen, L. Miao, Y. Yang, M. Wang, Nano Energy 48 (2018) 117-127.

[248] Y. Chen, Y. Lei, Y. Li, Y. Yu, J. Cai, M.-H. Chiu, R. Rao, Y. Gu, C. Wang, W. Choi, H. Hu, C. Wang, Y. Li, J. Song, J. Zhang, B. Qi, M. Lin, Z. Zhang, A.E. Islam, B. Maruyama, S. Dayeh, L.-J. Li, K. Yang, Y.-H. Lo, S. Xu, Nature 577 (2020) 209-215.

[249] W. Shockley, H.J. Queisser, J. Appl. Phys. 32 (1961) 510-519.

[250] S.P. Bremner, C. Yi, I. Almansouri, A. Ho-Baillie, M.A. Green, Sol. Energy 135 (2016) 750-757.

[251] T. Miyasaka, A. Kulkarni, G.M. Kim, S. Öz, A.K. Jena, Adv. Energy Mater. 10 (2020) 1902500.

[252] J.H. Noh, S.H. Im, J.H. Heo, T.N. Mandal, S.I. Seok, Nano Lett. 13 (2013) 1764-1769.

[253] F. Hao, C.C. Stoumpos, D.H. Cao, R.P.H. Chang, M.G. Kanatzidis, Nat. Photonics 8 (2014) 489-494.

[254] D. Sabba, H.K. Mulmudi, R.R. Prabhakar, T. Krishnamoorthy, T. Baikie, P.P. Boix, S. Mhaisalkar, N. Mathews, J. Phys. Chem. C 119 (2015) 1763-1767.

[255] F. Xu, T.Y. Zhang, G. Li, Y.X. Zhao, ChemSusChem 10 (2017) 2365-2369.

[256] B.-B. Yu, M. Liao, J. Yang, W. Chen, Y. Zhu, X. Zhang, T. Duan, W. Yao, S.-H. Wei, Z. He, J. Mater. Chem. A 7 (2019) 8818-8825.

[257] K.M. McCall, C.C. Stoumpos, O.Y. Kontsevoi, G.C.B. Alexander, B.W. Wessels, M.G. Kanatzidis, Chem. Mater. 31 (2019) 2644-2650.

[258] R. Prasanna, A. Gold-Parker, T. Leijtens, B. Conings, A. Babayigit, H.G. Boyen, M.F. Toney, M.D. McGehee, J. Am. Chem. Soc. 139 (2017) 11117-11124.

[259] K.Z. Du, W. Meng, X. Wang, Y. Yan, D.B. Mitzi, Angew. Chem. Int. Ed. 56 (2017) 8158-8162.

[260] M. Szafranski, A. Katrusiak, J. Phys. Chem. Lett. 7 (2016) 3458-3466.

[261] F. Ji, J. Klarbring, F. Wang, W. Ning, L. Wang, C. Yin, J.S.M. Figueroa, C.K. Christensen, M. Etter, T. Ederth, L. Sun, S.I. Simak, I.A. Abrikosov, F. Gao, Angew. Chem. Int. Ed. 59 (2020) 1-5.

[262] H. Choi, J. Jeong, H.-B. Kim, S. Kim, B. Walker, G.-H. Kim, J.Y. Kim, Nano Energy 7 (2014) 80-85.

[263] N. Pellet, P. Gao, G. Gregori, T.Y. Yang, M.K. Nazeeruddin, J. Maier, M. Grätzel, Angew. Chem. Int. Ed. 53 (2014) 3151-3157.

[264] Y. Yin, S. Fu, S. Zhou, Y. Song, L. Li, M. Zhang, J. Wang, P. Mariyappan, S.M. Alshehri, T. Ahamad, Y. Yamauchi, Electron. Mater. Lett. 16 (2020) 224-230.

[265] J. Zhao, L. Wei, C. Jia, H. Tang, X. Su, Y. Ou, Z. Liu, C. Wang, X. Zhao, H. Jin, P. Wang, G. Yu, G. Zhang, J. Liu, J. Mater. Chem. A 6 (2018) 20224-20232.

[266] M. Pena-Alvarez, E. del Corro, A. Morales-Garcia, L. Kavan, M. Kalbac, O. Frank, Nano Lett. 15 (2015) 3139-3146.

[267] H.J. Conley, B. Wang, J.I. Ziegler, R.F. Haglund Jr., S.T. Pantelides, K.I. Bolotin, Nano Lett. 13

(2013) 3626-3630.

[268] Q. Li, Y. Wang, W. Pan, W. Yang, B. Zou, J. Tang, Z. Quan, Angew. Chem. Int. Ed. 56 (2017) 15969-15973.

[269] L. Zhang, C. Liu, L. Wang, C. Liu, K. Wang, B. Zou, Angew. Chem. Int. Ed. 57 (2018) 11213-11217.

[270] K. Wu, A. Bera, C. Ma, Y. Du, Y. Yang, L. Li, T. Wu, Phys. Chem. Chem. Phys. 16 (2014) 22476-22481.

[271] M.I. Dar, G. Jacopin, S. Meloni, A. Mattoni, N. Arora, A. Boziki, S.M. Zakeeruddin, U. Rothlisberger, M. Grätzel, Sci. Adv. 2 (2016) e1601156.

[272] W. Ning, X.G. Zhao, J. Klarbring, S. Bai, F. Ji, F. Wang, S.I. Simak, Y. Tao, X.M. Ren, L. Zhang, W. Huang, I.A. Abrikosov, F. Gao, Adv. Funct. Mater. 29 (2019) 1807375.

[273] B. Hailegnaw, S. Kirmayer, E. Edri, G. Hodes, D. Cahen, J. Phys. Chem. Lett. 6 (2015) 1543-1547.

[274] A. Babayigit, A. Ethirajan, M. Muller, B. Conings, Nat. Mater. 15 (2016) 247-251.

[275] Y. Jiang, L. Qiu, E.J. Juarez-Perez, L.K. Ono, Z. Hu, Z. Liu, Z. Wu, L. Meng, Q. Wang, Y.B. Qi, Nat. Energy 4 (2019) 585-593.

[276] F. Yang, S. Wang, P. Dai, L. Chen, A. Wakamiya, K. Matsuda. J. Mater. Chem. A, 2020, DOI: 10.1039/D0TA07495K.

[277] F. Gu, Z. Zhao, C. Wang, H. Rao, B. Zhao, Z. Liu, Z. Bian, C. Huang, Sol. RRL 3 (2019) 1900213.

[278] I. Kopacic, B. Friesenbichler, S.F. Hoefler, B. Kunert, H. Plank, T. Rath, G. Trimmel, ACS Appl. Energy Mater. 1 (2018) 343-347.

Graphic abstract with a description:
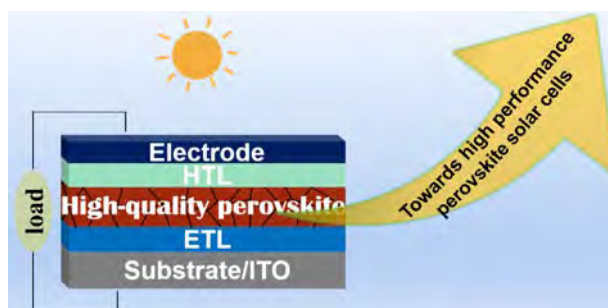
This review article focuses on providing a full picture of preparing high quality metal halide perovskite films for realizing high performance perovskite solar cells, including the strategies of antisolvent, Lewis acid-base, additive engineering, scaleable fabrication, strain engineering and band gap adjustment.